UNCLASSIFIED

SECURITY CLASSIFICATION OF THIS PAGE (When Data Entered)

REPORT DOCUMENTATION PAGE

READ INSTRUCTIONS BEFORE COMPLETING FORM

1. REPORT NUMBER: NSWC/DL-TR-3727
2. GOVT ACCESSION NO.
3. RECIPIENT'S CATALOG NUMBER
4. TITLE (and Subtitle): NONLINEAR ANALYSIS OF THE ROLLING MOTION OF A WRAP-AROUND FIN MISSILE AT ANGLES OF ATTACK FROM Ø TO 90° IN INCOMPRESSIBLE FLOW.
5. TYPE OF REPORT & PERIOD COVERED: Final rept. March 1975 - March 1977
6. PERFORMING ORG. REPORT NUMBER
7. AUTHOR(s): Samuel R. Hardy
8. CONTRACT OR GRANT NUMBER(s)
9. PERFORMING ORGANIZATION NAME AND ADDRESS: Naval Surface Weapons Center, Dahlgren Laboratory, Dahlgren, Virginia 22448
10. PROGRAM ELEMENT, PROJECT, TASK AREA & WORK UNIT NUMBERS: 62332N/F32323/WF32323201/DK04AA101
11. CONTROLLING OFFICE NAME AND ADDRESS: Naval Air Systems Command, Washington, DC 20361
12. REPORT DATE: September 1977
13. NUMBER OF PAGES: 95
14. MONITORING AGENCY NAME & ADDRESS (if different from Controlling Office): 85p.
15. SECURITY CLASS. (of this report): UNCLASSIFIED
15a. DECLASSIFICATION/DOWNGRADING SCHEDULE
16. DISTRIBUTION STATEMENT (of this Report): Approved for public release; distribution unlimited.
16. F32323 F32399
17. WF32323201, WF32399999
17. DISTRIBUTION STATEMENT (of the abstract entered in Block 20, if different from Report)
18. SUPPLEMENTARY NOTES
19. KEY WORDS (Continue on reverse side if necessary and identify by block number)

wrap-around fin missile
rolling motion
subsonic wind tunnel test
dynamic wind tunnel test

20. ABSTRACT (Continue on reverse side if necessary and identify by block number)

Dynamic subsonic wind tunnel test data are presented for a wrap-around fin (WAF) missile configuration in pure rolling motion at angles of attack from 0 through 90°. A nonlinear second-order differential equation of motion which describes the rolling motion of the four-finned WAF missile is discussed. This equation of motion is utilized in a "global" nonlinear least-squares fitting procedure to extract linear and nonlinear aerodynamic roll moment coefficients from the wind tunnel test data. The equation of motion together →

DD FORM 1 JAN 73 1473 EDITION OF 1 NOV 65 IS OBSOLETE S/N 0102-LF-014-6601

UNCLASSIFIED

SECURITY CLASSIFICATION OF THIS PAGE (When Data Entered)

A046368

391 598

AB

with four extracted coefficients are shown to adequately explain the subsonic rolling motion of a WAF missile configuration at angles of attack from 0 through 90°

FOREWORD

This report documents wind tunnel test data and nonlinear roll moment coefficients extracted from test data for a wrap-around fin (WAF) missile configuration. The work was conducted under a program to investigate the nonlinear rolling motion of finned bodies at both small and large angles of attack.

This work was supported by the Naval Air Systems Command (Mr. W. C. Volz, AIR-320C) under AIRTASK A03W-350D/004B-6F32-300-000.

This report was reviewed and approved by Mr. Frank L. Stevens, Aeromechanics Branch, Dr. Frankie G. Moore, Head, Aeromechanics Branch, and Mr. Herman Caster, Head, Exterior Ballistics Division of the Warfare Analysis Department.

Released by:

Ralph A. Niemann

RALPH A. NIEMANN, Head
Warfare Analysis Department

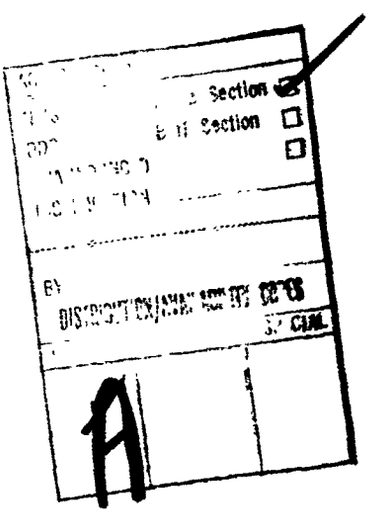

TABLE OF CONTENTS

Metric Conversion Table

To Convert From	To	Multiply By
in.	cm	2.54
ft	m	0.30479
deg	rad	0.1686
ft/s	m/s	0.3479
lb/ft^2 (force)	Pa	4.788026

LIST OF ILLUSTRATIONS

LIST OF ILLUSTRATIONS (Continued)

LIST OF ILLUSTRATIONS (Continued)

LIST OF ILLUSTRATIONS (Continued)

INTRODUCTION

The work described herein is the conclusion of a larger program to investigate the roll behavior of finned bodies at small and large angles of attack. The objective of these efforts was to provide a theoretical and experimental understanding of rolling motion in order to improve the dynamic stability characteristics of finned missiles.

The stability characteristics of finned missiles are dependent on the missile's roll behavior. Because of missile asymmetries such as manufacturing tolerances and bent fins, many unguided missiles are designed to spin to avoid large dispersions. When the missile spins, potential problems of roll/yaw coupling, roll resonance, and Magnus instability may arise. A thorough understanding of a configuration's roll behavior is needed to reduce or eliminate these roll problems.

The Naval Surface Weapons Center, Dahlgren Laboratory (NSWC/DL), Dahlgren, Virginia, was tasked to experimentally determine static and dynamic aerodynamic roll moment coefficients for a typical wrap-around fin (WAF) missile configuration. The roll coefficients were to completely describe the subsonic rolling motion characteristics of the WAF configuration at both small and large angles of attack.

Rolling motion data for the missile configuration were obtained from subsonic, free-rolling wind tunnel tests by recording the actual motion with a movie camera. The data films were then digitized to provide roll angle versus time data. A "global" nonlinear least-squares fitting procedure, which had been previously developed, was used to extract the roll moment coefficients from the rolling motion data.

The objective of this report is to document the results of the analysis and to discuss the subsonic roll characteristics of the WAF configuration versus the more familiar cruciform configuration.

WIND TUNNEL TESTS

The WAF missile configuration selected for study was similar to the standard WAF configuration chosen by The Technical Cooperation Program (TTCP), Panel O-7.[1*] This configuration, shown in Figure 1, was selected because some basic aerodynamic data were known for this standard configuration.

Figure 2 shows the 3-in. diameter WAF model installed in the David W. Taylor Naval Ship Research and Development Center's 7x10-ft subsonic wind tunnel. The model was free to roll on a low friction air bearing. The air bearing was attached to a sting that provided yaw only in the horizontal plane. As a result, the yaw angle was the total angle of

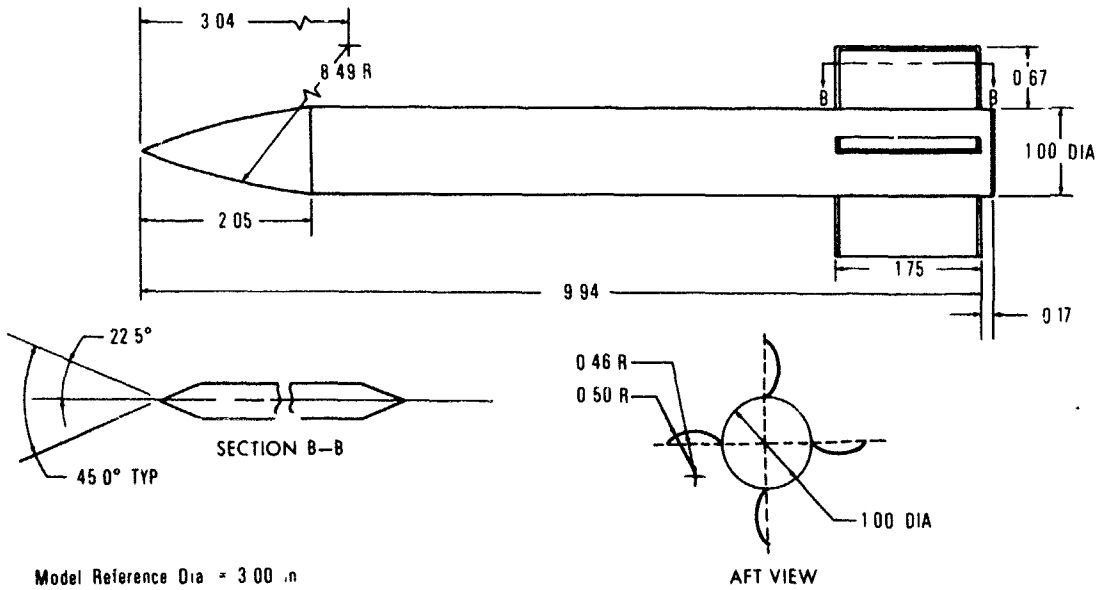

Figure 1. WAF Missile Configuration Dimensions

* Raised numerals refer to identically numbered references listed at the end of the text.

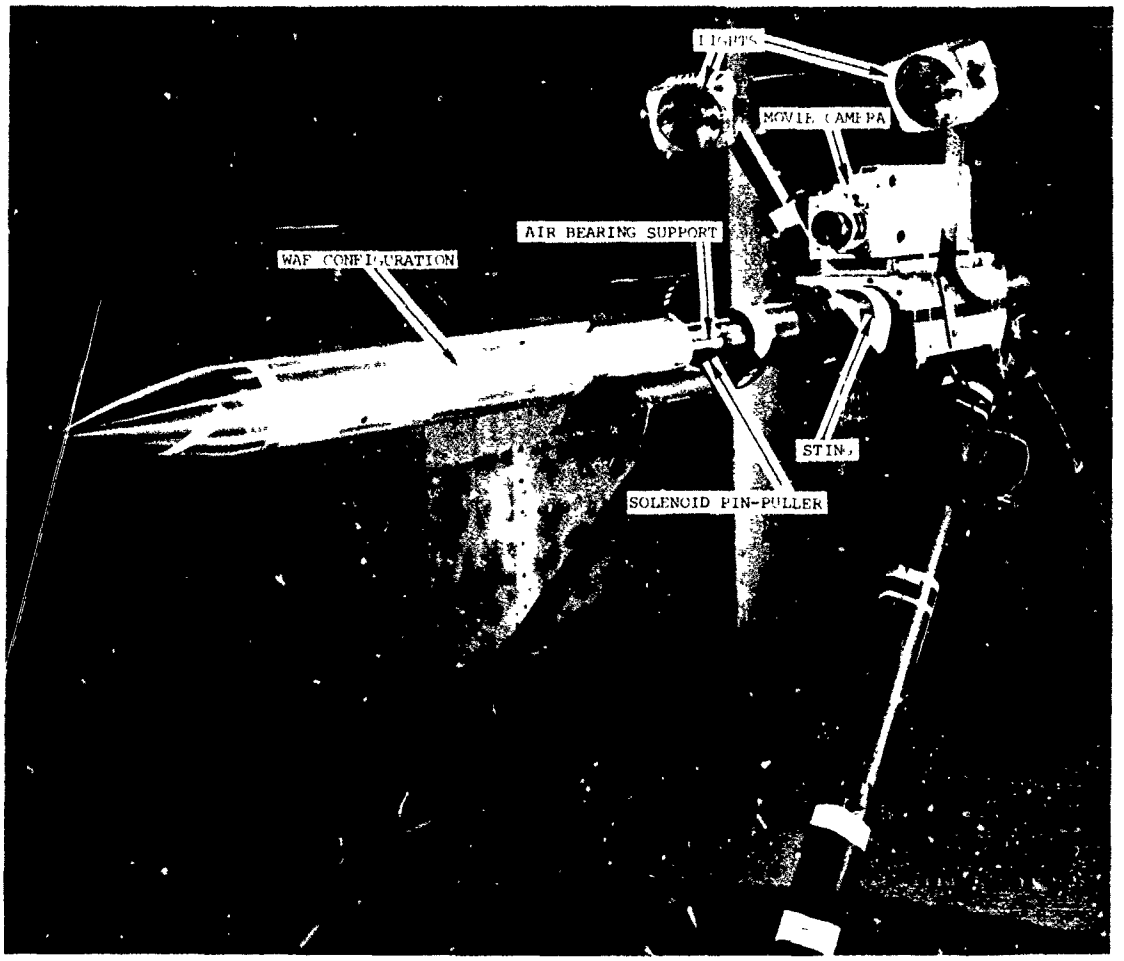

Figure 2. WAF Missile Model Installed in Subsonic Wind Tunnel

attack. The configuration was tested at a free-stream velocity of about 80 ft/s and at angles of attack of 0 through 90°.

Dynamic pressure during the test was about 8.0 lb/ft^2 with a Reynolds number of approximately $5.1x10^5$/ft. Figure 3 shows the coordinate system and defines several terms used in this report.

Rolling motion of the model was recorded at each selected angle of attack using a high-speed movie camera. The camera was mounted on the

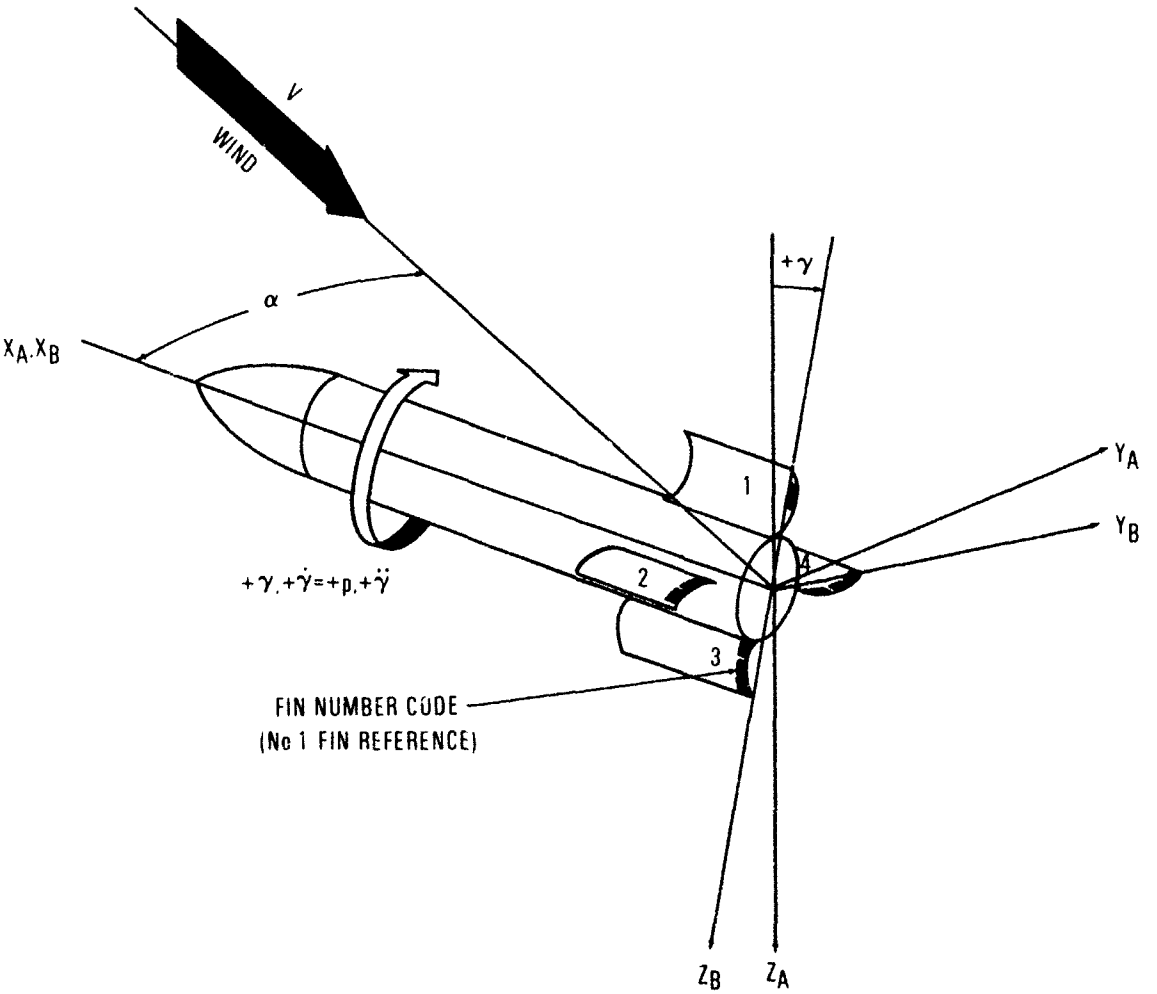

V = Free-Stream Velocity

X_A, Y_A, Z_A = Wind Tunnel Axis System

X_B, Y_B, Z_B = Body Axis System

γ = Missile Roll Angle

$\dot{\gamma} = p$ = Missile Spin Rate

$\ddot{\gamma}$ = Missile Roll Angular Acceleration

α = Missile Angle of Attack

Figure 3. Definition of Terms and Coordinate System

sting with the axis of the lens always parallel to the axis of rotation of the missile. The trailing edges of the fins were coded so that the roll orientation of the model could be determined from each frame of the

movie film. A timing light provided reference marks on the film at the rate of 120 mark/s so that the film frame number could be correlated to time. Thus, the digitized film provided records of roll angle versus time.[2]

Different types of rolling motion were obtained from the model by controlling its initial conditions. A solenoid-actuated pin located at the base of the model locked the model at a fixed roll angle until the wind tunnel had stabilized at test conditions. At the beginning of some data runs, the pin was pulled unlocking the model so it could roll freely. In other runs, the missile was spun up to high spin rates using an air jet, which was created by a nozzle on the end of a high pressure pipe. The jet blew against the missile's fins spinning the missile. At the beginning of a data run, the jet was removed and the camera was then turned on. The initial conditions used on runs at a particular angle of attack depended on the type of rolling motion that was exhibited. Attempts were made to record all of the modes of motion at each of the angles of attack tested.

EQUATION OF MOTION

The "global" nonlinear least-squares fitting procedure used to extract the roll moment coefficients required an equation of motion which could adequately describe the roll characteristics of the test configuration in order to fit the observed test data. The equation used in this analysis was one which had been previously developed for cruciform configurations. The general form of the equation allowed consideration of coefficients for the WAF missile which, because of symmetry considerations, would be identically zero for a cruciform missile.

The equation of motion for the cruciform-finned missile was developed from observation of its basic free-rolling motion characteristics.

Nicolaides[2,3,4] labeled these characteristics as "linear" rolling motion, roll "slowdown," roll "lock-in," roll "break-out," and roll "speed-up." These phenomena occur as the missile increases in angles of attack from 0 to 90°. Figure 4 shows these roll characteristics (steady-state roll rates) as a function of the angle of attack for a typical cruciform-finned missile with/without fin cant at low subsonic speeds.

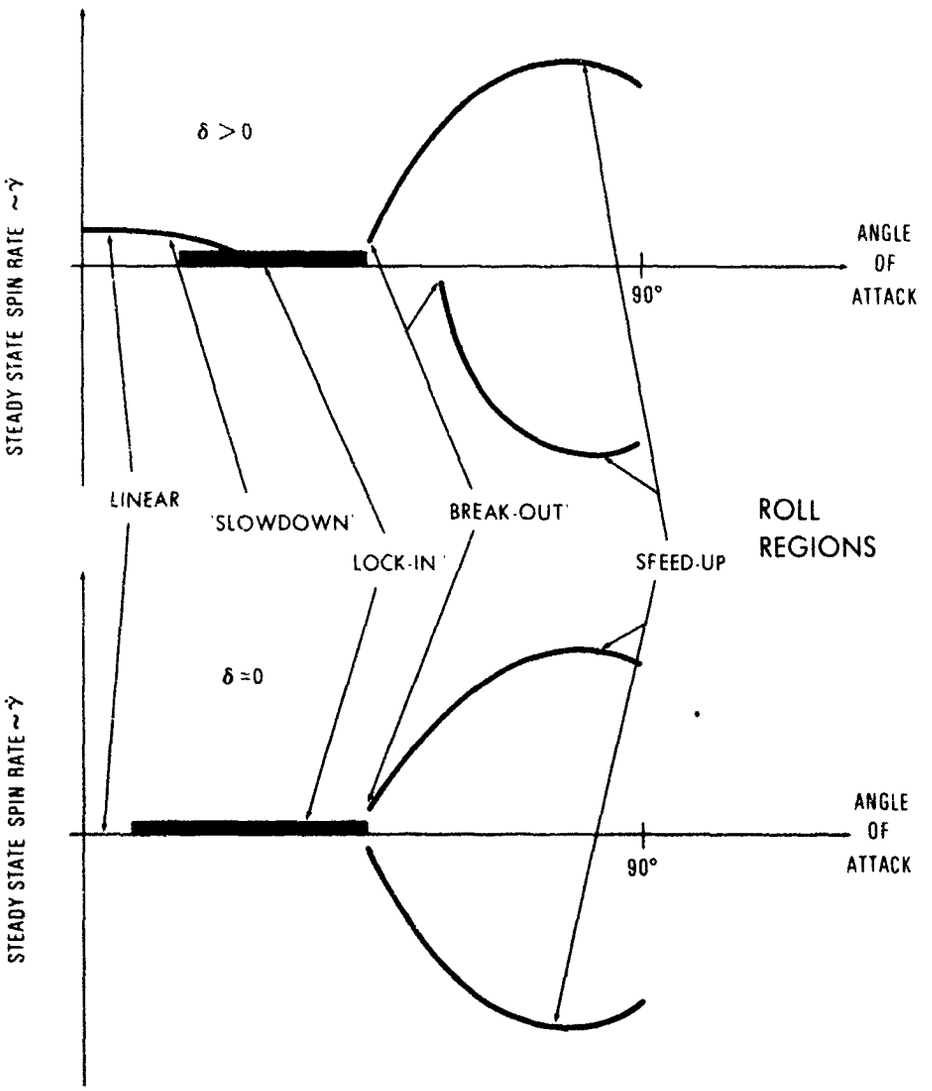

Figure 4. Characteristic Rolling Motion Regions of Cruciform-Finned Missiles With/ Without Fin Cant

Detailed discussion of this characteristic rolling motion and the evolution of the differential equation describing it are contained in References 5 through 9 and will not be repeated here. The complete equation of motion, taken from Reference 7, is:

$$\ddot{\gamma} = \frac{Q}{} \sum_{j=0}^{J} \left(\frac{\dot{\gamma}d}{2V}\right)^{j} \sum_{k=0}^{K} \left(C_{jk} \cos 4k\gamma + S_{jk} \sin 4k\gamma\right) \qquad (1)$$

$$+ C_{ac} \cos \gamma + S_{as} \sin \gamma$$

$$\gamma(0) = \gamma_0 \qquad \dot{\gamma}(0) = \dot{\gamma}_0$$

Equation (1) was believed to be adequate for fitting the rolling motion of the WAF configuration since it appeared that the motion observed in the tests could be described by the equation. The correspondence between the aerodynamic coefficients used in Equation (1) and more conventional coefficient nomenclature is shown in Table 1. The 15 coefficients shown in Table 1 were considered in fitting the roll data. Fourteen of these coefficients were considered in previous work done by Cohen, Clare, and Stevens[7] when they applied the analysis technique to a cruciform-finned configuration. In the present analysis, an additional coefficient, $C_{\ell_{p^2}}$, was considered because of possible differences in the damping torque in the positive and negative spin directions because of WAF fin curvature. Because of the similarities in the roll data between WAF and cruciform-finned missiles, the techniques used by Cohen, Clare, and Stevens[7] were applied directly to the WAF configuration data.

DISCUSSION OF WIND TUNNEL DATA

Figures A-1 through A-28 show plots of roll angle versus frame number which were obtained by digitizing film data from the wind tunnel tests. The roll angle scale was plotted on a scale from 0 to 360° in

Table 1. Aerodynamic Roll Moment Coefficients Considered in Data Fits

Nomenclature		Description
Standard	Equation	
$C_{\ell_\delta}{}^{\delta}$	C_{00}	Static roll moment coefficient
$C_{\ell_{\delta(4\gamma)}}{}^{\delta}$	C_{01}	Variation of static roll moment coefficient with roll angle (γ)
$C_{\ell_{\delta(8\gamma)}}{}^{\delta}$	C_{02}	
C_{ℓ_p}	C_{10}	Linear roll damping moment coefficient
$C_{\ell_{p(4\gamma)}}$	C_{11}	Variation of linear roll damping moment coefficients with roll angle
$C_{\ell_{p(8\gamma)}}$	C_{12}	
$C_{\ell_{p^2}}$	C_{20}	Quadratic roll damping moment coefficient
$C_{\ell_{p^3}}$	C_{30}	Cubic roll damping moment coefficient
$C_{\ell(4\gamma)}$	S_{01}	Induced static roll moment coefficients
$C_{\ell(8\gamma)}$	S_{02}	
$C_{\ell(12\gamma)}$	S_{03}	
$C_{\ell(16\gamma)}$	S_{04}	
$C_{\ell(20\gamma)}$	S_{05}	
C_{ac}	C_{06}	Aerodynamic/mass asymmetric roll moment coefficients
S_{as}	S_{06}	

order to make usable-sized plots. There are two data runs with different initial conditions for each angle of attack that were tested.

Examination of the data in Figures A-1 through A-28 allows some relevant comparisons of the rolling motion between WAF and cruciform-finned configurations. (Steady-state roll rates of a cruciform missile versus angle of attack are shown qualitatively in Figure 4. Reference 8 presents actual roll angle history data for a cruciform missile at high angles of attack.) The WAF rolling motion data at angles of attack of 0 and 5°, Figures A-1 through A-4, show that if the missile was initially spun up the roll rate damped to a zero steady-state rate. Figures A-2 and A-4 show small roll rates at the end of the data runs. Because the camera film magazine was small, the camera stopped before the motion reached a zero steady-state rate. Small static roll moments at a 0° angle of attack have been measured at various Mach numbers for the WAF configuration. These moments have been small and appear to be due to the WAF curvature.[1] Because there was no intentional fin cant and the asymmetry moment may have been larger than the static roll moment, the model did not exhibit a steady-state roll rate at a 0° angle of attack. A cruciform-finned configuration with no fin cant would exhibit similar motion at low angles of attack. At these small angles of attack, oscillations in the roll angle, γ, indicate that the model has a slight aerodynamic asymmetry or mass imbalance.

At angles of attack from 10 through 30°, Figures A-5 through A-12, the WAF configuration exhibited a positive steady-state roll rate that increased with increasing angle of attack. A cruciform-finned missile with fin cant would have exhibited a "slowdown" or decrease in the spin rate with increasing angle of attack. At each angle of attack, two different initial conditions were used. When the model was spun up to a high negative spin rate, it reversed the roll direction to a positive steady-state rate. When the WAF model was released at a fixed roll angle with zero roll rate, it spun up again to a positive steady-state rate.

This type of motion at a particular angle of attack is similar to motion of a cruciform missile with large fin cant.

The WAF missile's rolling motion showed strong nonlinearities that are evident in the angular roll data at angles of attack above 30°. At a 35° angle of attack, Figures A-13 and A-14, the missile exhibits motion similar to the motion at lower angles of attack except for fluctuations in the roll rate at low roll rates. These fluctuations indicate the presence of the induced roll moment which is dependent on the missile roll angle, γ, and on the angle of attack. Roll "lock-in," which can be attributed to the induced roll, was also observed at a 35° angle of attack during the test. However, irregularities in the run showing "lock-in" at a 35° angle of attack precluded its analysis. Dual modes of motion are possible at a 35° angle of attack depending on the initial conditions, γ_0 and $\dot{\gamma}_0$. Similarly, dual modes may be exhibited by a cruciform-finned missile with fin cant at a 35° angle of attack.

At a 40° angle of attack, the damping is no longer a linear function of the spin rate. At moderately negative spin rates, Figure A-15, the damping torque is nearly zero. In Figure A-16, the damping is positive at low spin rates near zero and negative at the positive steady-state spin rate. These same damping characteristics are exhibited by a cruciform-finned missile with fin cant in the beginning of the roll "speed-up" region.

At a 45° angle of attack, Figures A-17 and A-18, the roll oscillation amplitude grows, "breaks-out," indicating that the damping is positive at low spin rates when the model is released. However, at this angle of attack, the WAF missile has both positive and negative steady-state spin rates that are nearly equal. These characteristics are again similar to a cruciform-finned missile with no fin cant in the roll "speed-up" region where the damping has a cubic form. It is also important to notice that slightly different initial roll angles can cause the model

to "break-out" in either positive or negative spin direction; a characteristic of a nonlinear system.

Above a 45° angle of attack, Figures A-19 through A-28, the WAF configuration exhibits roll "break-out" and roll "speed-up" only in the positive direction. Similar characteristics are exhibited by cruciform-finned missiles with large positive fin cants at angles of attack in the beginning of the roll "speed-up" region.[5]

All of the rolling motion data shown in Figures A-1 through A-28 were repeatable and, therefore, are predominantly a steady aerodynamic phenomenon. The motion is nonlinear in nature and requires a nonlinear equation to completely describe the dynamics throughout the 0 to 90° angle of attack range. However, the WAF motion and its nonlinearities were found to be quite similar in many respects to those observed previously for a cruciform-finned missile.

EXTRACTION OF AERODYNAMIC ROLL MOMENT COEFFICIENTS

A "global" nonlinear least-squares procedure formulated by Cohen and Clare[6] was used to extract roll moment coefficients from the observed angular roll data. This procedure fits Equation (1) to observed data and extracts a set of roll moment coefficients for a particular angle of attack.

The fitting process requires the variation of the sum of the squares of the residuals (between observed and computed roll angle) with respect to each of the perturbed (fit for) coefficients to vanish. The coefficients are incremented in an iterative fashion until the sum of the squares of the residuals converge. All of the observed data for a particular angle of attack are fit at the same time. The observed data are divided into segments because the sum of the squares of the residuals may become too large for convergence when all the data are fit in a

single segment. Large residuals may be due to truncation of the equation of motion, unmodeled turbulence, or other unmodeled transients in the wind tunnel.

Estimates of C_{00}, C_{10}, C_{30}, and S_{01} were used to begin the fitting process. Estimates of the initial roll angle and roll rate were determined from observed data. Equation (1) was fit "locally" to each of the observed data segments using the constant estimates of the roll moment coefficients to determine the initial conditions (γ_0 and $\dot{\gamma}_0$) for that segment independently of the other segments. Then, all of the segments of observed data were fit "globally" to obtain a new set of roll moment coefficients and new segment initial conditions. Once a fit was obtained, additional coefficients were included in an iterative fashion until all of the desired coefficients were obtained or until the fitting process would not converge if additional coefficients were introduced. Because the data were segmented, jumps or discontinuities occurred in γ and $\dot{\gamma}$ at the beginning of each segment. Segmenting the data allowed restart of the motion in regions where the roll motion was sensitive to accumulated error in γ or $\dot{\gamma}$. In order to improve the accuracy of extracted roll moment coefficients, the segments were made as large as possible while allowing for convergence. These techniques were applied to each data run until a set of roll moment coefficients were obtained at each angle of attack tested.

The methods and equations employed in the "global" nonlinear least-squares fitting procedure are contained in detail in References 6 and 7. A description of the computer program utilizing the fitting technique is presented in Reference 10.

DISCUSSION OF RESULTS

Table 1 shows the roll moment coefficients which were introduced in the extraction process. Attempts were made to extract all 15 coefficients

at each angle of attack. However, some of the higher order terms which varied with roll angle, γ, could not be extracted at all angles of attack because the fitting technique would not converge when these coefficients were introduced. There may not have been sufficient rolling motion data of the particular nature required to extract all of the coefficients at each angle of attack. Analysis of extraction statistics also indicated that most of the high order terms which varied with roll angle did not improve the fits significantly. Values of some higher order terms are believed to be fit to system noise, and those results were not considered to be reliable. However, the most important, first-order roll moment coefficients were extracted at all angles of attack and those results are presented. These four basic coefficients are (1) static roll moment coefficients, $C_{\ell_\delta}\delta$, (2) linear roll damping moment coefficient, C_{ℓ_p}, (3) cubic roll damping, $C_{\ell_p}3$, and (4) induced roll moment coefficient, $C_{\ell_{(4\gamma)}}$. These coefficients appear to adequately explain the rolling motion characteristics of WAF at all angles of attack tested.

Figures B-1 through B-27 show comparison plots of the observed roll data and the computed roll angular data. The observed data corresponds to the data shown in Figures A-1 through A-28 after the frame numbers have been converted into time. The computed data were generated at each angle of attack using Equation (1) and the entire set of roll moment coefficients. The roll moment coefficient sets used to make the comparison plots included all of the higher order terms.

The small lines normal to the computed plots indicate where segments occurred in the computed data. Both data runs at each angle of attack were fit simultaneously. Figures B-1 through B-27 show the portions of the observed data that were actually used in the fitting process to determine the roll moment coefficients. The deleted data exhibited motion that appeared to be due to unmodeled wind tunnel transients. No comparison plot is presented for data Run 23 (α = 90°) because only a few small

segments of this run were included in the fitting process.[10] In general, Figures B-1 through B-27 show that the computed data match the observed data well.

Figure 5 shows comparison plots of the computed steady-state roll rate and the last observed spin rates versus angle of attack for the WAF configuration. The computed steady-state roll rates were calculated using the entire extracted set of roll moment coefficients at each angle of attack. The agreement between the computed and observed rates is good. The last observed rates were taken from the data runs and were not considered to be actual observed steady-state rates because the camera magazine size limited the data run recording time, and the motion may not have completely reached the steady-state motion in that time period. As a result, the last photographed spin rate at a 70° angle of attack was much less than the actual observed steady-state rate. It should be noted that observed rates at a 45° angle of attack indicate both positive and negative steady-state spin rates. The roll "lock-in" observed at a 35° angle of attack is denoted by the darkened bar on the angle of attack axis.

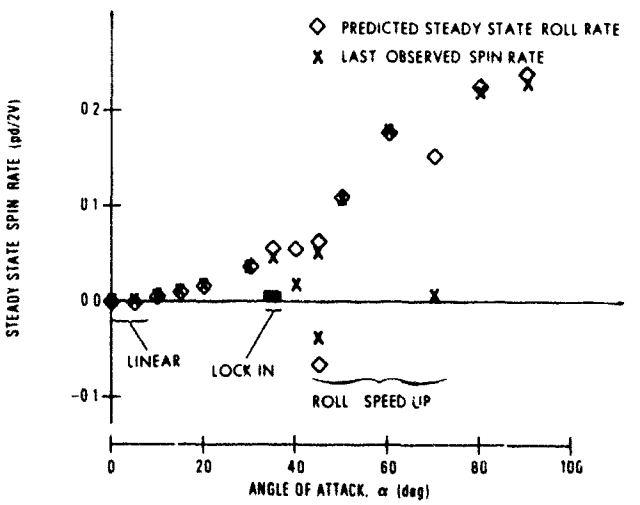

Figure 5. Comparison of Computed and Observed Steady-State Roll Rates for WAF Missile Configuration

By comparing Figures 4 and 5, the qualitative differences in rolling motion characteristics between a cruciform-finned missile and the WAF missile can be seen. The WAF missile has "linear," "lock-in," "break-out," and roll "speed-up" regions similar to the cruciform-finned missile with significant differences in these regions. These differences can be explained by examining the variation in the four, first-order roll moment coefficients with angle of attack. Figures 6 through 9 show plots of these four basic coefficients versus angle of attack.

The WAF configuration's "linear" region occurs between a 0 and 5° angle of attack. As discussed in Reference 5 for the cruciform-finned missile, the linear damping moment and the static roll moment (fin cant moment) are the predominant moments acting on the missile in the "linear" region. Because the WAF configuration had no intentional fin cant and the static roll moments were smaller than the asymmetry moments, the steady-state roll rates were zero. Although the steady-state rates are zero in this region, the region is not truly "linear" because the magnitude of the linear damping moment increases with the angle of attack. The other roll moment coefficient values are insignificant in this region.

As the angle of attack increases from 5 to 30°, the steady-state roll rates of the WAF missile increase rapidly. The static roll moment coefficient, shown in Figure 8, is increasing almost exponentially with the angle of attack in this region. However, Figure 6 shows that there is an increase in the negative damping torque with an increasing angle of attack. Because the static moment increases more rapidly than the damping moment, the steady-state roll rate increases with the angle of attack. A cruciform-finned missile with fin cant would exhibit a constant or decreasing static moment in this region while the damping moment increased; thus, a roll "slowdown" region occurs at these angles of attack. Increases in the cubic damping coefficient in this region indicate that the damping moment is becoming more nonlinear at higher spin rates. The

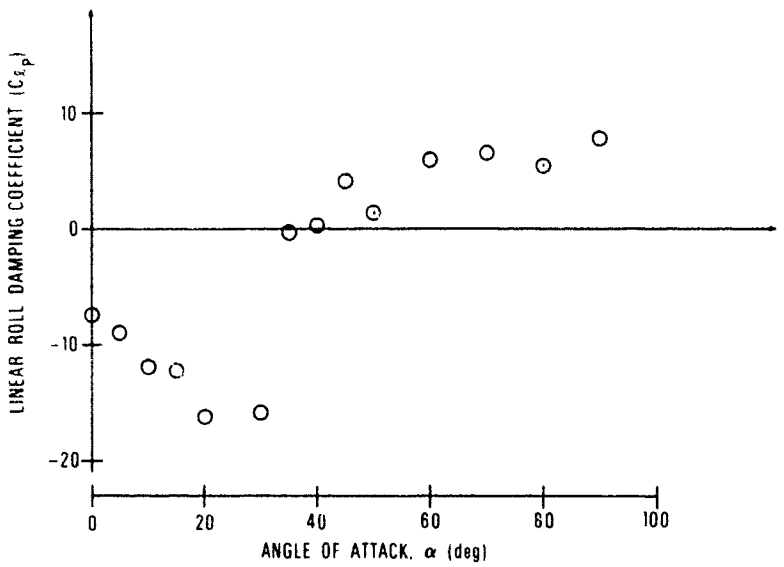

Figure 6. Linear Roll Damping Coefficient Versus Angle of Attack for WAF Missile Configuration

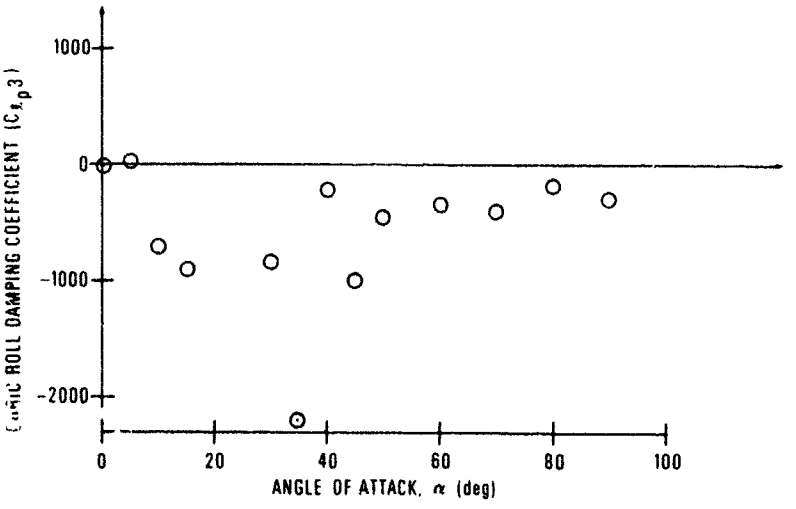

Figure 7. Cubic Roll Damping Coefficient Versus Angle of Attack for WAF Missile Configuration

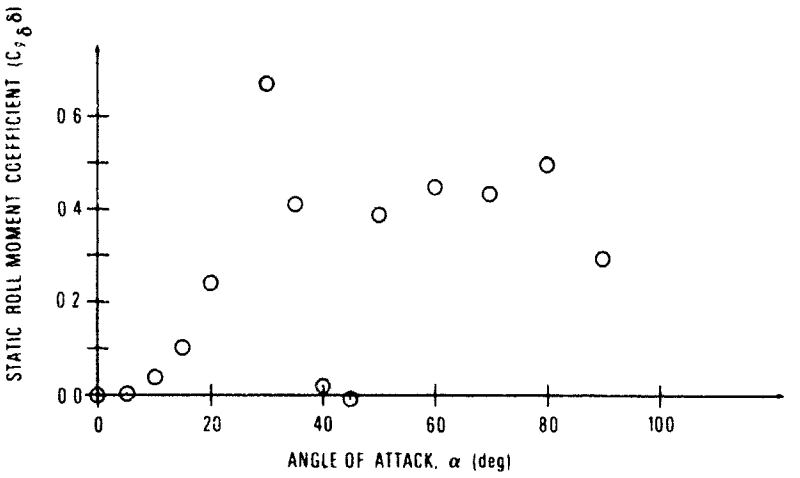

Figure 8. Static Roll Moment Coefficient Versus Angle of Attack for WAF Missile Configuration

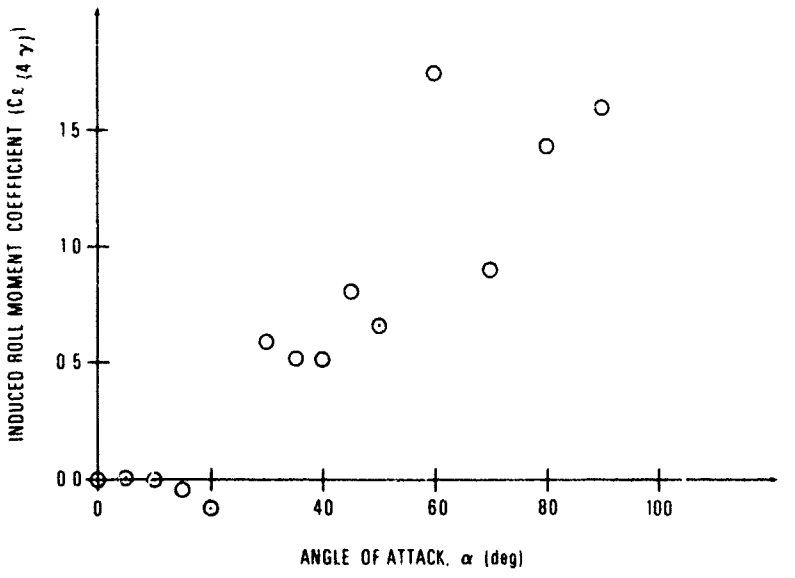

Figure 9. Induced Roll Moment Coefficient Versus Angle of Attack for WAF Missile Configuration

amplitude of the induced roll moment is increasing with the angle of attack in this region. Because the static roll moment is always large, no oscillatory motion is possible.

However, at a 35° angle of attack, the induced roll moment is larger than the static roll moment and the linear damping torque is negative. Because these two conditions are satisfied, it is possible to have dual modes; (1) a steady-state roll rate and (2) roll "lock-in" motion. The linear roll damping coefficient is very small and the cubic damping coefficient is large indicating that the roll damping torque is a nonlinear function of spin rate even at moderate spin rates.

At a 40° angle of attack, the linear damping coefficient is slightly positive and the cubic damping coefficient is negative indicating the beginning of the roll "speed-up" region. There is no negative steady-state roll rate because the positive static roll moment drives the missile in the positive spin direction after roll "break-out." However, at a 45° angle of attack, the static roll moment is nearly zero and the WAF configuration exhibits both positive and negative steady-state rates. This motion is characteristic of a cruciform-finned missile with no fin cant in the roll "speed-up" region.

At angles of attack from 50 to 90°, the damping moment is a cubic function of the spin rate. The WAF configuration "breaks-out" and "speeds-up" only in the positive direction because there is a positive static roll moment driving the motion.

By examining the average roll moment coefficient, the nonlinearity of the roll damping moment and the effect of the static roll moment may be seen at particular angles of attack. Neglecting the coefficients that vary with roll angle, γ, the average roll moment coefficient may be defined as:

$$\overline{C_\ell} = C_{\ell_\delta}\delta + C_{\ell_p}\left(\frac{\dot{\gamma}d}{2V}\right) + C_{\ell_p 2}\left(\frac{\dot{\gamma}d}{2V}\right)^2 + C_{\ell_p 3}\left(\frac{\dot{\gamma}d}{2V}\right)^3 \qquad (2)$$

Figures C-1 through C-14 show plots of $\overline{C_\ell}$ versus nondimensional spin rate ($\dot{\gamma}d/2V$) at all of the angles of attack tested. Steady-state roll rates can be determined from these figures. When $\overline{C_\ell} = 0$ and $\delta\overline{C_\ell}/\delta(\dot{\gamma}d/2V) < 0$, then a steady-state solution exists.

Figures C-1 through C-6 show that the roll damping moment is nearly linear at angles of attack from 0 to 30°. Note that at a 20° angle of attack, $C_{\ell_p}2$ and $C_{\ell_p}3$ were not included in the calculation of $\overline{C_\ell}$ because the extracted values of these coefficients were incorrect. The incorrect coefficient values would have predicted infinite steady-state rates. Spin rates may not have been high enough to extract these higher order damping coefficients correctly. The cubic damping coefficient appears to contribute little to the damping moment at these low angles of attack, especially at low spin rates. Also, the cubic damping coefficient is not needed at low angles of attack to explain the WAF rolling motion characteristics.

At 35 and 40° angles of attack, Figures C-7 and C-8 show that the roll damping moment is nonlinear. This is a region of transition from a negative linear damping coefficient at a 30° angle of attack to a positive linear damping coefficient with a negative cubic damping coefficient at a 45° angle of attack. The cubic damping coefficient ($C_{\ell_p}3$) becomes important in this region and at higher angles of attack. At 35°, only one steady-state roll rate is shown in Figure C-7; however, two steady-state roll rates were observed (dual modes). The other steady-state condition is roll "lock-in" caused by the large induced roll moment coefficient ($C_{\ell_{(4\gamma)}}$) that was neglected when calculating the average roll moment coefficient. Figure C-8 shows that at a 40° angle of attack there is a large spin rate region where the roll damping moment is nearly zero. In the region where the damping is small, the motion may not be repeatable because of the high susceptibility to wind tunnel transients. Both the linear damping coefficient and the cubic damping coefficient are

needed to explain the rolling motion at these angles of attack, even though the WAF missile is not in its roll "speed-up" region.

At a 45° angle of attack, Figure C-9, the roll damping moment has a cubic form similar to the cubic form shown for the cruciform-finned missile with no fin cant.[7] Both positive and negative steady-state rates are predicted in Figure C-9 At angles of attack above 45°, the roll damping moment is cubic in nature; however, the static roll moment is large and only a positive steady-state solution exists. Figures C-10 through C-14 show that the major difference in WAF configuration and a typical cruciform-finned missile in the roll "speed-up" region is the WAF's large static roll moment.

The static induced roll moment coefficient ($C_{\ell(4\gamma)}$) extracted for the WAF configuration showed trends similar to a cruciform-finned missile. Figure 10 shows a comparison plot of the induced roll moment coefficient versus angle of attack for the WAF and cruciform-finned missile.

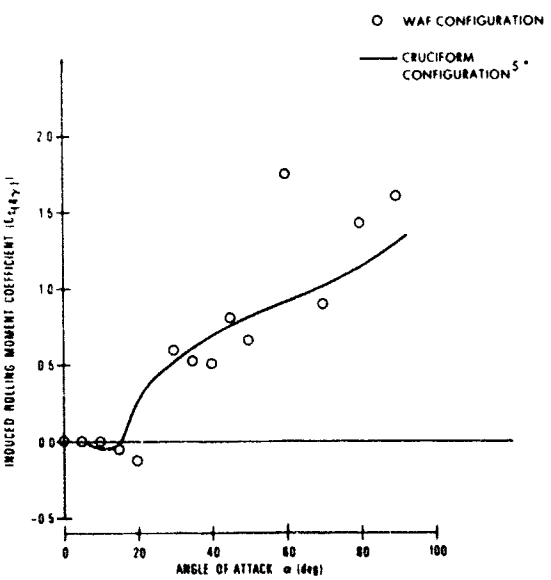

* Daniels, P. "A Study of the Nonlinear Rolling Motion of a Four-Finned Missile," Journal of Spacecraft and Rockets, Volume 7, No. 4, April, 1970

Figure 10. Comparison of WAF and Cruciform-Finned Missile Induced Rolling Moment Coefficient

Insufficient quadratic damping coefficients ($C_{\ell_p 2}$) were extracted to determine differences in the roll damping moment in the positive and negative spin directions.

Phase planes of $\dot{\gamma}$ versus γ were generated at various angles of attack by integrating the roll equation of motion, Equation (1), using the four, first-order roll moment coefficients and the two roll asymmetry terms. Different initial conditions were used to start each trajectory. The phase planes exhibited the same general characteristics of motion observed in the wind tunnel data runs. Figures 11 through 15 show the types of motion exhibited at 0, 30, 35, 45, and 70° angles of attack. The phase planes show all of the general types of motion exhibited in the different roll regions.

SUMMARY AND FUTURE PLANS

Four basic roll moment coefficients were extracted from dynamic subsonic wind tunnel test data of a WAF missile configuration at angles of attack from 0 to 90°. A set of coefficients was extracted at each angle of attack tested. These four basic coefficients were static roll moment, static induced roll moment, linear roll damping, and cubic roll damping. They were shown to be adequate to explain the rolling motion characteristics of the WAF missile over the entire angle of attack range. A comparison of the basic coefficients for a cruciform-finned configuration and the WAF configuration showed that the primary difference in the configurations is the WAF's static roll moment coefficient. This static roll moment is thought to be due to the curvature of the WAF. The damping roll moments and induced roll moments appeared to be similar to the moments for a cruciform-finned missile. The variation of the roll damping moment with spin rate was presented for angles of attack from 0 to 90°. The roll damping moment was nearly a linear function of spin rate up to angles of attack of 30°. At higher angles of attack, the damping

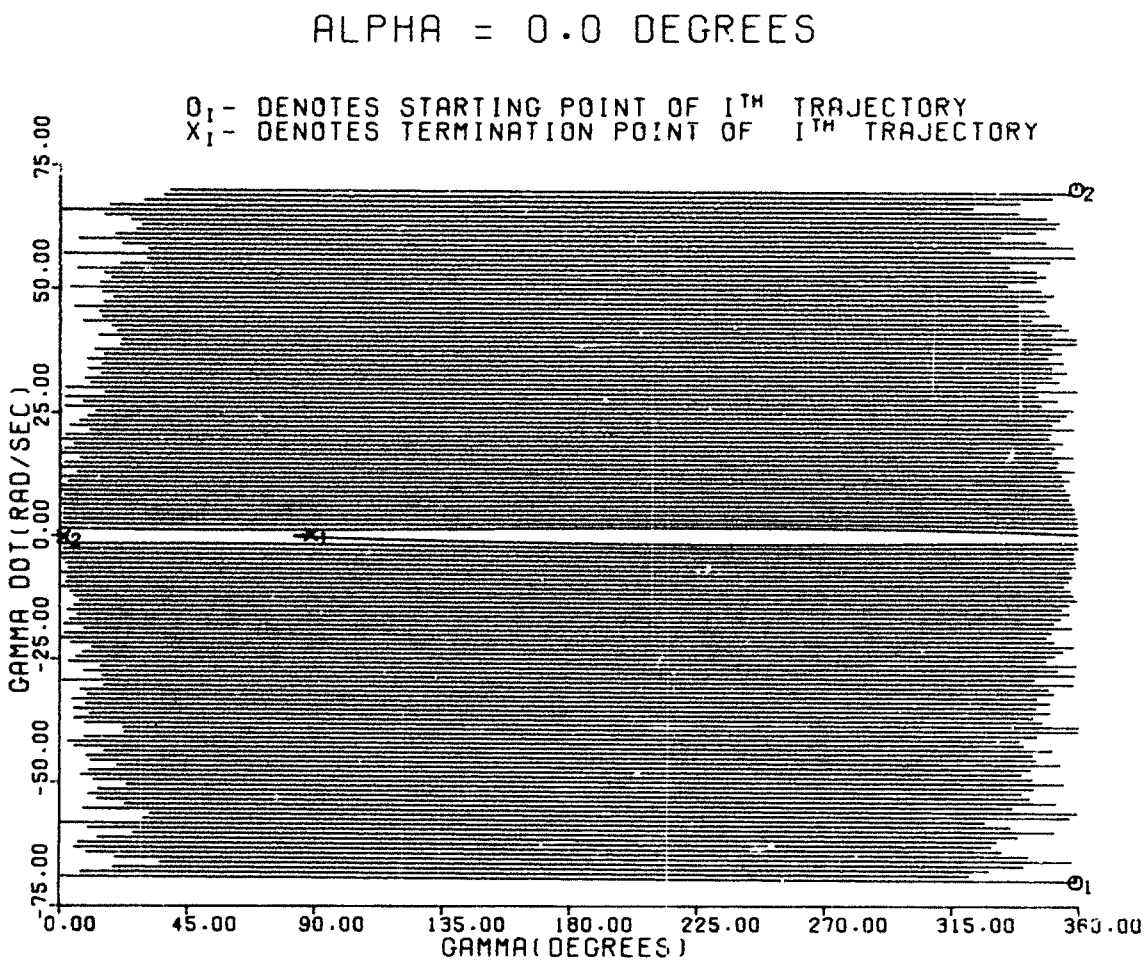

Figure 11. Phase Plane at a 0° Angle of Attack

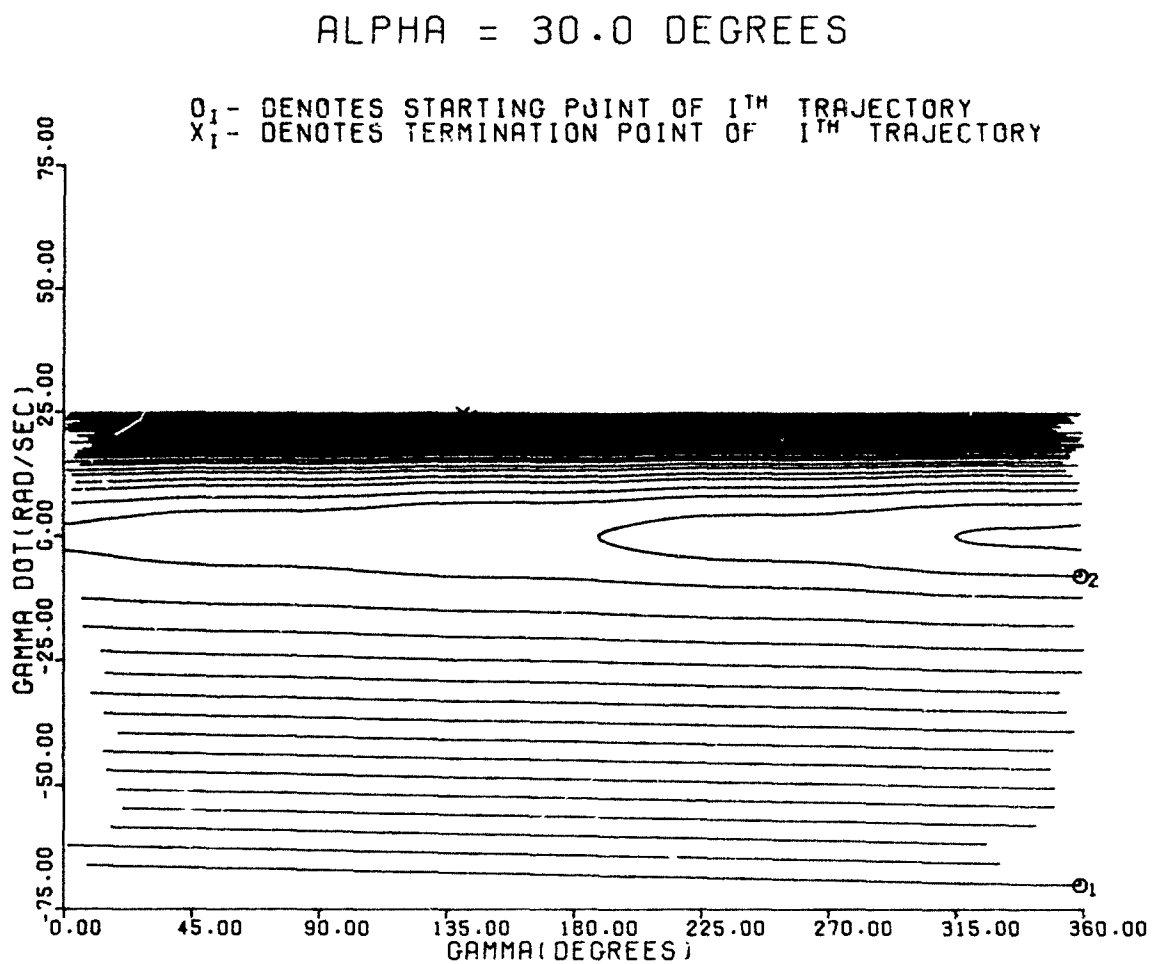

Figure 12. Phase Plane at a 30° Angle of Attack

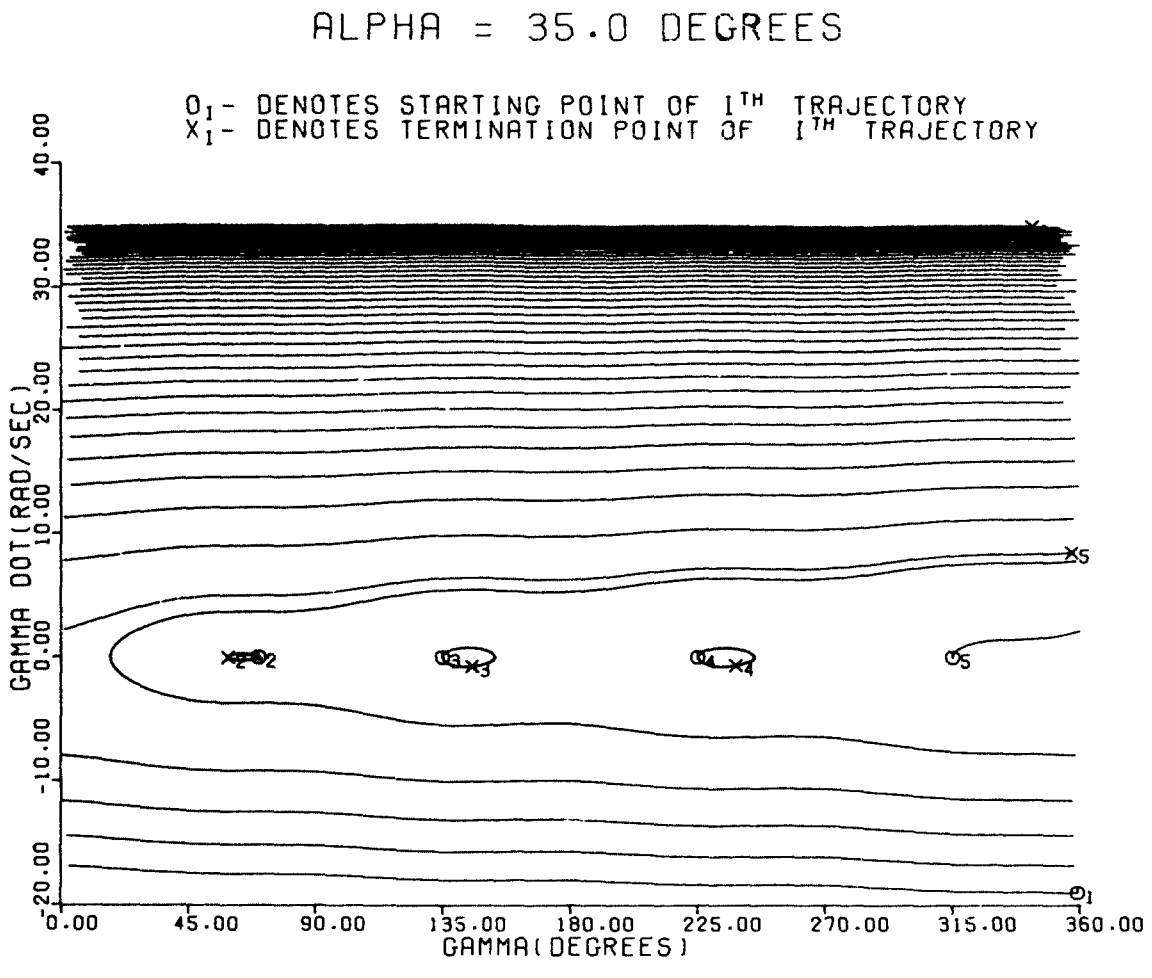

Figure 13. Phase Plane at a 35° Angle of Attack

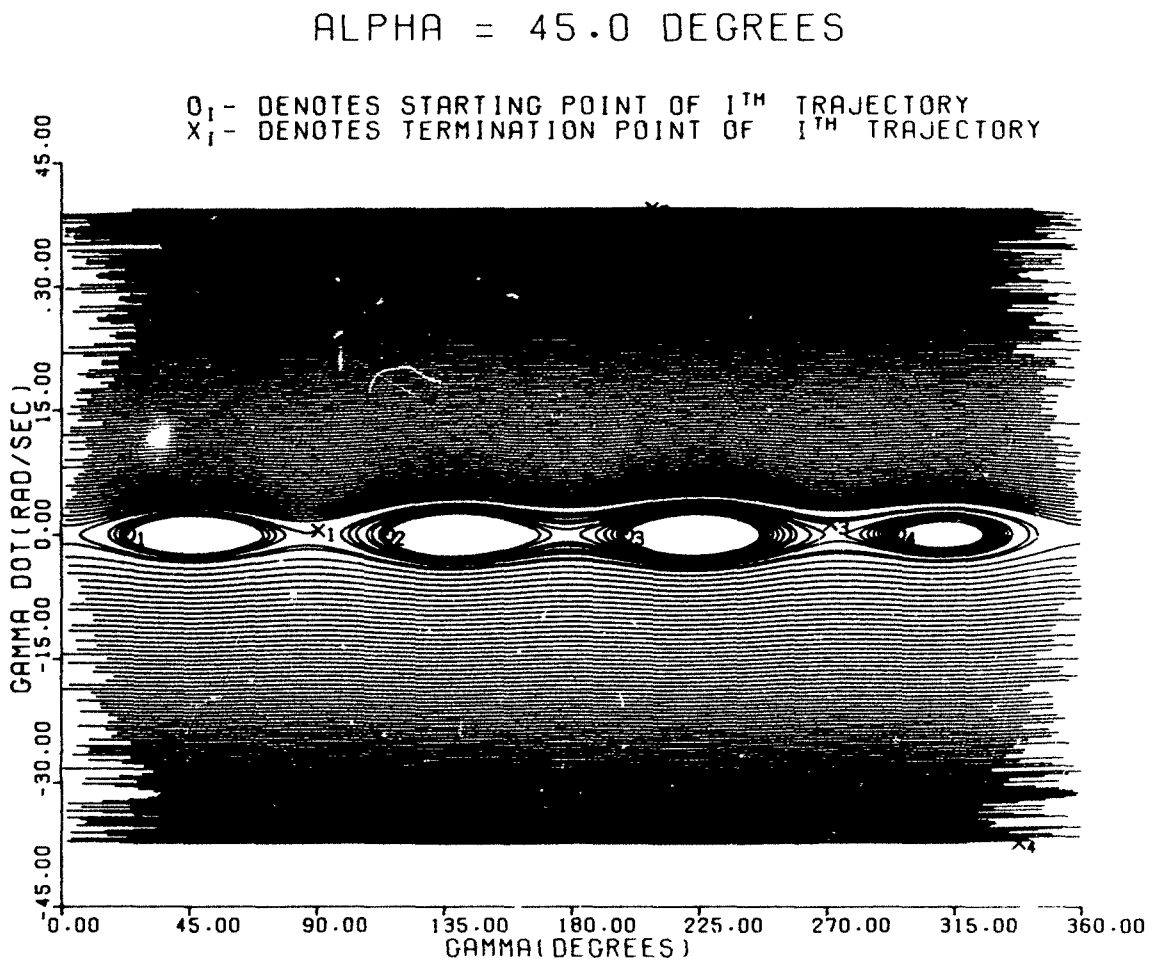

Figure 14. Phase Plane at a 45° Angle of Attack

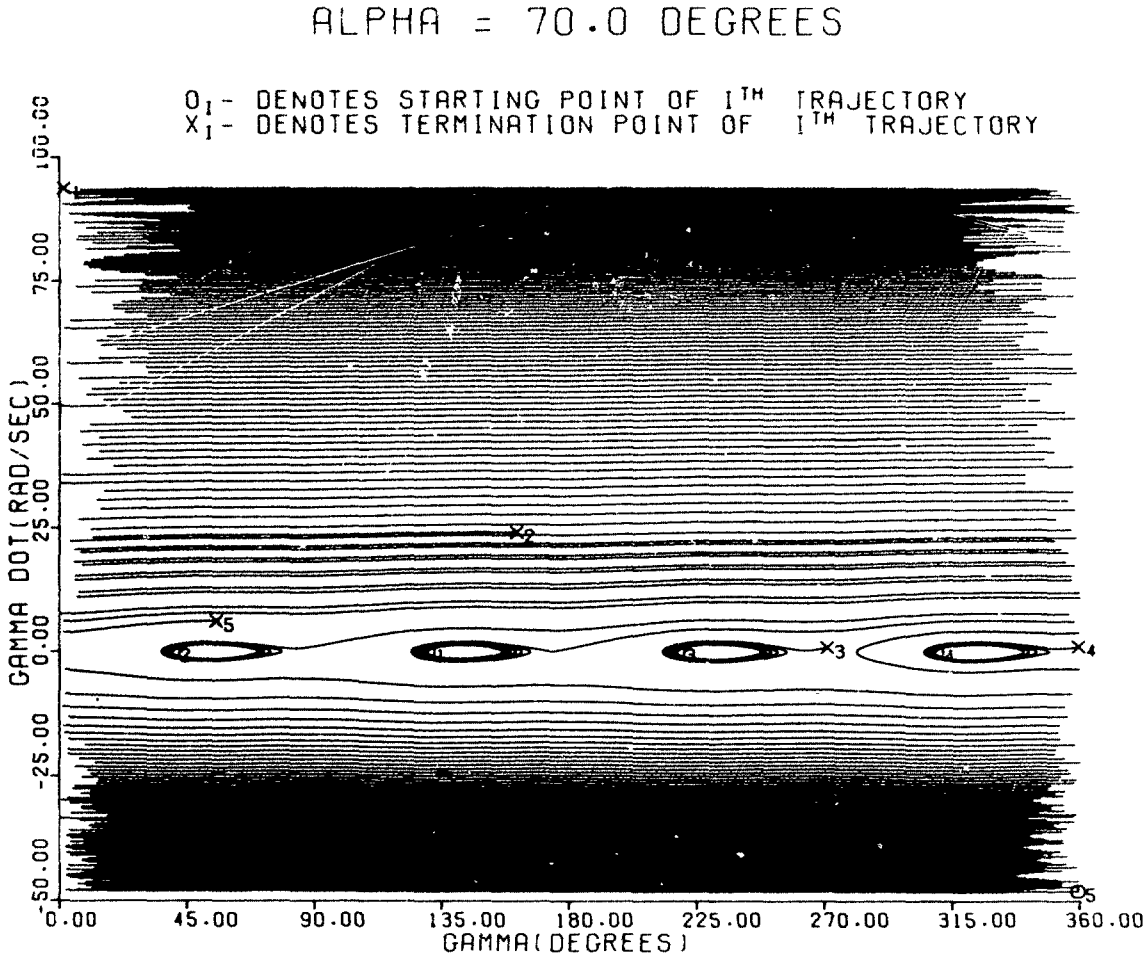

Figure 15. Phase Plane at a 70° Angle of Attack

required both linear and cubic coefficients to describe its variation with spin rate. Extracted induced roll moment coefficient ($C_{\ell_{(4\gamma)}}$) results were similar to those measured statically for a cruciform-finned missile.

REFERENCES

1. Holmes, J. E., *Wrap-Around Fin (WAF) Pressure Distribution*, NSWC/WOL Technical Report TR-73-107, Naval Surface Weapons Center, White Oak Laboratory, Silver Spring, MD, October 1973.

2. Nicolaides, J. D., *On the Rolling Motion of Missiles*, TN 33, Bureau of Ordnance, U.S. Navy, Washington, DC, March 1957.

3. Nicolaides, J. D., *An Hypothesis for Catastrophic Yaw*, TN-18, Bureau of Ordnance, U.S. Navy, Washington, DC, September 1955.

4. Nicolaides, J. D., *Missile Flight and Astrodynamics*, TN-100A, Bureau of Naval Weapons, Washington, DC, 1961.

5. Daniels, P., "A Study of the Nonlinear Rolling Motion of a Four-Finned Missile," Journal of Spacecraft and Rockets, Volume 7, No. 4, April, 1970.

6. Cohen, C. J. and T. A. Clare, *Analysis of the Rolling Motion of Finned Missiles at Large Angles of Attack*, NSWC/DL Technical Report TR-2671, Naval Surface Weapons Center, Dahlgren Laboratory, Dahlgren, VA, February 1972.

7. Cohen, C. J., T. A. Clare, and F. L. Stevens, "Analysis of the Nonlinear Rolling Motion of Finned Missile," AIAA Paper No. 72-980, Palo Alto, CA, 1972.

8. Stevens, F. L., *Subsonic Wind Tunnel Tests of the Basic Finner Missile in Pure Rolling Motion*, NSWC/DL Technical Note TN-K-4/72, Naval Surface Weapons Center, Dahlgren Laboratory, Dahlgren, VA, February 1972.

9. Hardy, S. R., *Subsonic Wind Tunnel Tests of a Canard-Control Missile Configuration in Pure Rolling Motion*, NSWC/DL Technical Report TR-3615, Naval Surface Weapons Center, Dahlgren Laboratory, Dahlgren, VA, June 1977.

REFERENCES (Continued)

10. Reynolds, J. H., *RØMØF, a CDC 6700 Computer Program for Fitting Rolling Motion Data of Cruciform-Finned Missiles*, NSWC/DL Technical Note TN-K-42/76, Naval Surface Weapons Center, Dahlgren Laboratory, Dahlgren, VA, July 1973.

APPENDIX A

OBSERVED ROLL ANGLE VERSUS FRAME NUMBER

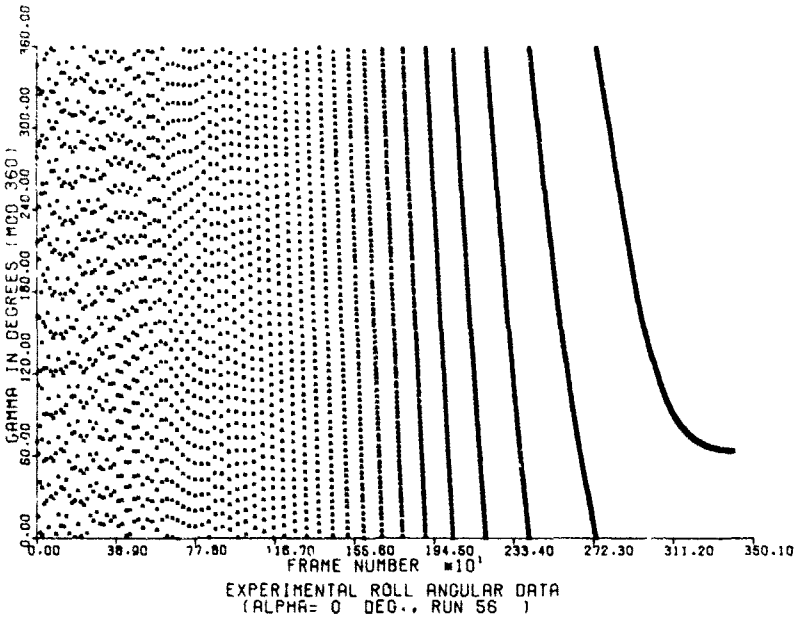

Figure A-1. Observed Roll Angle Versus Frame Number at a 0° Angle of Attack for Run 56

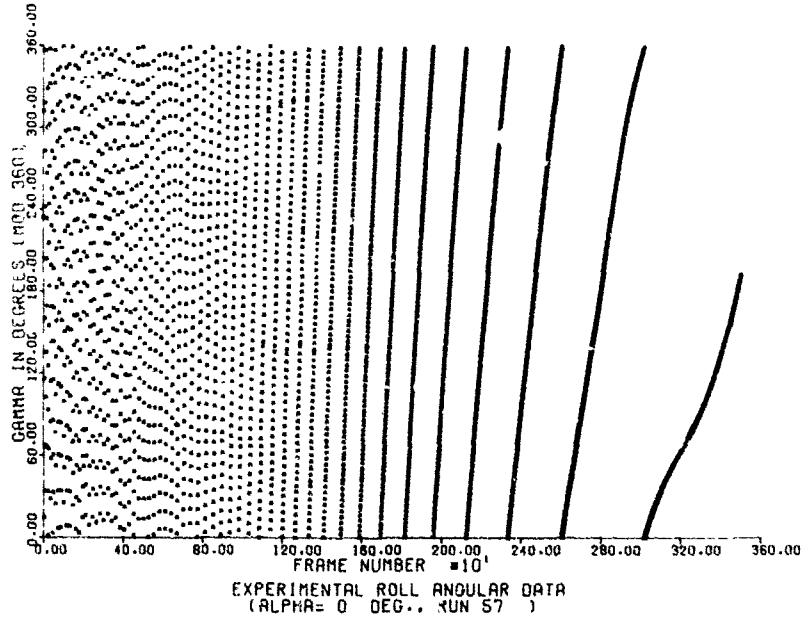

Figure A-2. Observed Roll Angle Versus Frame Number at a 0° Angle of Attack for Run 57

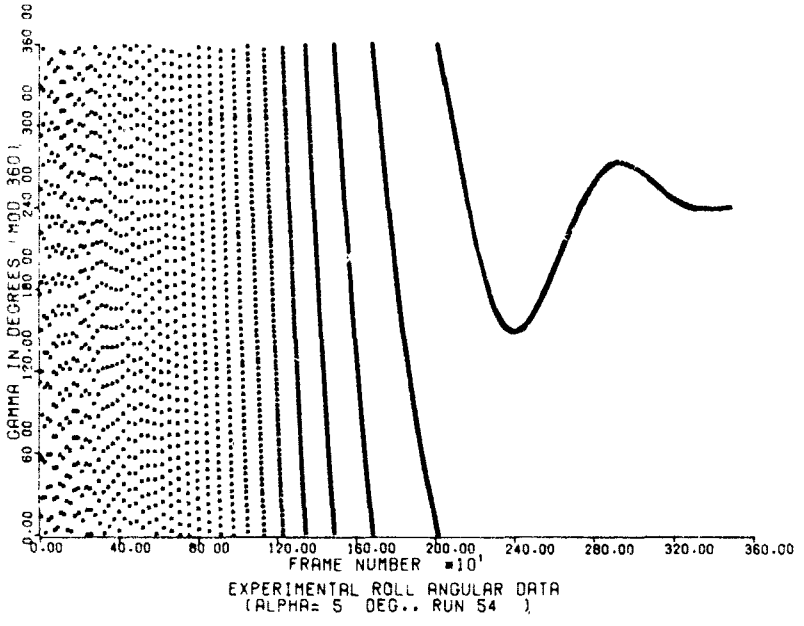

Figure A-3. Observed Roll Angle Versus Frame Number at a 5° Angle of Attack for Run 54

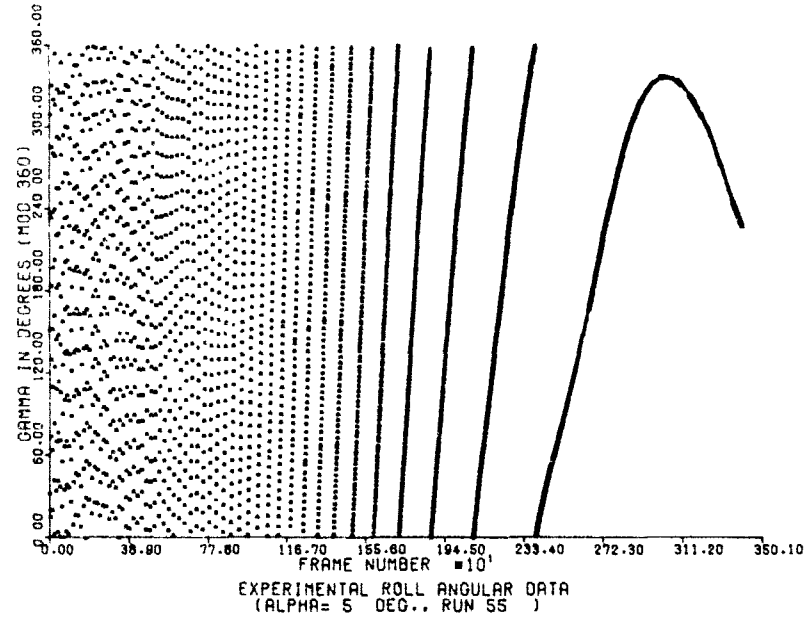

Figure A-4. Observed Roll Angle Versus Frame Number at a 5° Angle of Attack for Run 55

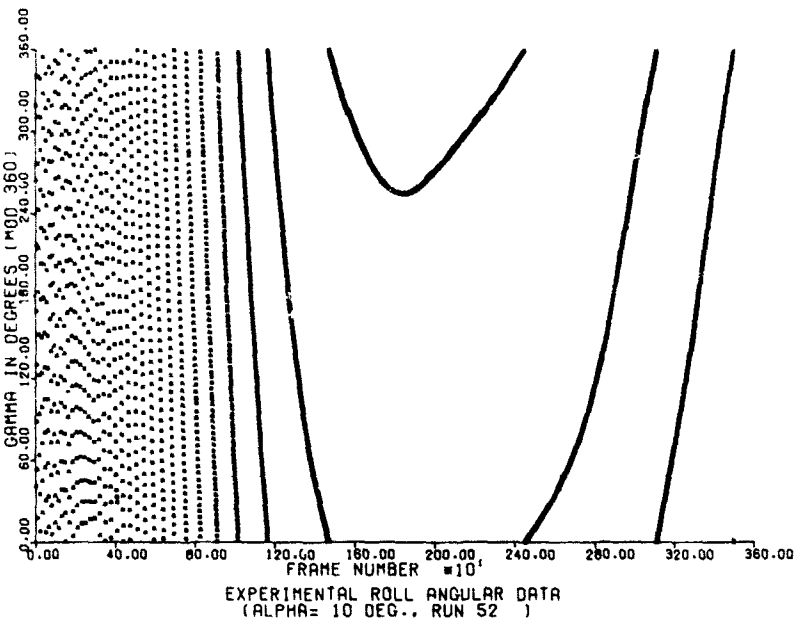

Figure A-5. Observed Roll Angle Versus Frame Number at a 10° Angle of Attack for Run 52

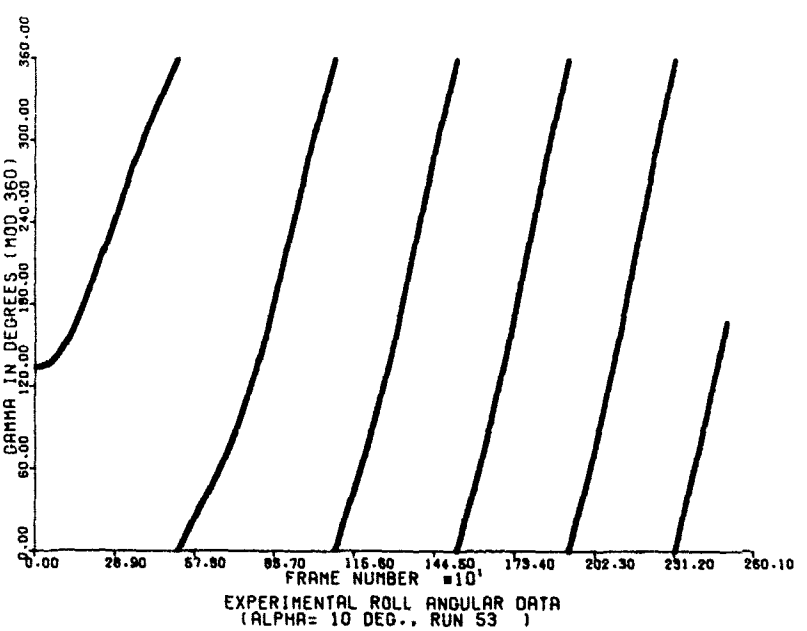

Figure A-6. Observed Roll Angle Versus Frame Number at a 10° Angle of Attack for Run 53

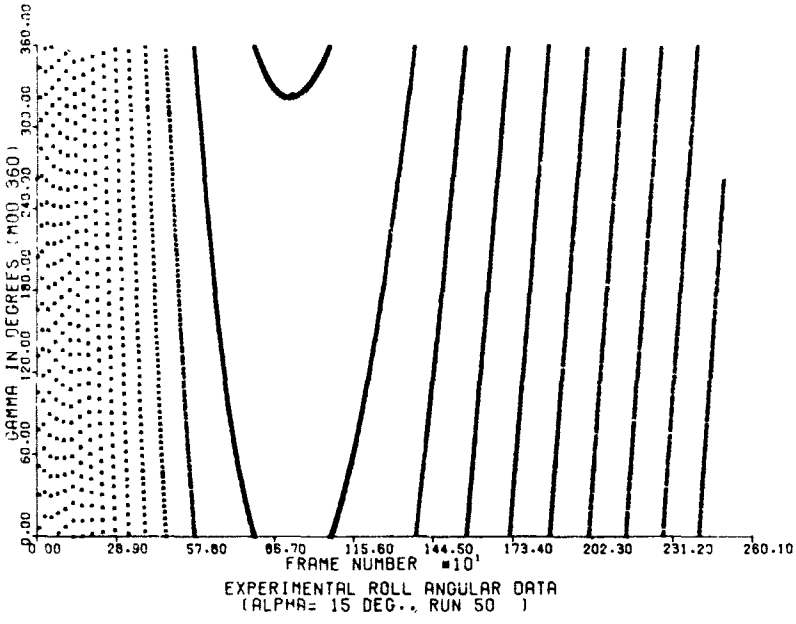

Figure A-7. Observed Roll Angle Versus Frame Number at a 15° Angle of Attack for Run 50

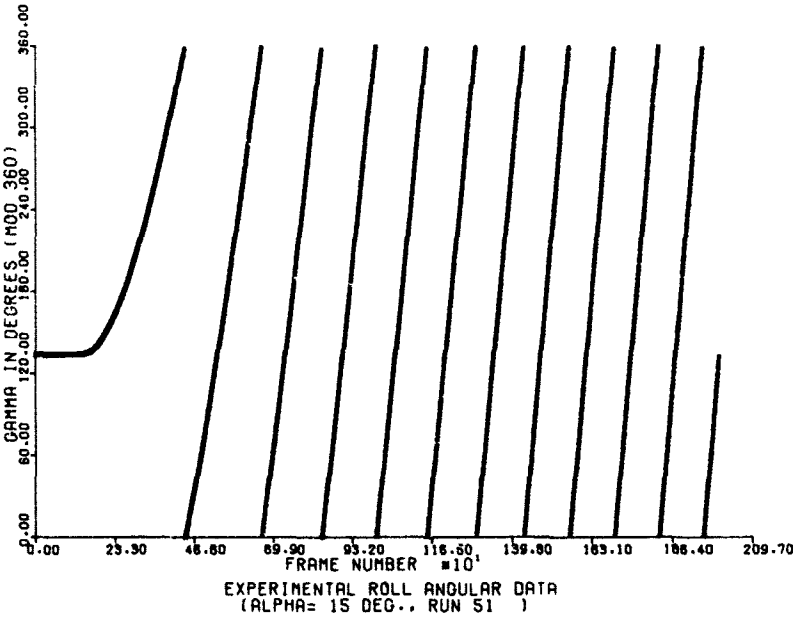

Figure A-8. Observed Roll Angle Versus Frame Number at a 15° Angle of Attack for Run 51

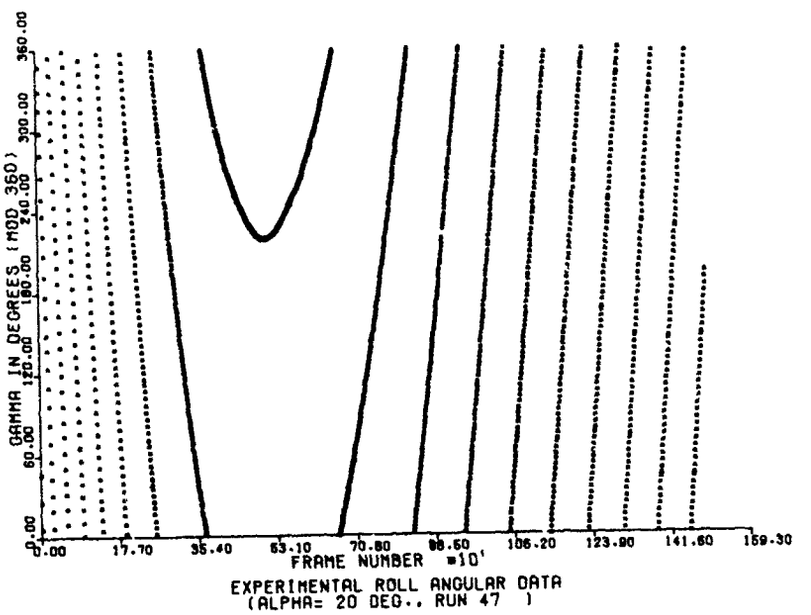

Figure A-9. Observed Roll Angle Versus Frame Number at a 20° Angle of Attack for Run 47

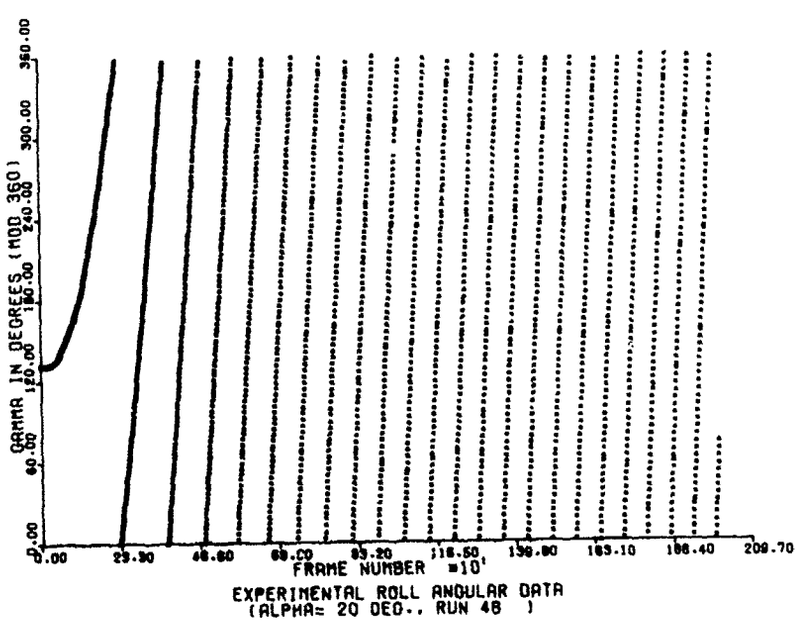

Figure A-10. Observed Roll Angle Versus Frame Number at a 20° Angle of Attack for Run 48

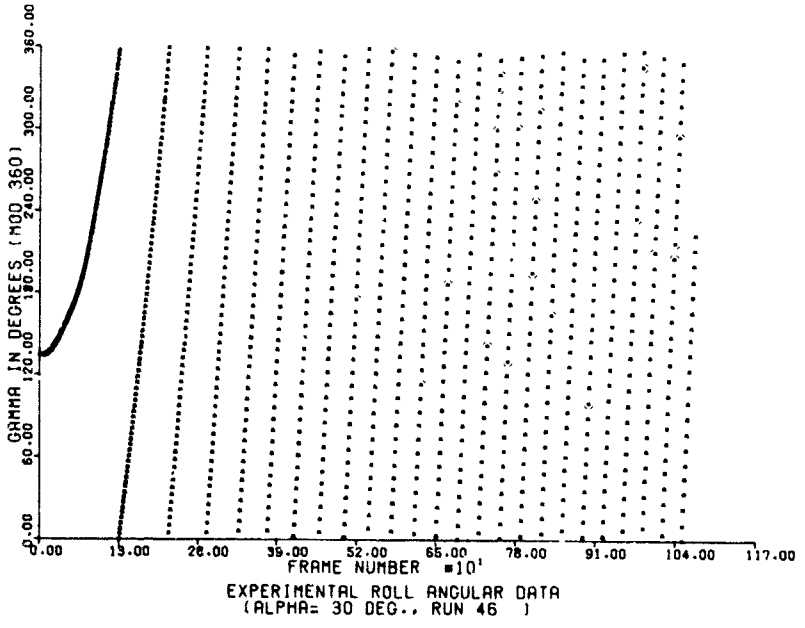

Figure A-11. Observed Roll Angle Versus Frame Number at a 30° Angle of Attack for Run 46

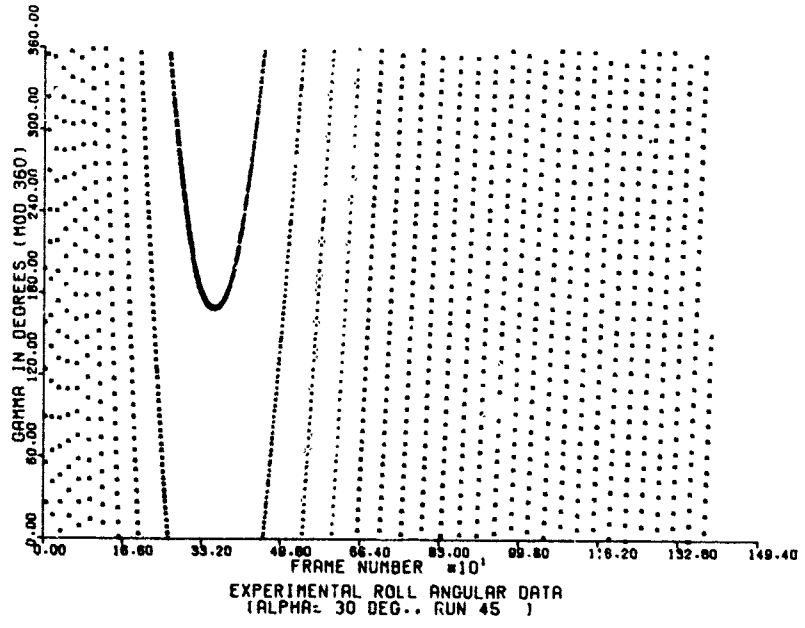

Figure A-12. Observed Roll Angle Versus Frame Number at a 30° Angle of Attack for Run 45

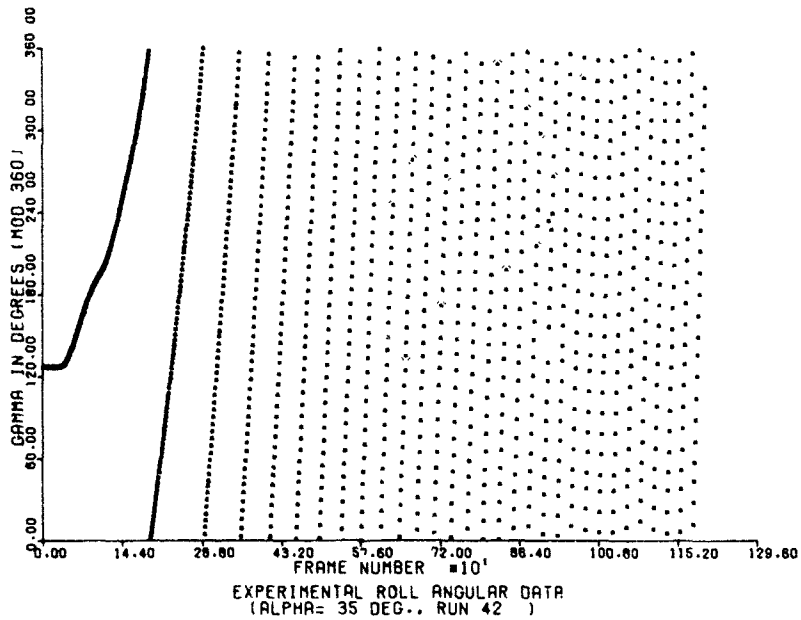

Figure A-13. Observed Roll Angle Versus Frame Number at a 35° Angle of Attack for Run 42

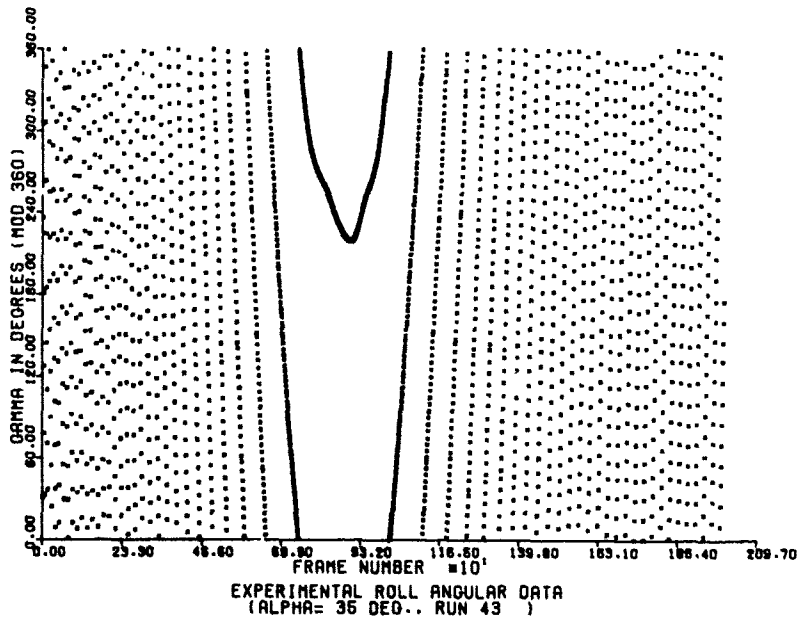

Figure A-14. Observed Roll Angle Versus Frame Number at a 35° Angle of Attack for Run 43

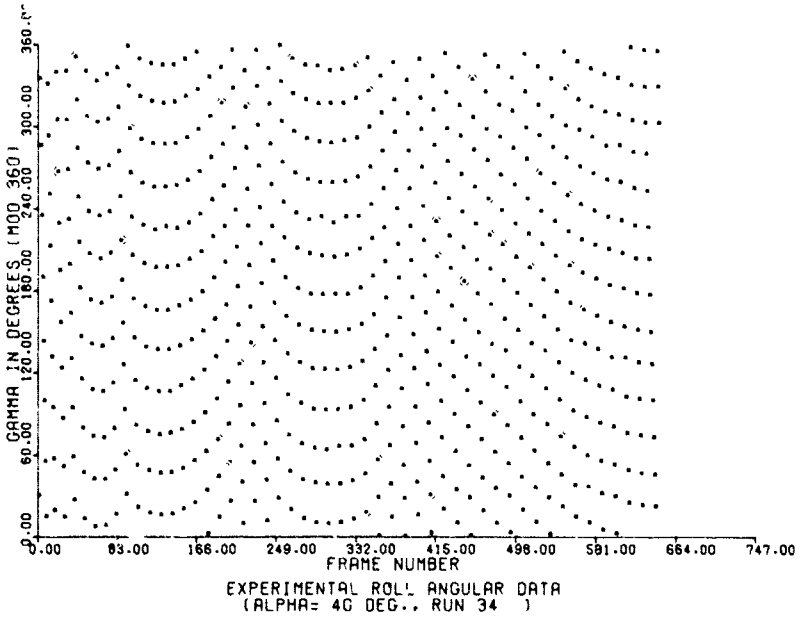

Figure A-15. Observed Roll Angle Versus Frame Number at a 40° Angle of Attack for Run 34

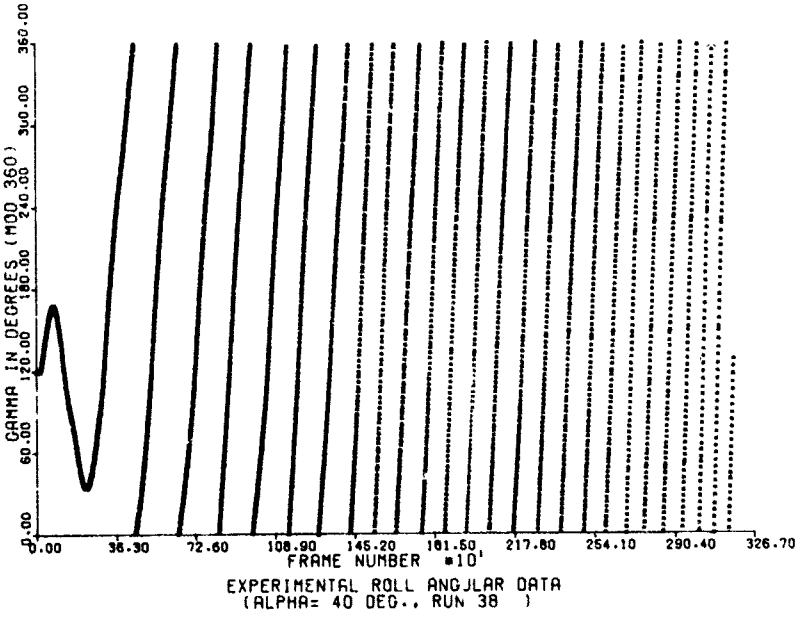

Figure A-16. Observed Roll Angle Versus Frame Number at a 40° Angle of Attack for Run 38

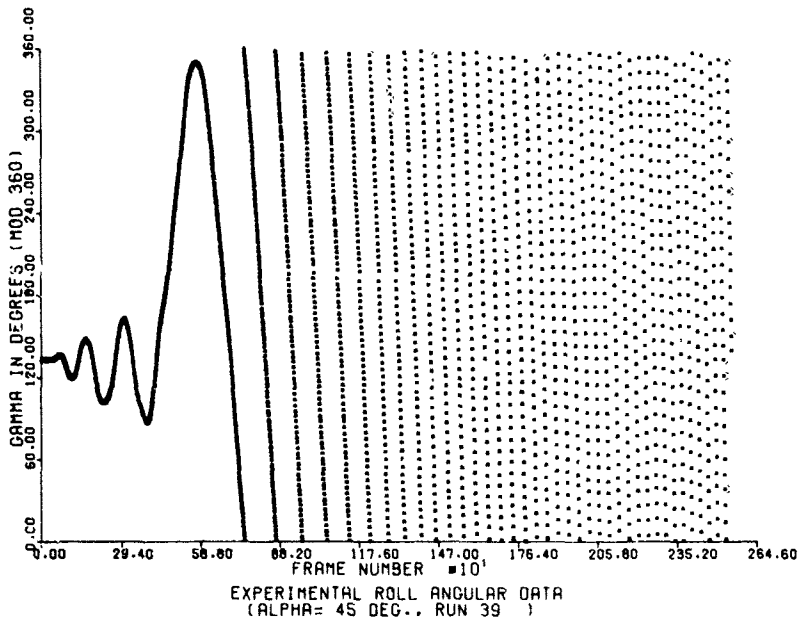

Figure A-17. Observed Roll Angle Versus Frame Number at a 45° Angle of Attack for Run 39

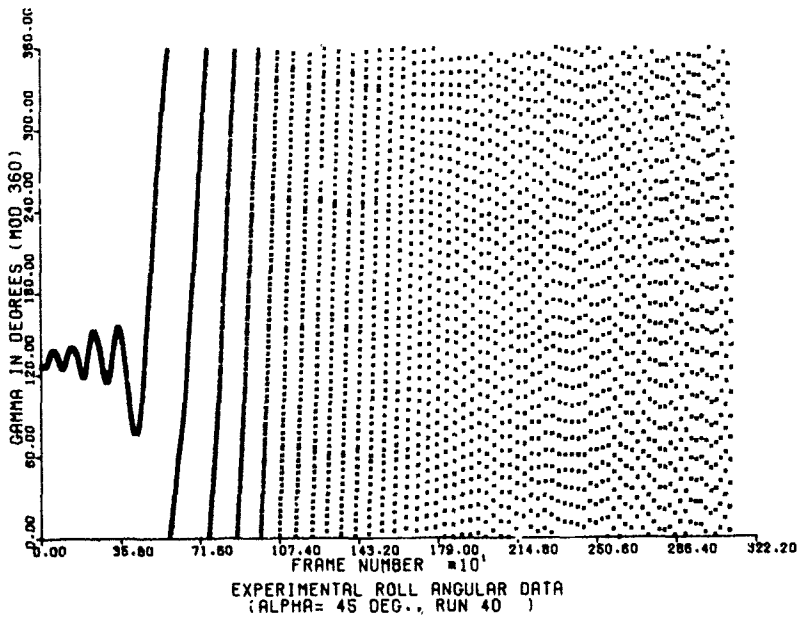

Figure A-18. Observed Roll Angle Versus Frame Number at a 45° Angle of Attack for Run 40

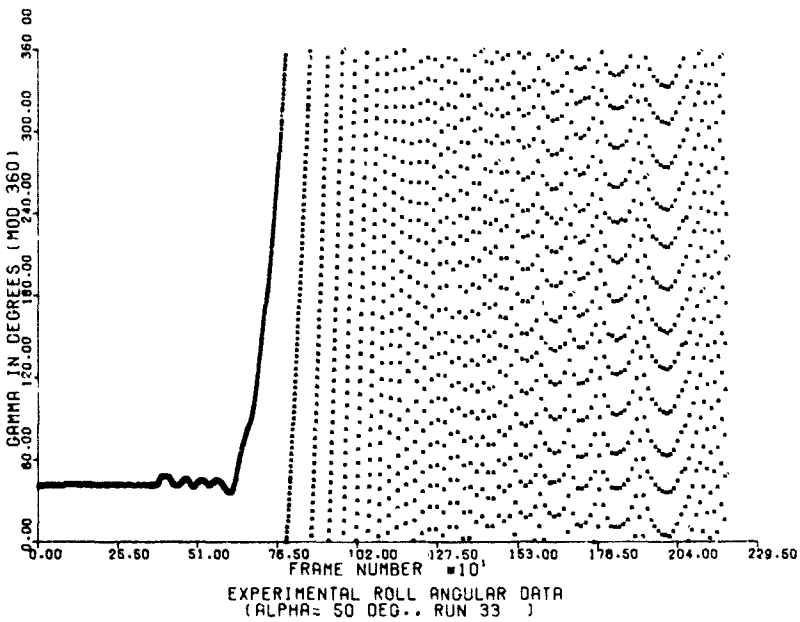

Figure A-19. Observed Roll Angle Versus Frame Number at a 50° Angle of Attack for Run 33

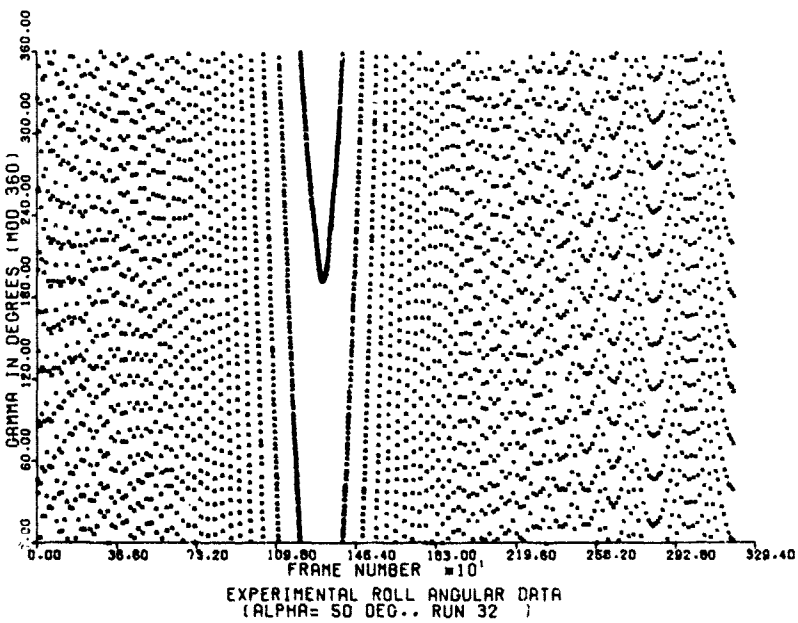

Figure A-20. Observed Roll Angle Versus Frame Number at a 50° Angle of Attack for Run 32

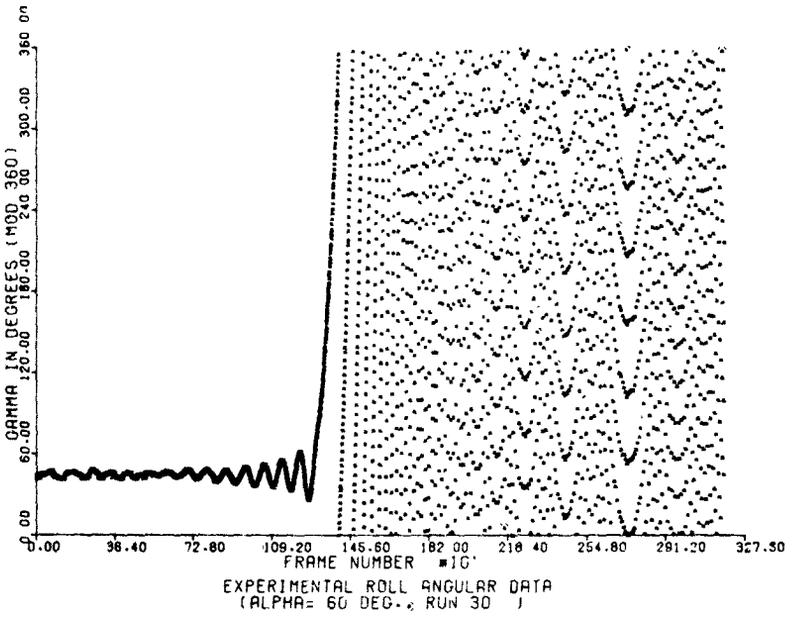

Figure A-21. Observed Roll Angle Versus Frame Number at a 60° Angle of Attack for Run 30

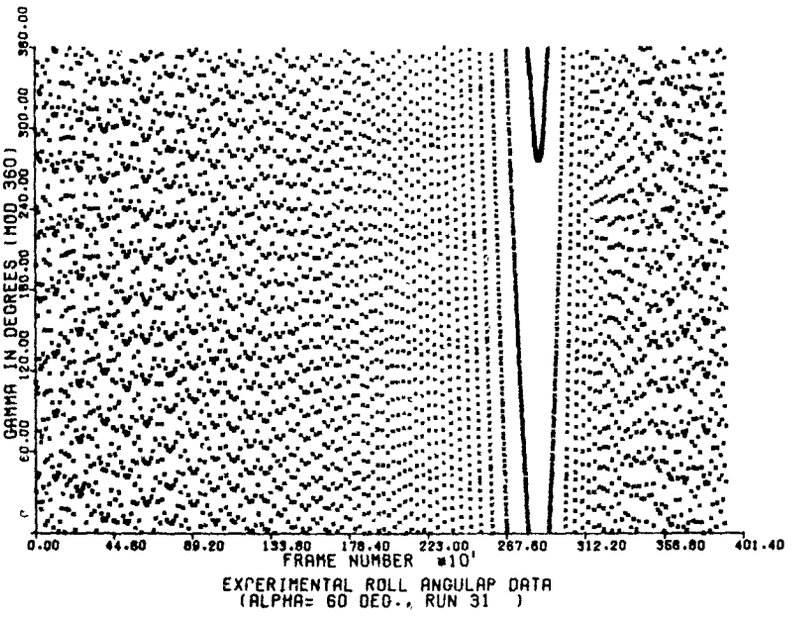

Figure A-22. Observed Roll Angle Versus Frame Number at a 60° Angle of Attack for Run 31

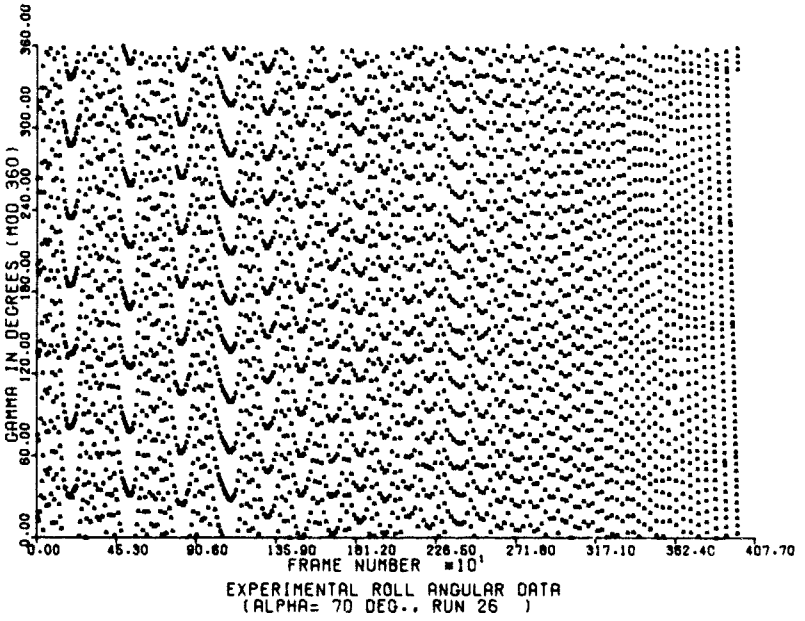

Figure A-23. Observed Roll Angle Versus Frame Number at a 70° Angle of Attack for Run 26

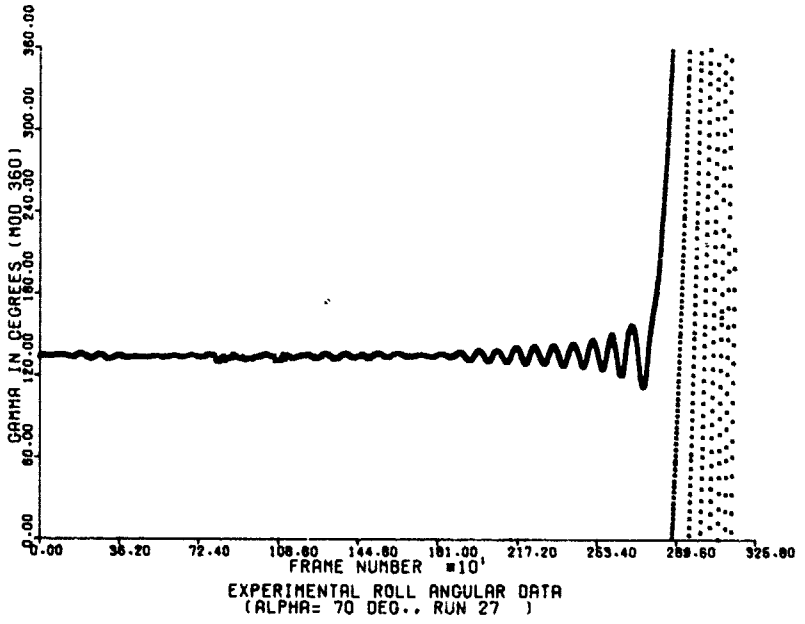

Figure A-24. Observed Roll Angle Versus Frame Number at a 70° Angle of Attack for Run 27

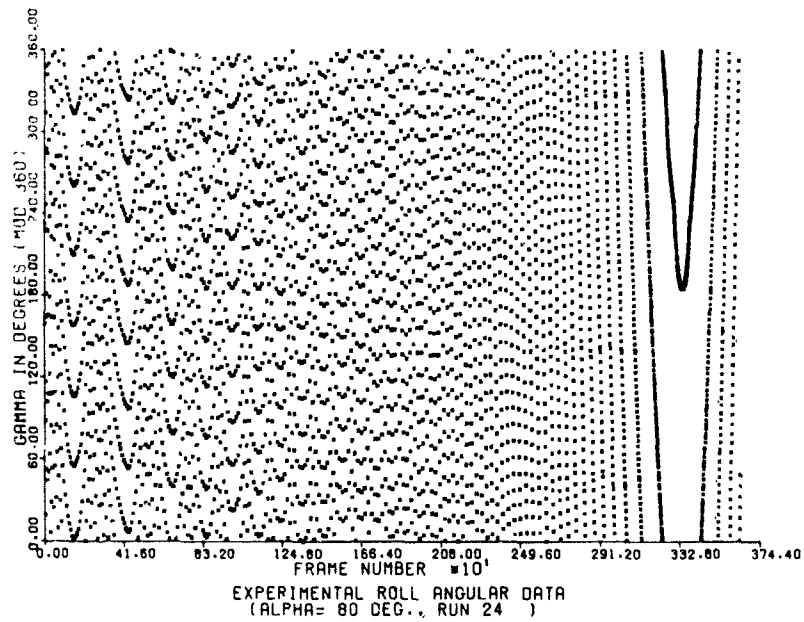

Figure A-25. Observed Roll Angle Versus Frame Number at an 80° Angle of Attack for Run 24

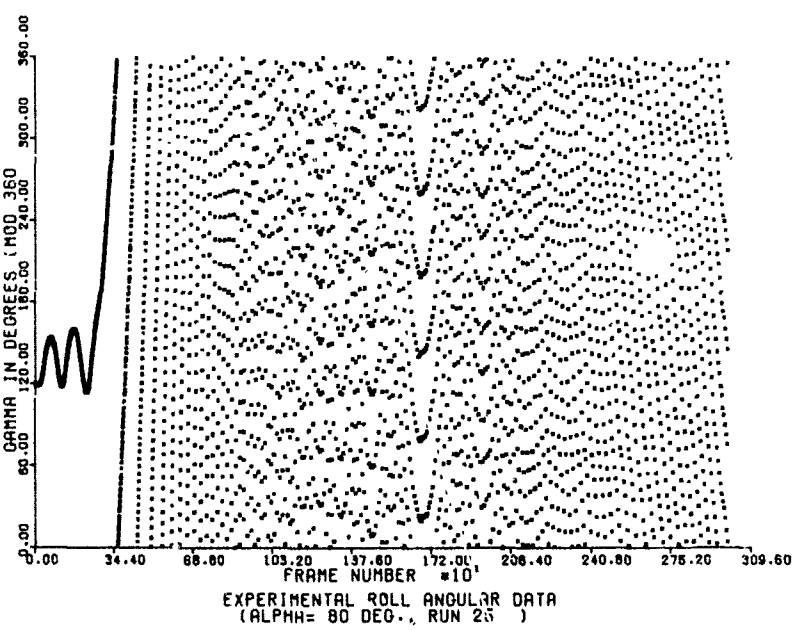

Figure A-26. Observed Roll Angle Versus Frame Number at an 80° Angle of Attack for Run 25

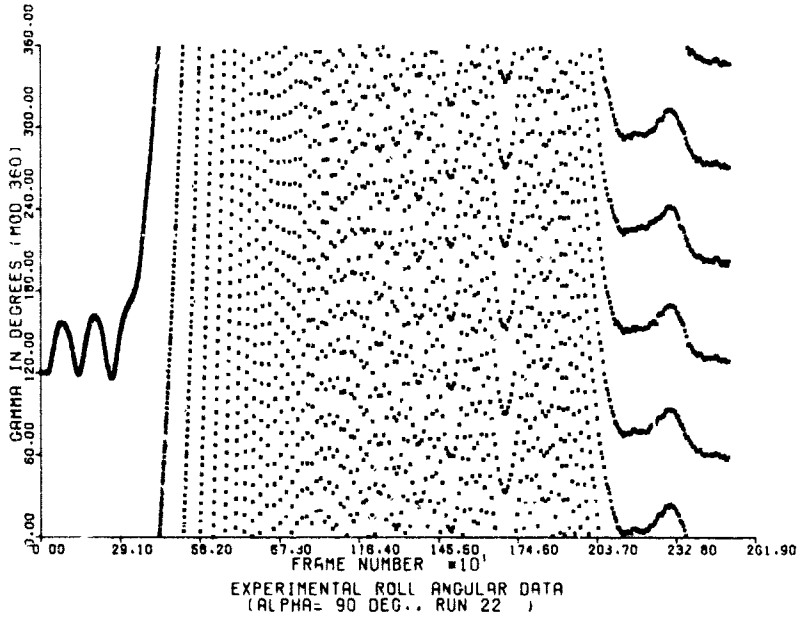

Figure A-27. Observed Roll Angle Versus Frame Number at a 90° Angle of Attack for Run 22

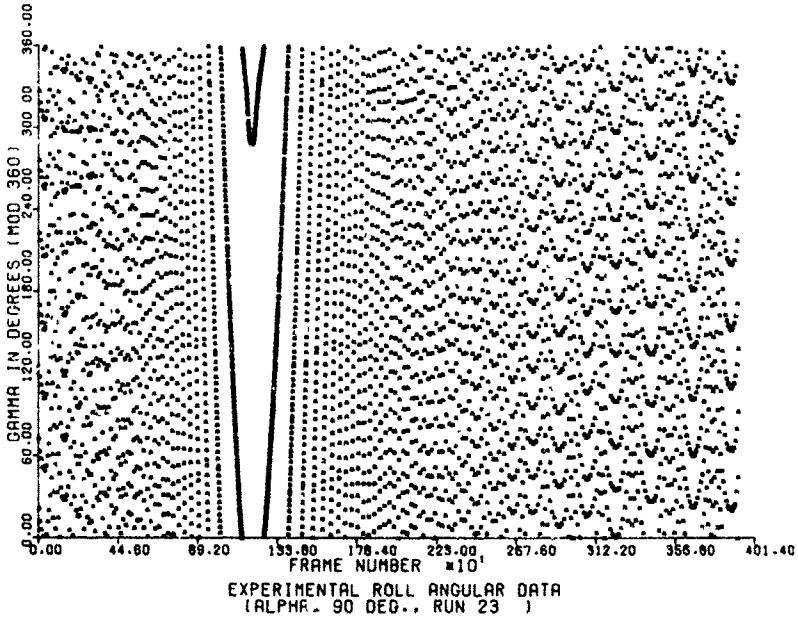

Figure A-28. Observed Roll Angle Versus Frame Number at a 90° Angle of Attack for Run 23

APPENDIX B

COMPARISON OF OBSERVED AND COMPUTED ROLL DATA

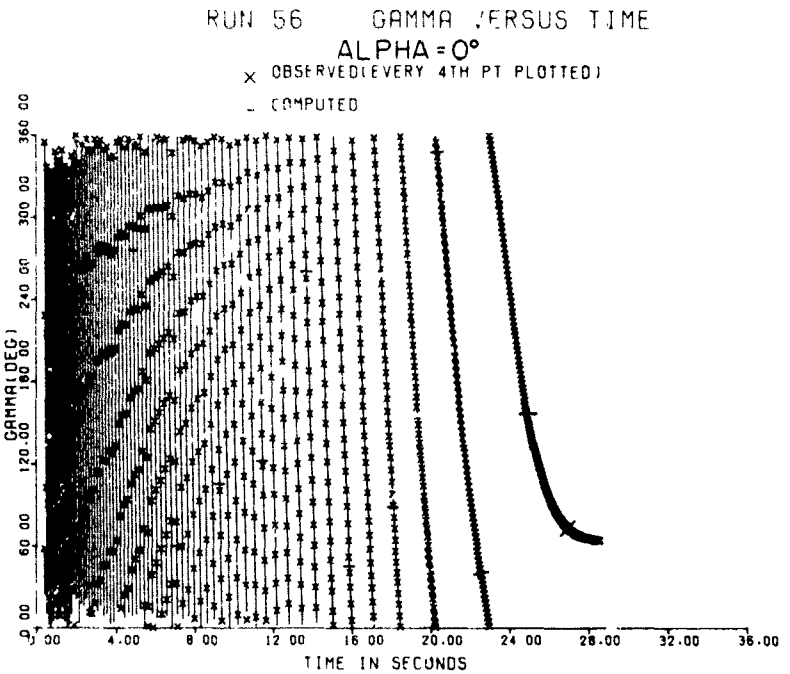

Figure B-1. Comparison of Observed and Computed Roll Angles at a 0° Angle of Attack for Run 56

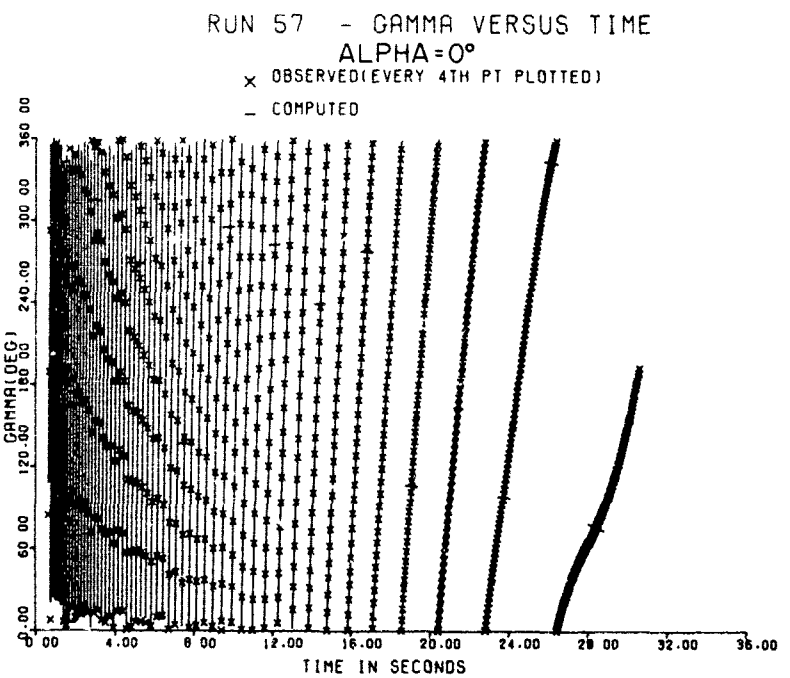

Figure B-2. Comparison of Observed and Computed Roll Angles at a 0° Angle of Attack for Run 57

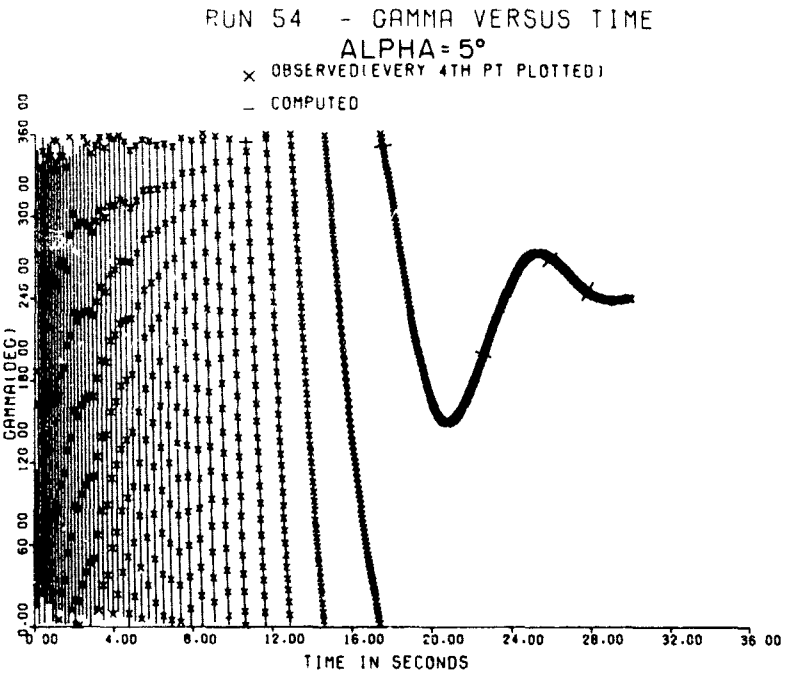

Figure B-3. Comparison of Observed and Computed Roll Angles at a 5° Angle of Attack for Run 54

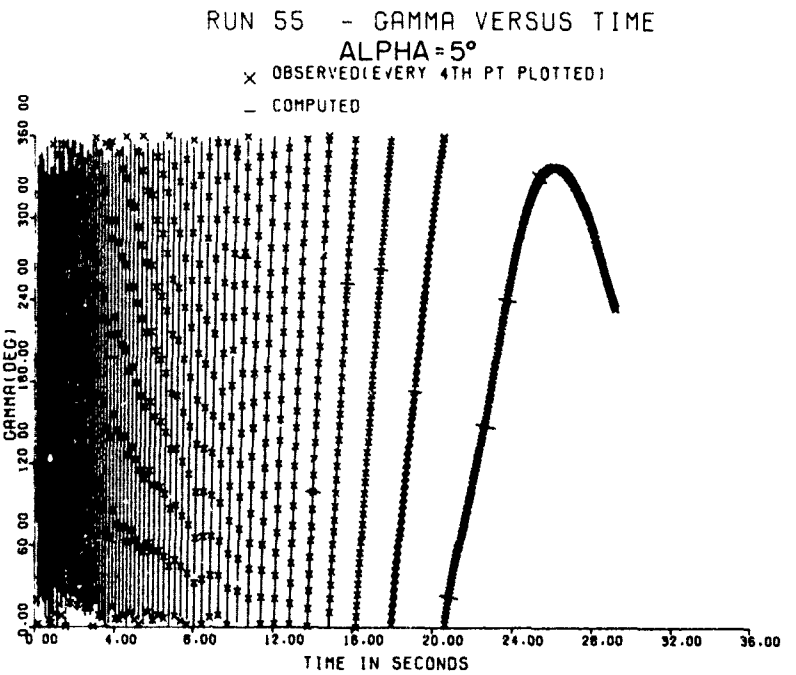

Figure B-4. Comparison of Observed and Computed Roll Angles at a 5° Angle of Attack for Run 55

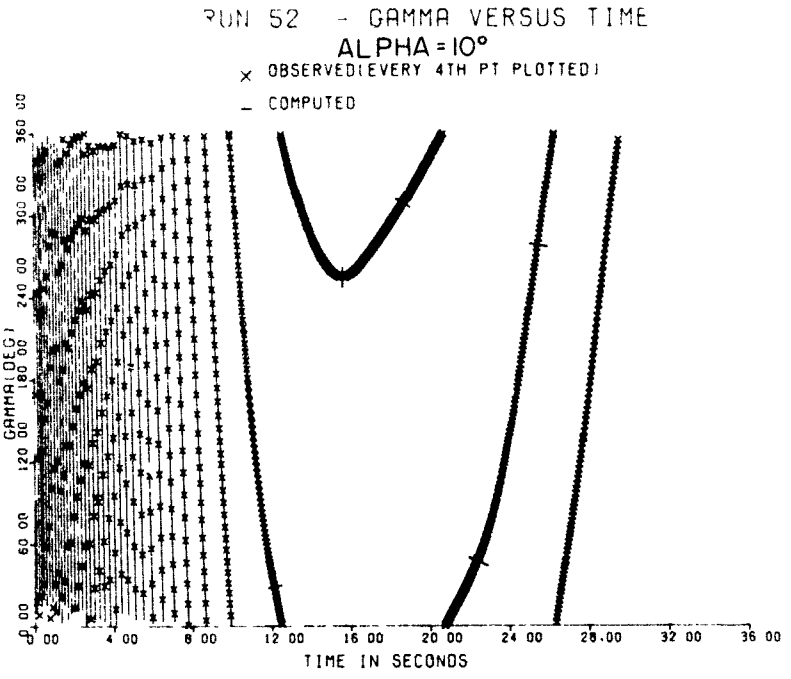

Figure B-5. Comparison of Observed and Computed Roll Angles at a 10° Angle of Attack for Run 52

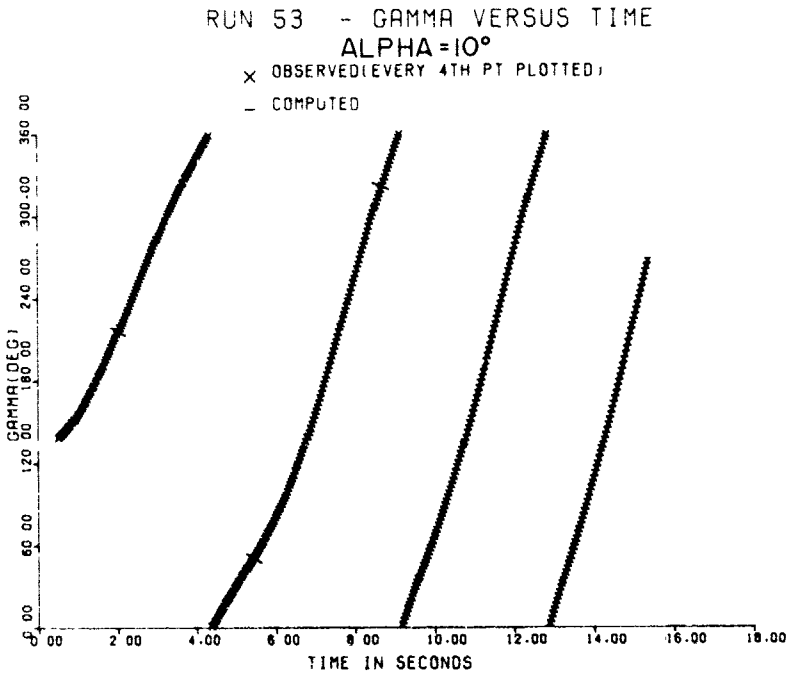

Figure B-6. Comparison of Observed and Computed Roll Angles at a 10° Angle of Attack for Run 53

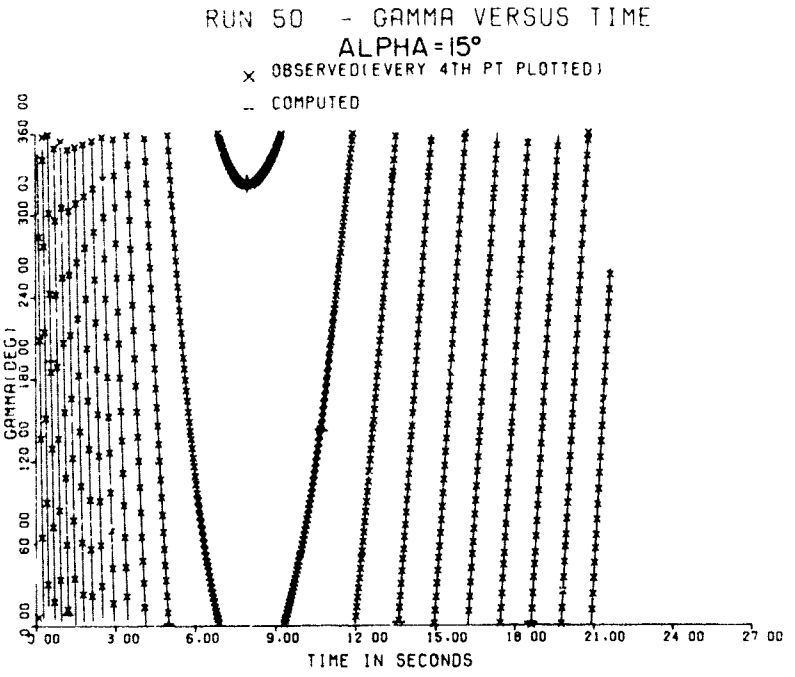

Figure B-7. Comparison of Observed and Computed Roll Angles at a 15° Angle of Attack for Run 50

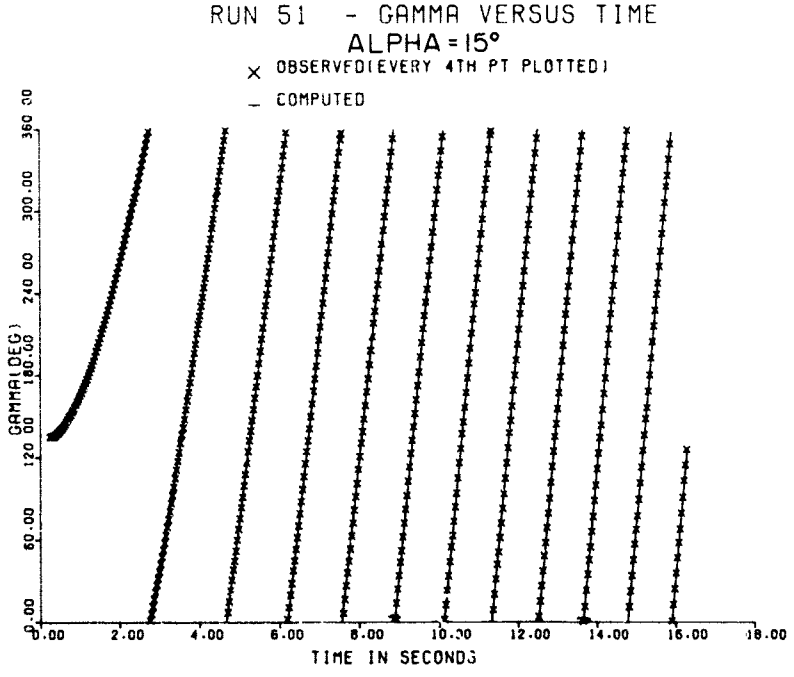

Figure B-8. Comparison of Observed and Computed Roll Angles at a 15° Angle of Attack for Run 51

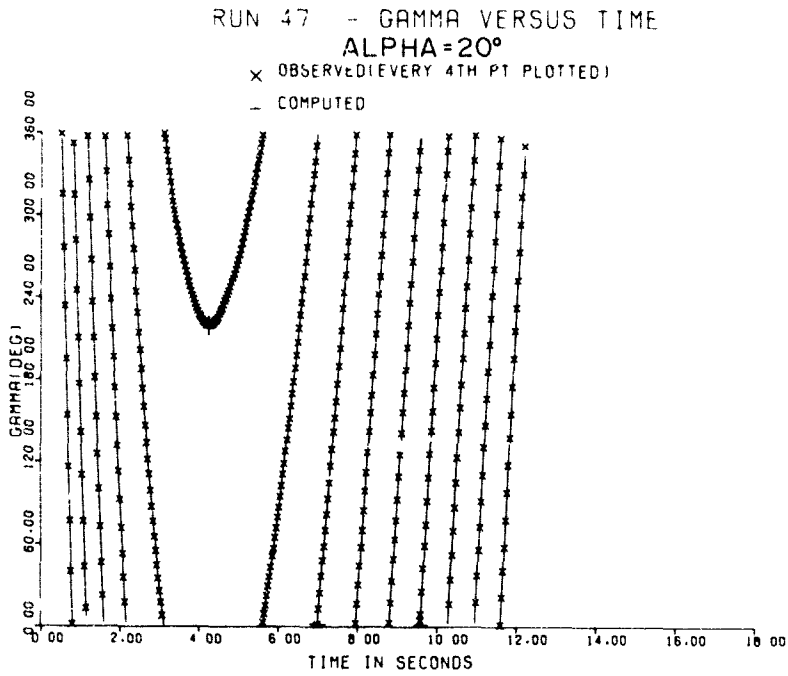

Figure B-9. Comparison of Observed and Computed Roll Angles at a 20° Angle of Attack for Run 47

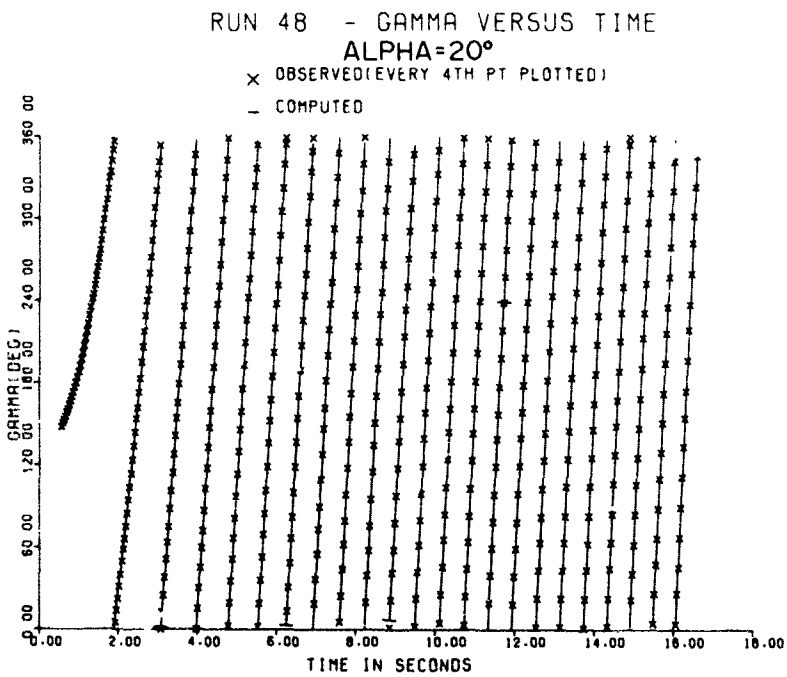

Figure B-10. Comparison of Observed and Computed Roll Angles at a 20° Angle of Attack for Run 48

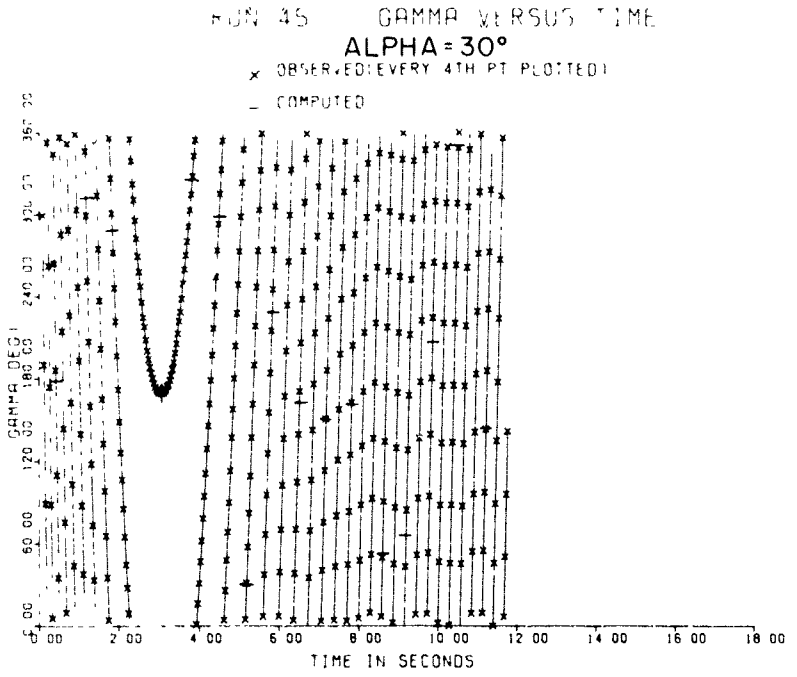

Figure B-11. Comparison of Observed and Computed Roll Angles at a 30° Argle of Attack for Run 45

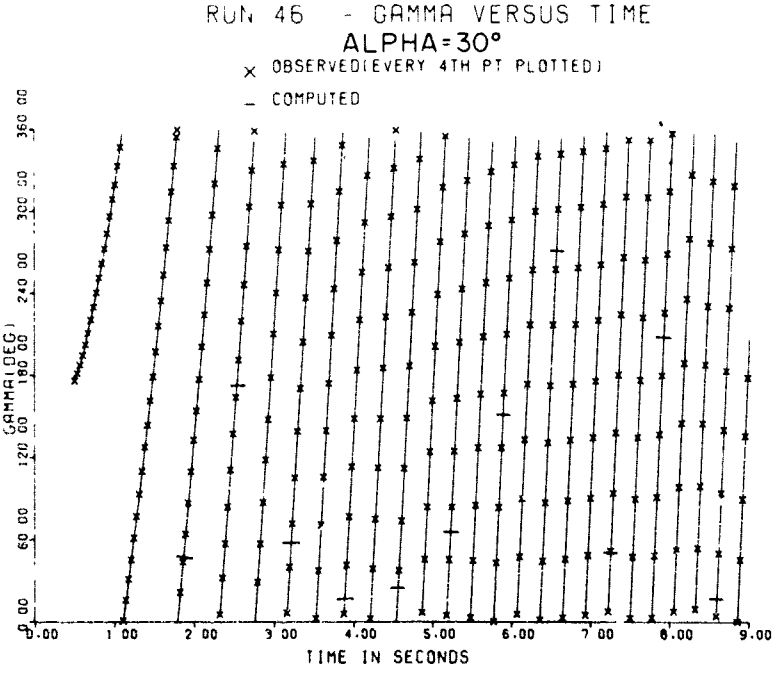

Figure B-12. Comparison of Observed and Computed Roll Angles at a 30° Angle of Attack for Run 46

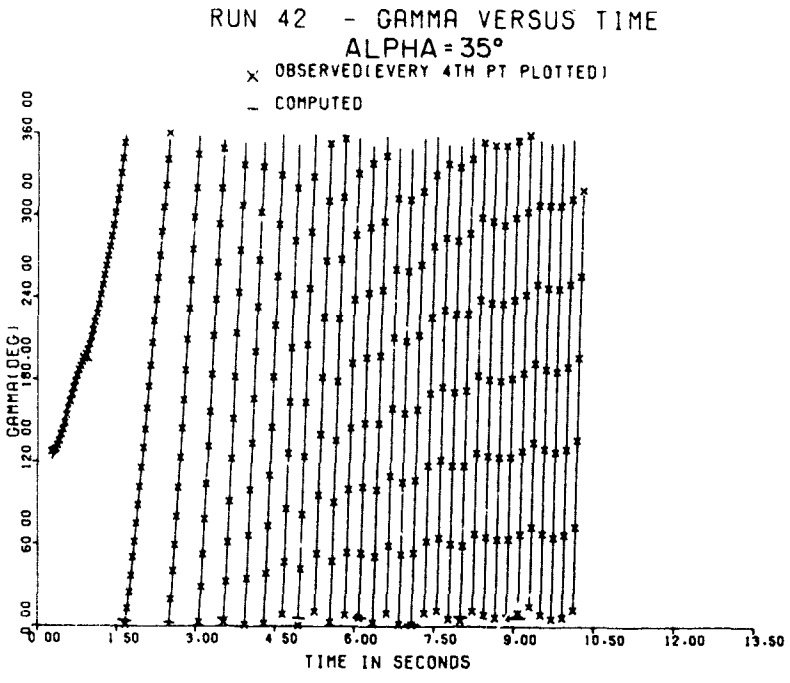

Figure B-13. Comparison of Observed and Computed Roll Angles at a 35° Angle of Attack for Run 42

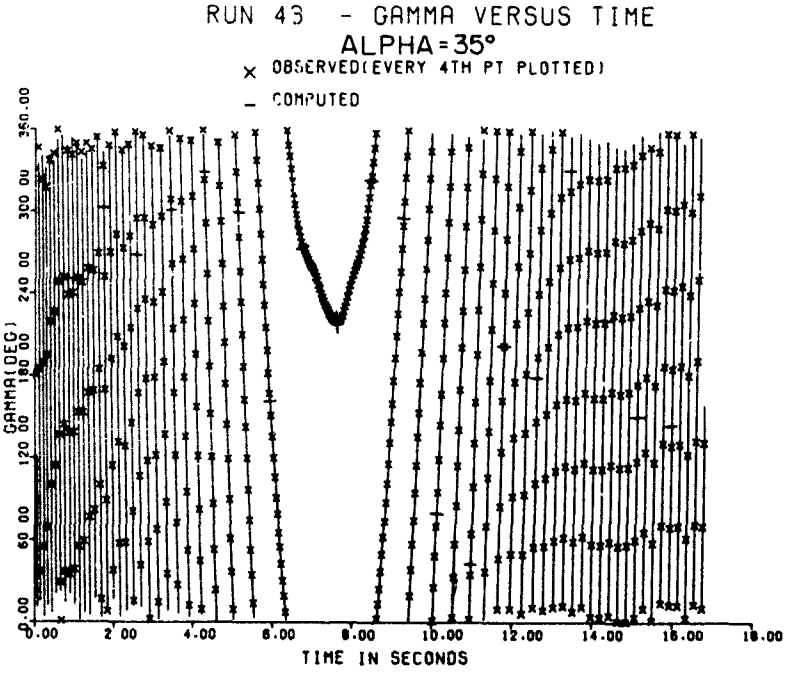

Figure B-14. Comparison of Observed and Computed Roll Angles at a 35° Angle of Attack for Run 43

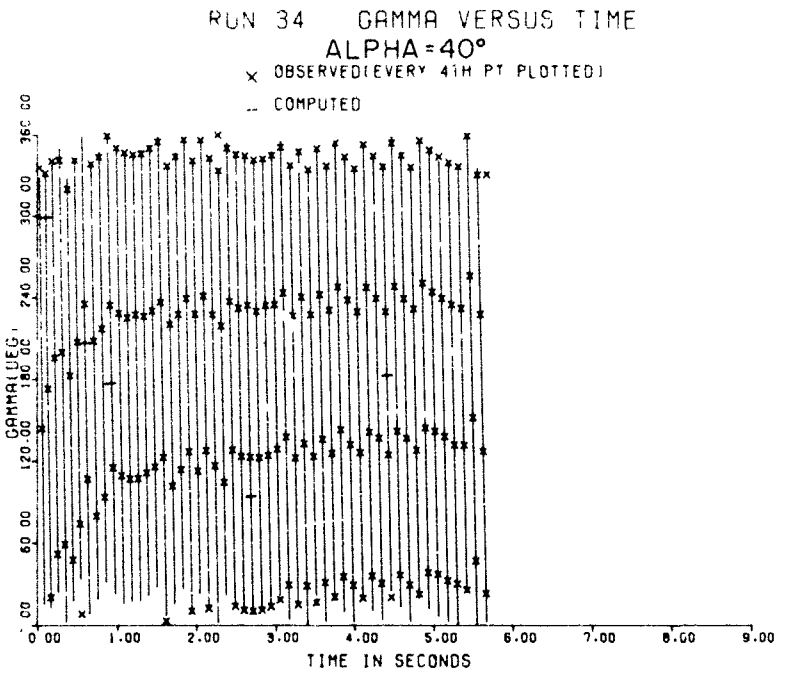

Figure B-15. Comparison of Observed and Computed Roll Angles at a 40° Angle of Attack for Run 34

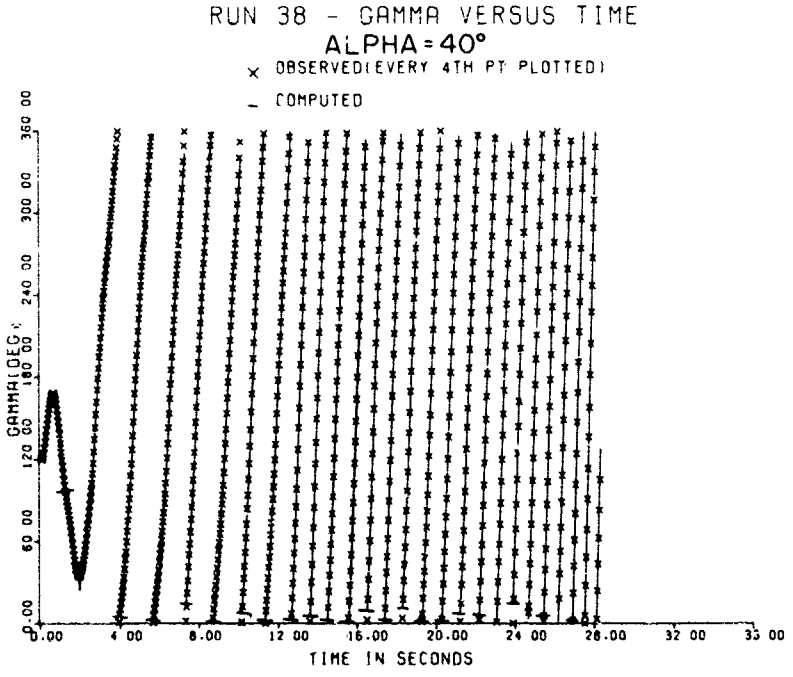

Figure B-16. Comparison of Observed and Computed Roll Angles at a 40° Angle of Attack for Run 38

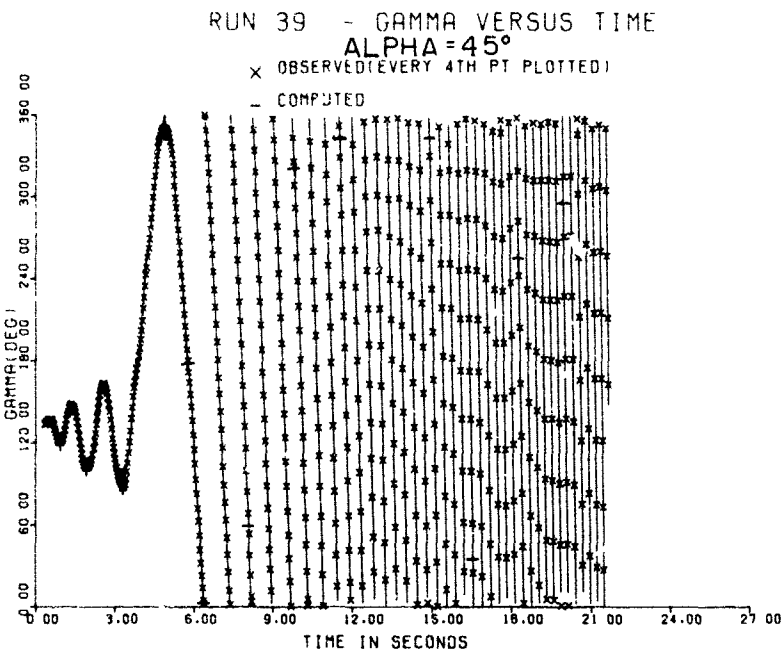

Figure B-17. Comparison of Observed and Computed Roll Angles at a 45° Angle of Attack for Run 39

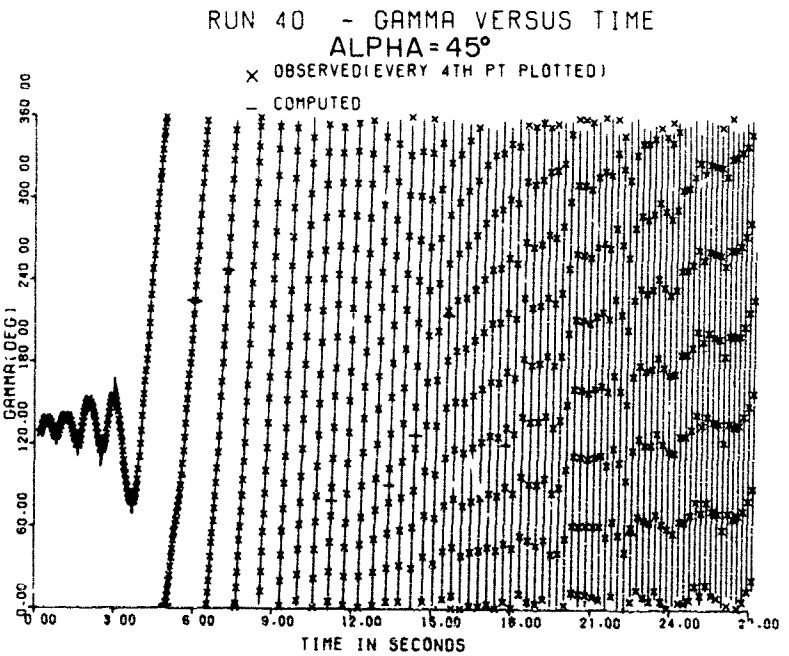

Figure B-18. Comparison of Observed and Computed Roll Angles at a 45° Angle of Attack for Run 40

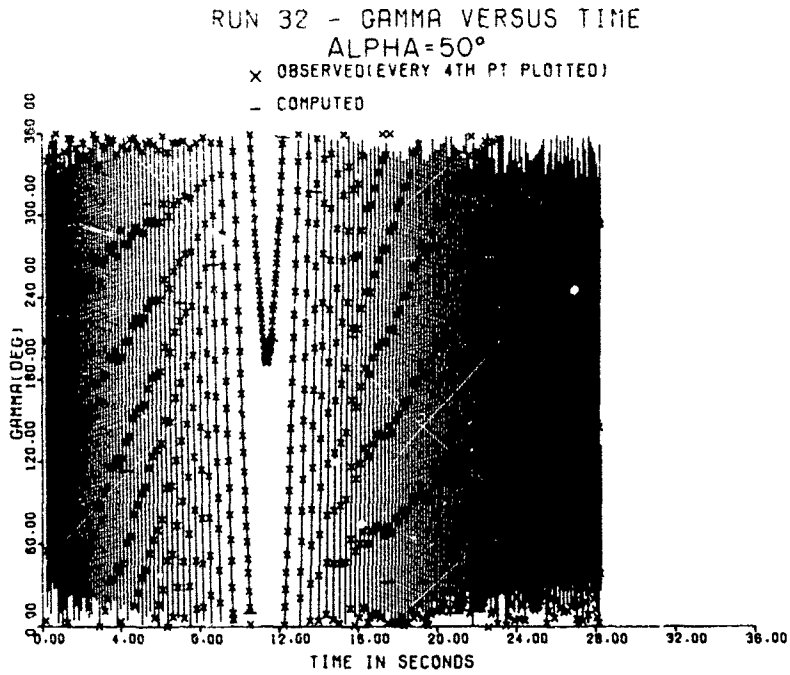

Figure B-19. Comparison of Observed and Computed Roll Angles at a 50° Angle of Attack for Run 32

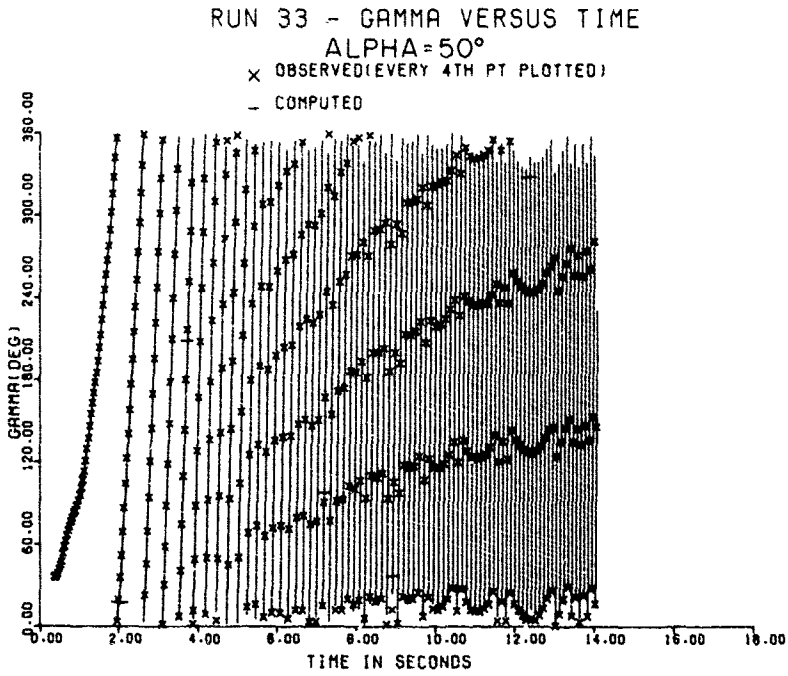

Figure B-20. Comparison of Observed and Computed Roll Angles at a 50° Angle of Attack for Run 33

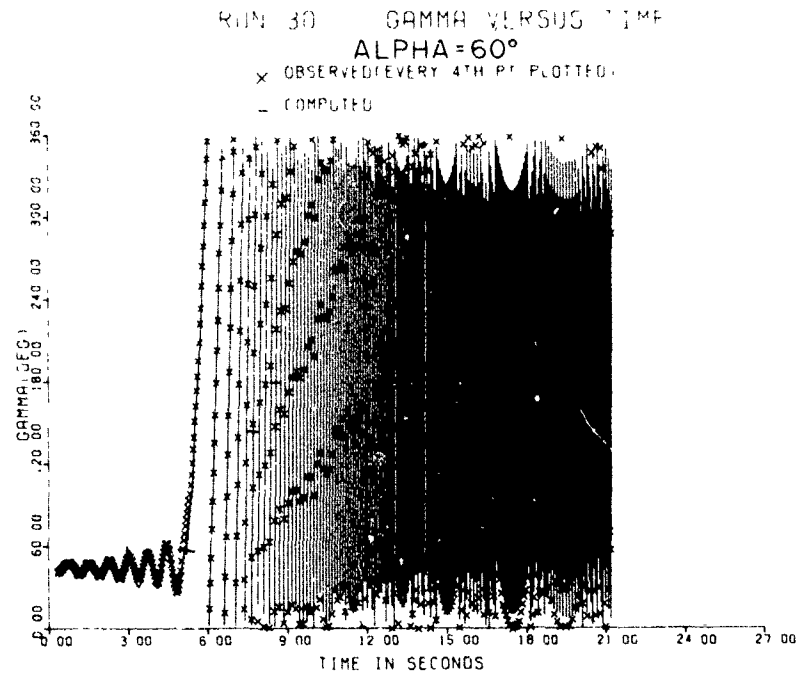

Figure B-21. Comparison of Observed and Computed Roll Angles at a 60° Angle of Attack for Run 30

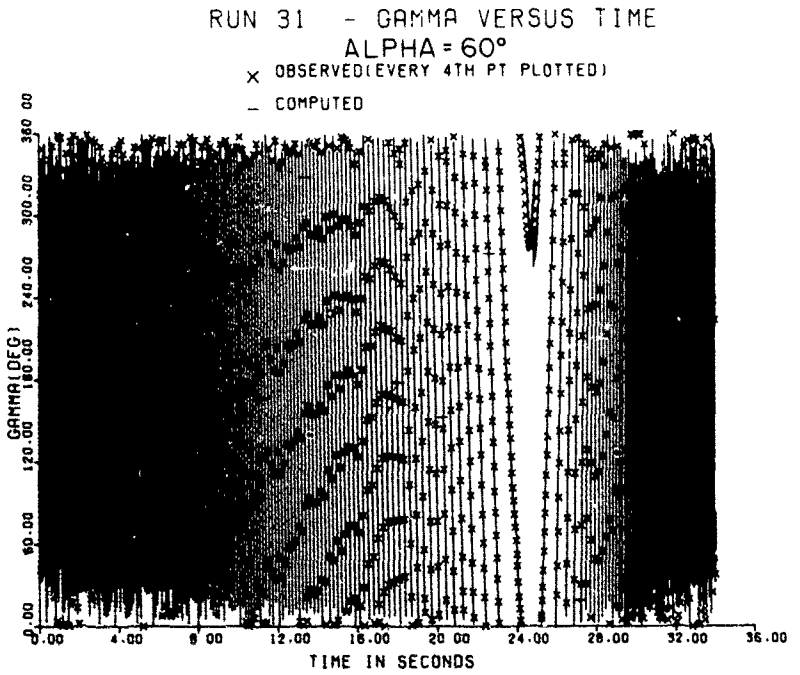

Figure B-22. Comparison of Observed and Computed Roll Angles at a 60° Angle of Attack for Run 31

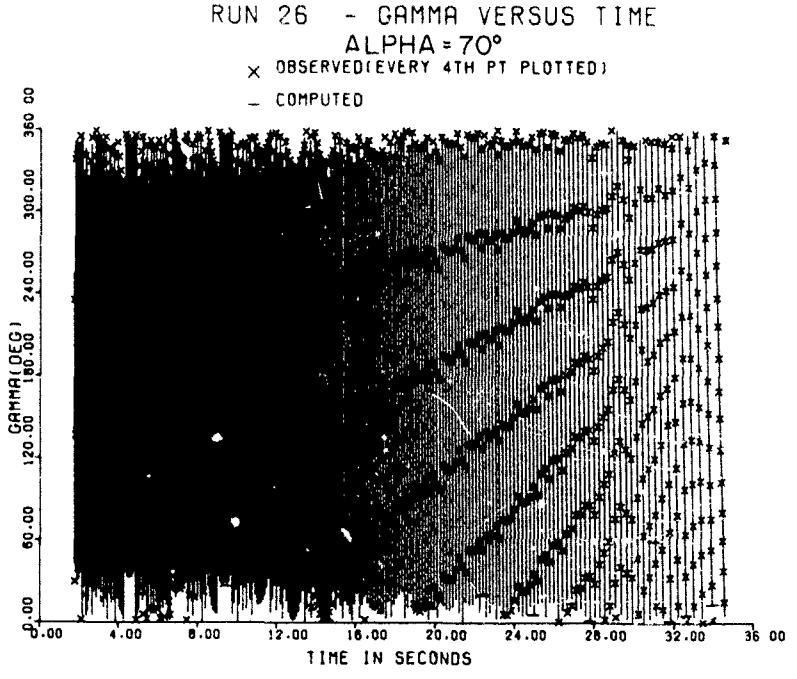

Figure B-23. Comparison of Observed and Computed Roll Angles at a 70° Angle of Attack for Run 26

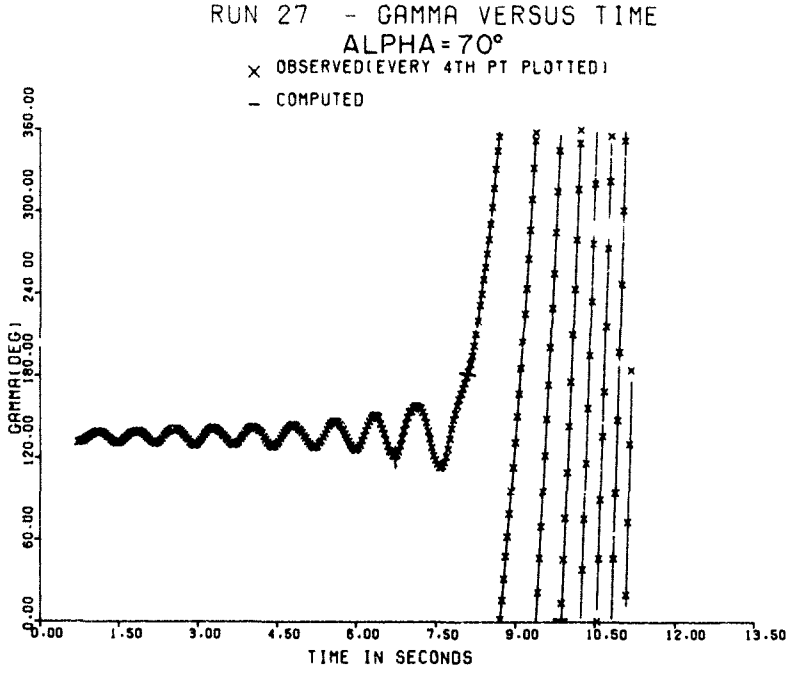

Figure B-24. Comparison of Observed and Computed Roll Angles at a 70° Angle of Attack for Run 27

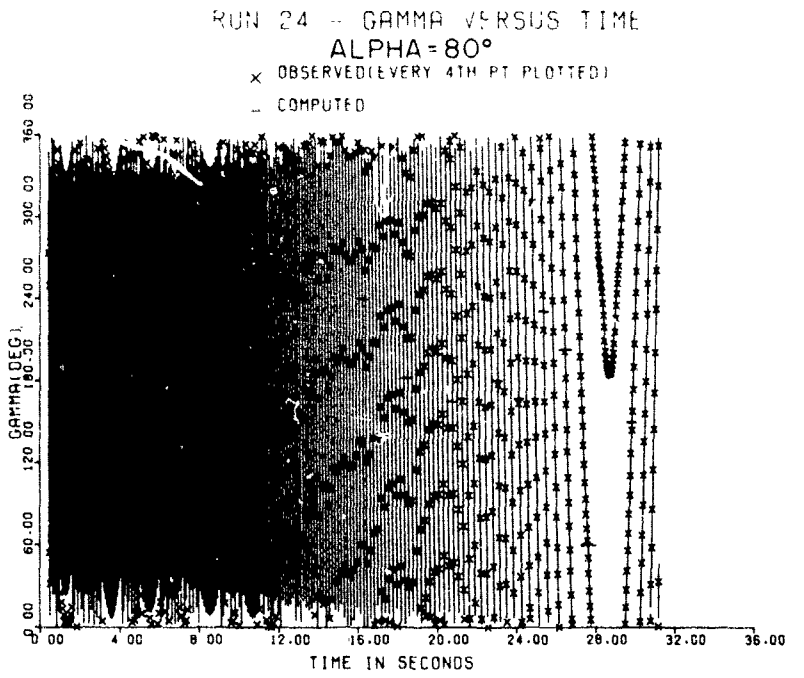

Figure B-25. Comparison of Observed and Computed Roll Angles at an 80° Angle of Attack for Run 24

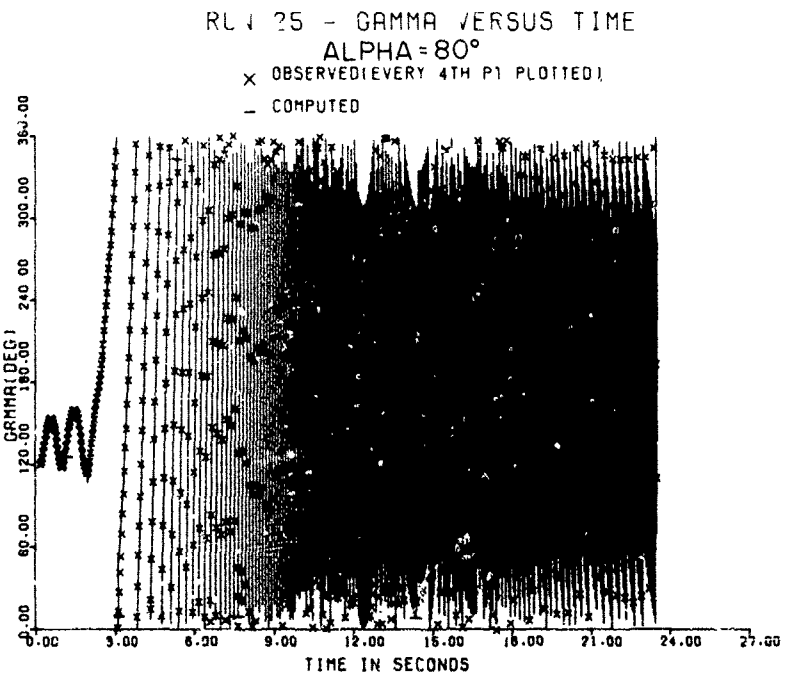

Figure B-26. Comparison of Observed and Computed Roll Angles at an 80° Angle of Attack for Run 25

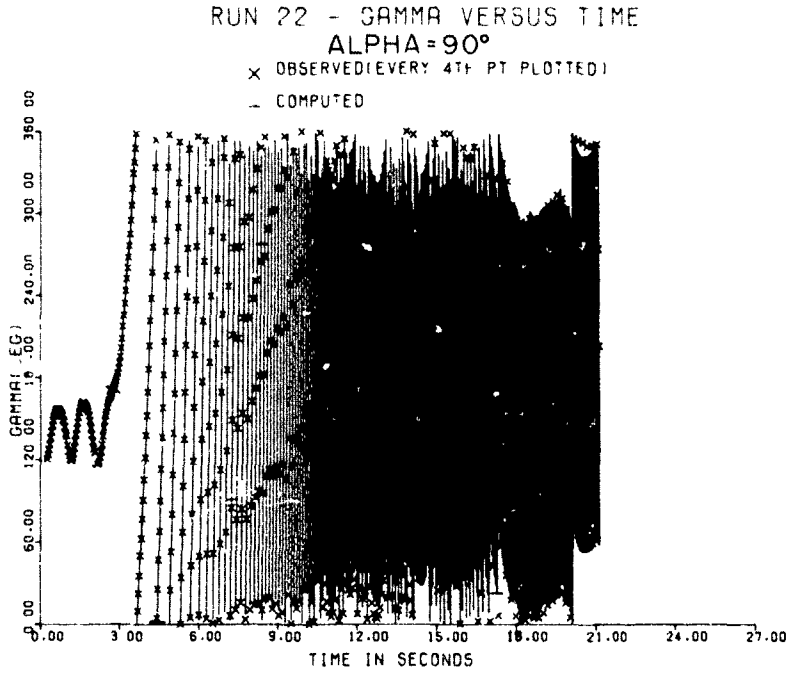

Figure B-27. Comparison of Observed and Computed Roll Angles at a 90° Angle of Attack for Run 22

APPENDIX C

AVERAGE ROLL MOMENT COEFFICIENT VERSUS SPIN RATE

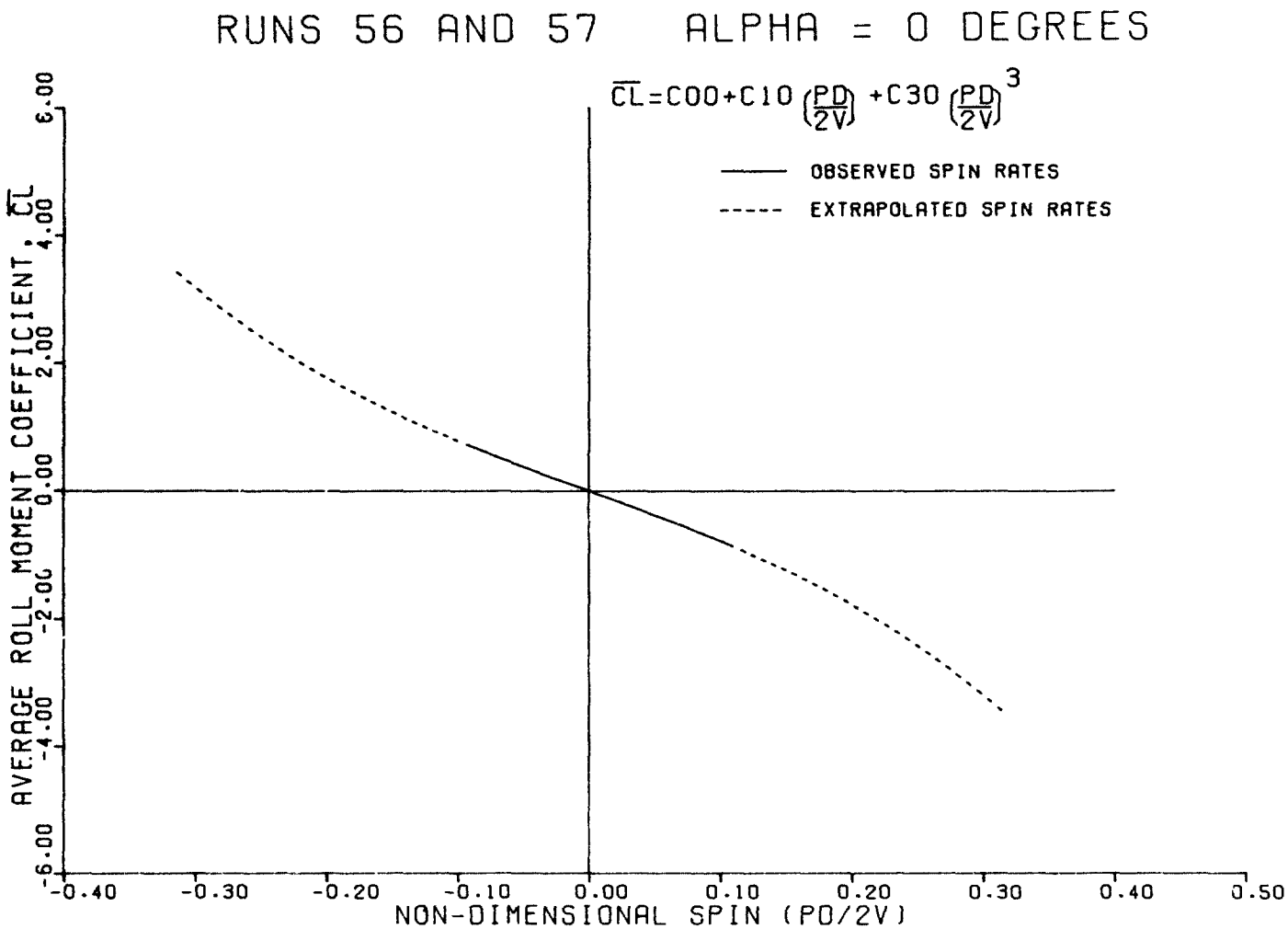

Figure C-1. Average Roll Moment Coefficient Versus Spin Rate at a 0° Angle of Attack for Runs 56 and 57

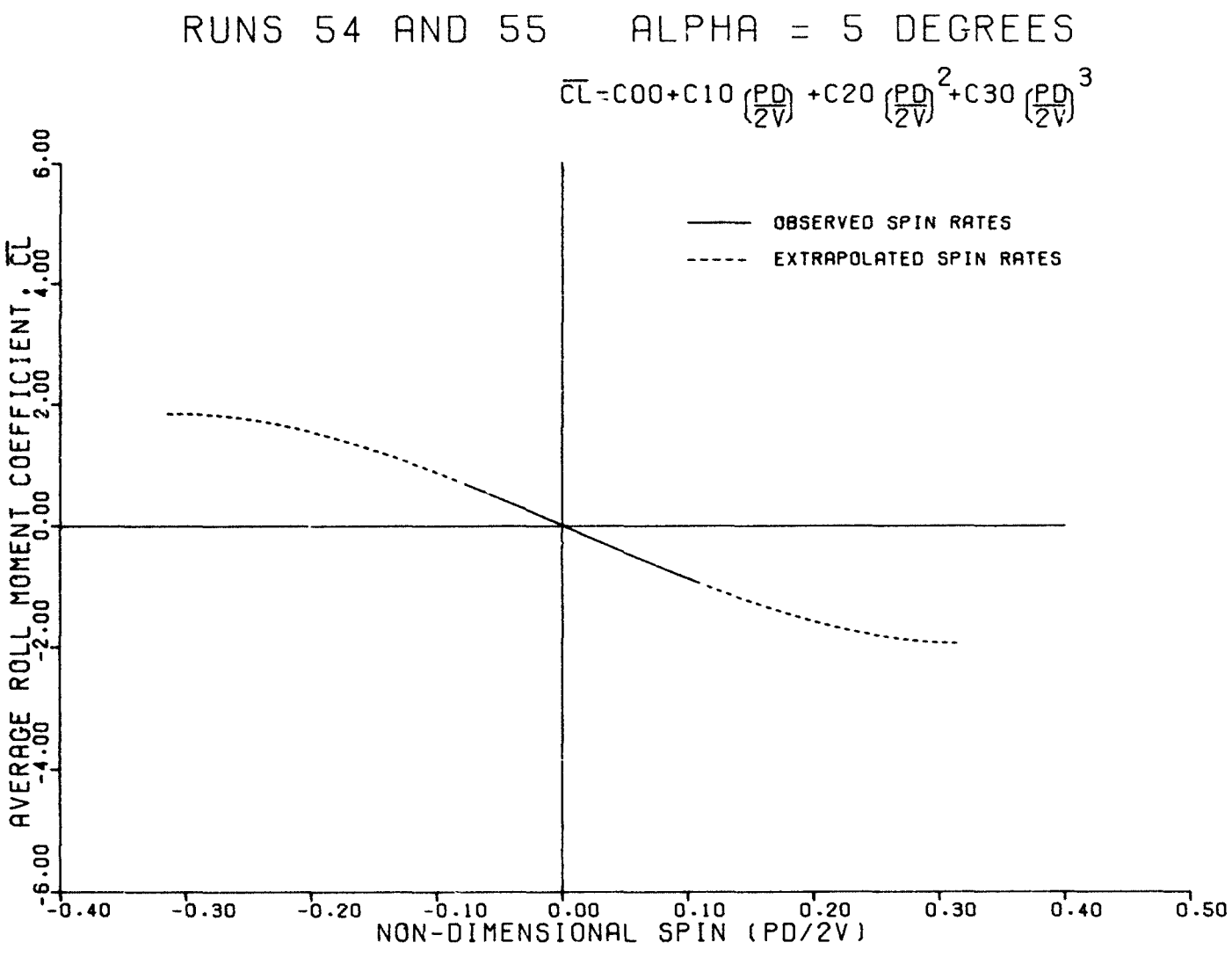

Figure C-2. Average Roll Moment Coefficient Versus Spin Rate at a 5° Angle of Attack for Runs 54 and 55

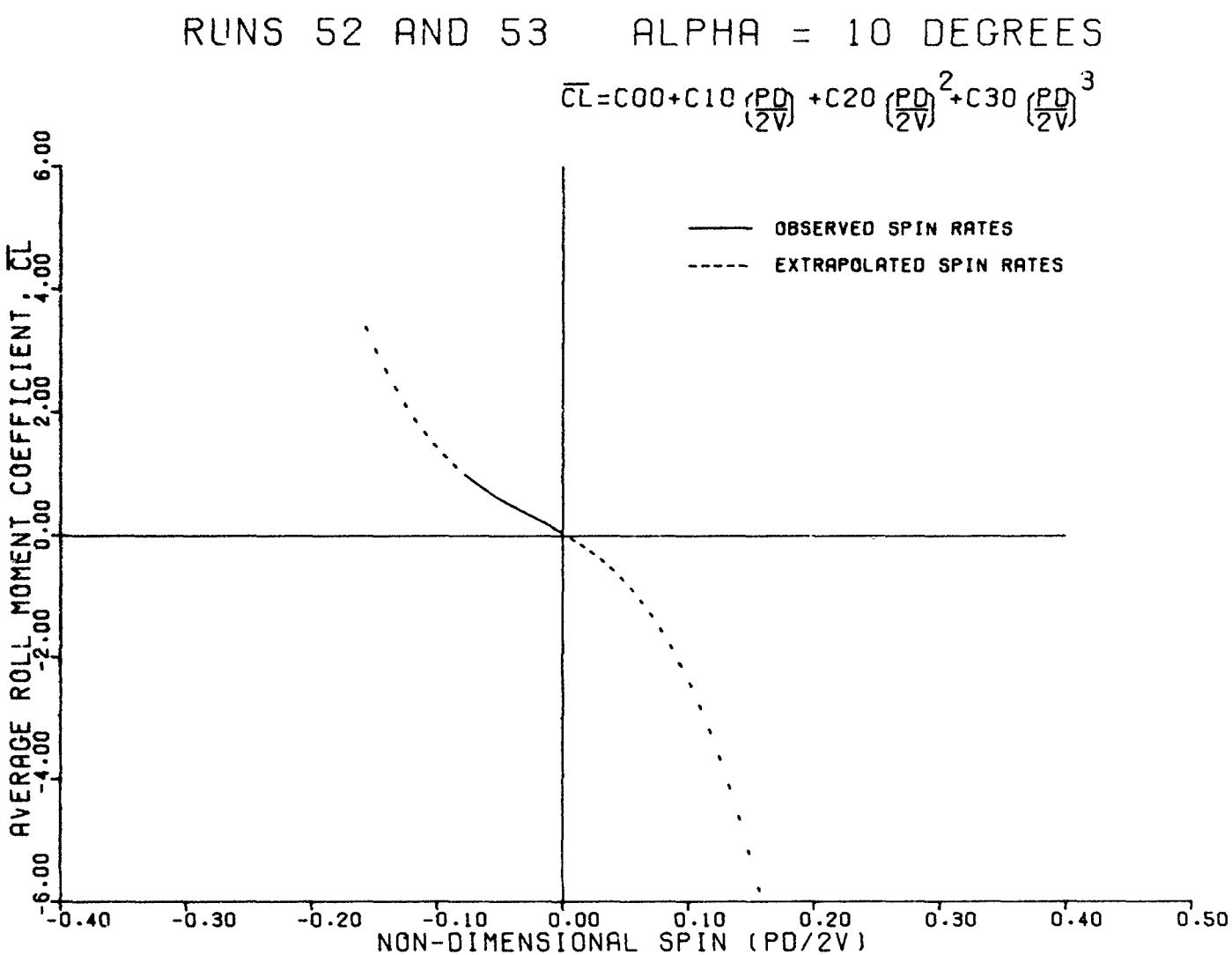

Figure C-3. Average Roll Moment Coefficient Versus Spin Rate at a 10° Angle of Attack for Runs 52 and 53

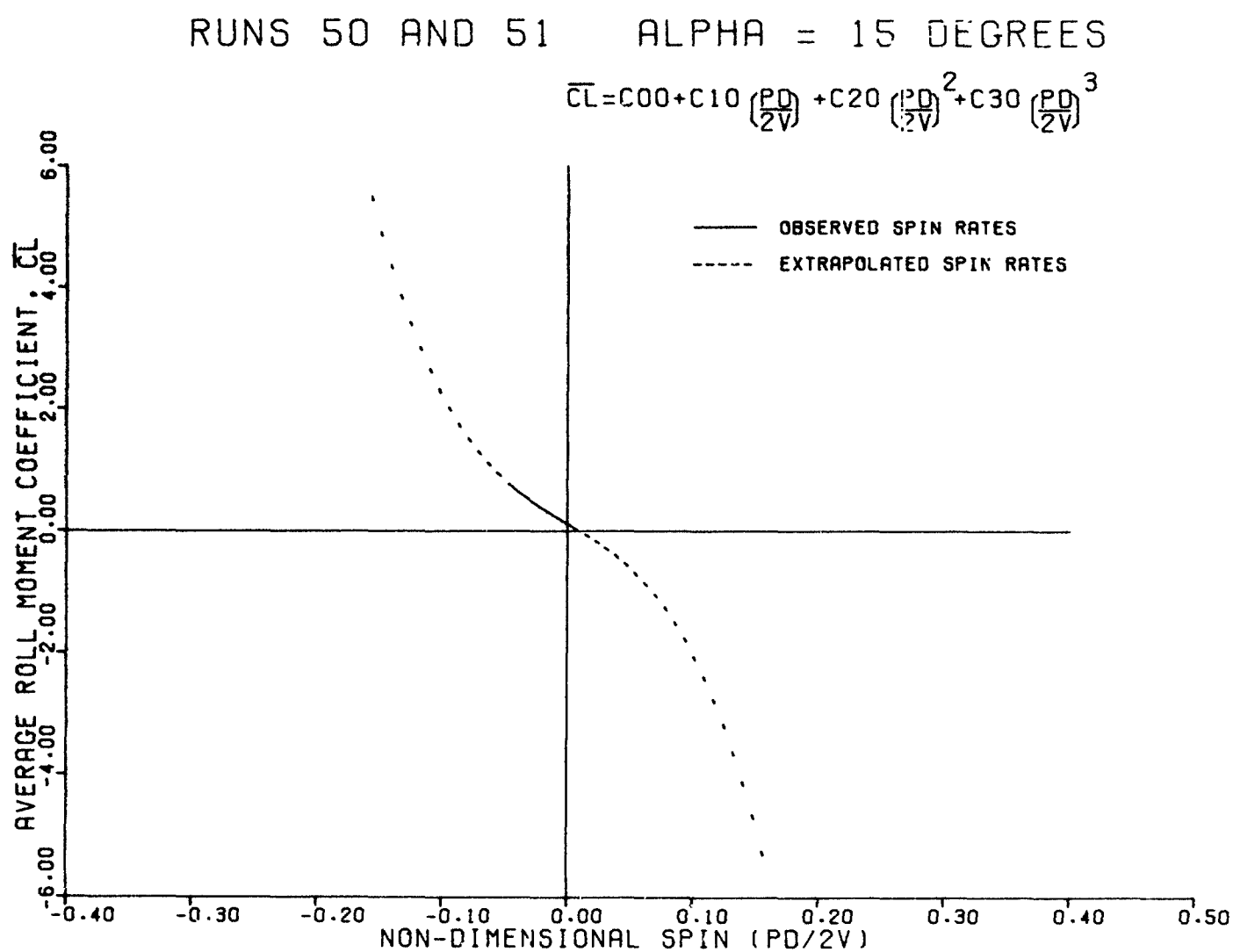

Figure C-4. Average Roll Moment Coefficient Versus Spin Rate at a 15° Angle of Attack for Runs 50 and 51

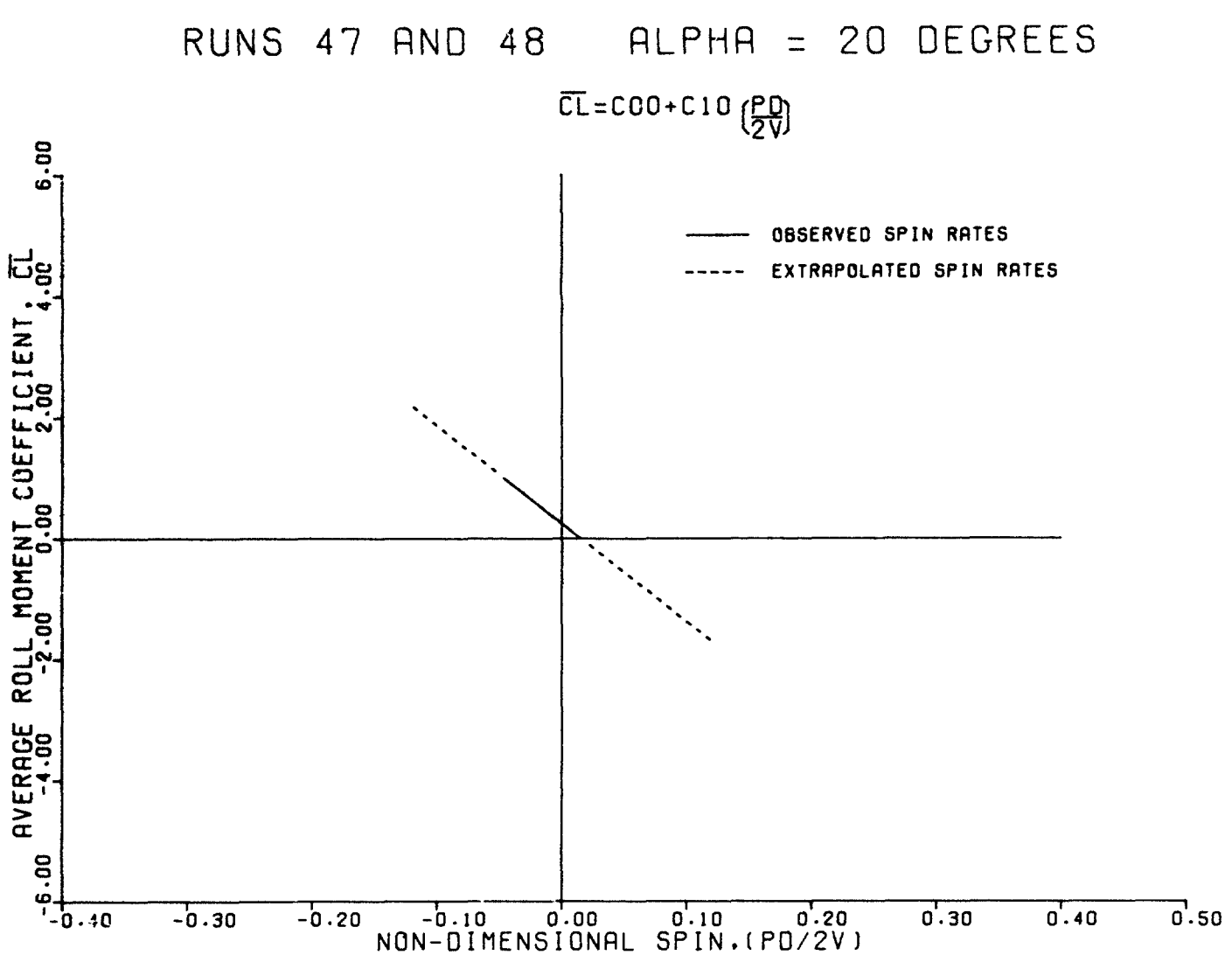

Figure C-5. Average Roll Moment Coefficient Versus Spin Rate at a 20° Angle of Attack for Runs 47 and 48

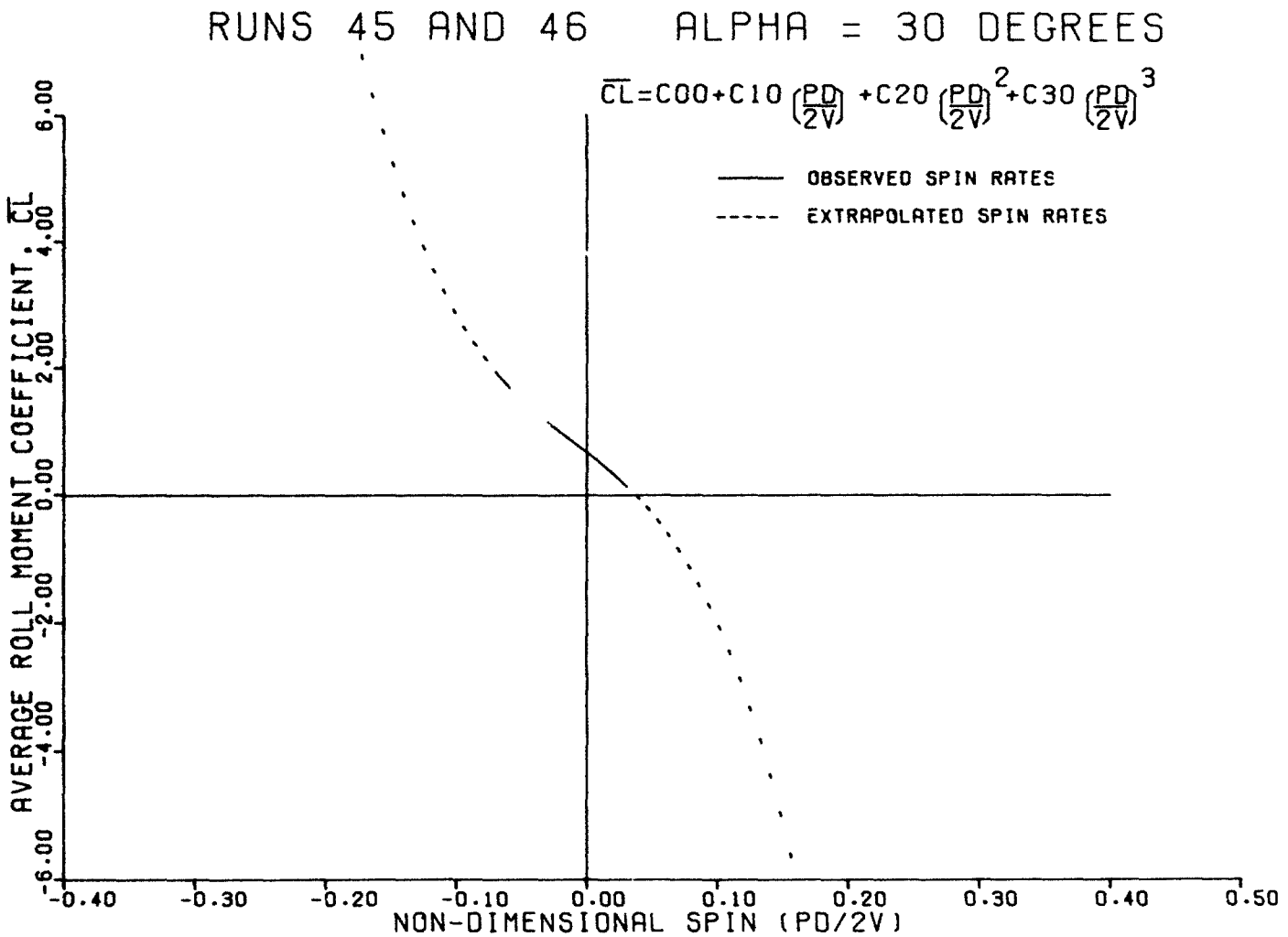

Figure C-6. Average Roll Moment Coefficient Versus Spin Rate at a 30° Angle of Attack for Runs 45 and 46

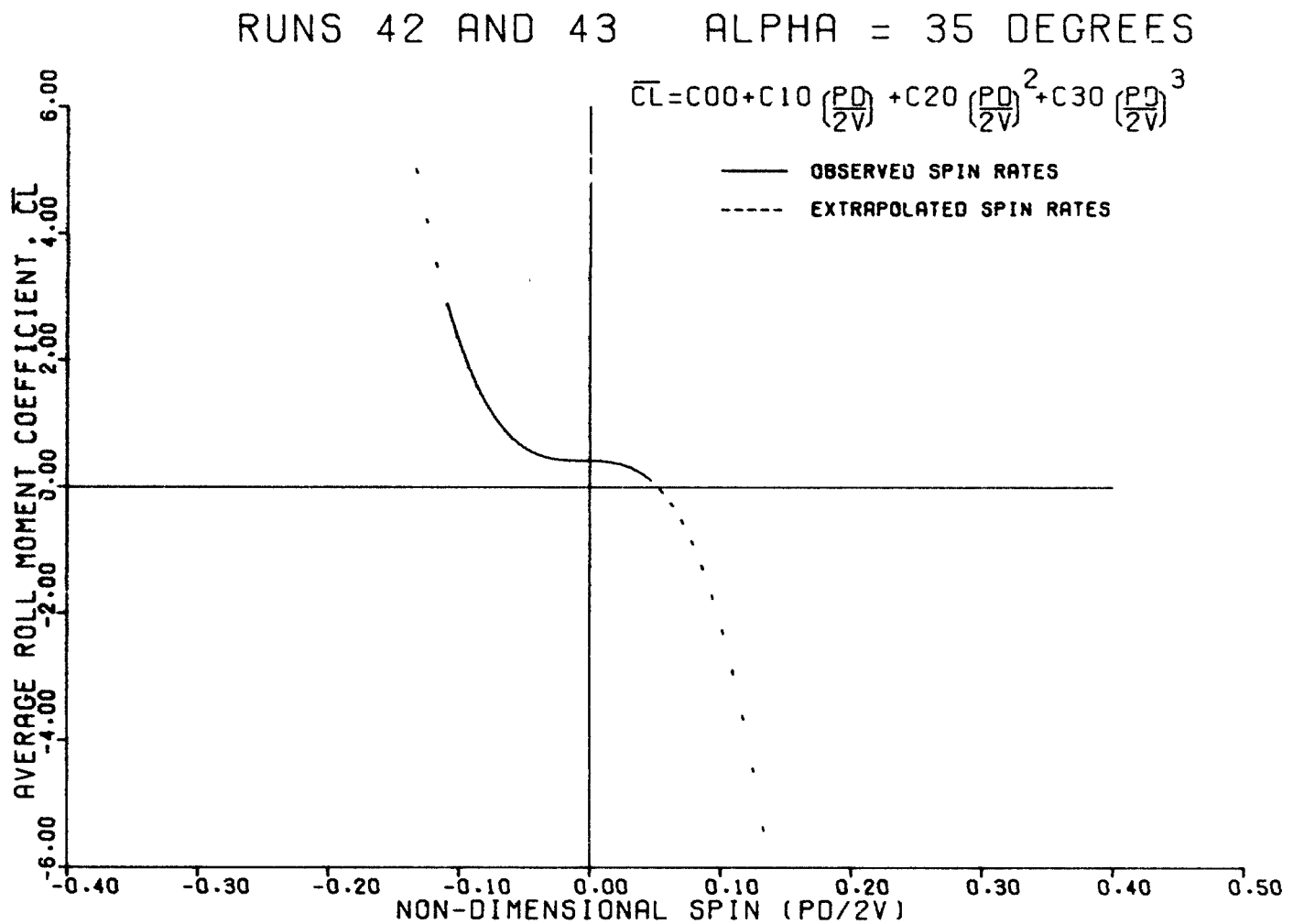

Figure C-7. Average Roll Moment Coefficient Versus Spin Rate at a 35° Angle of Attack for Runs 42 and 43

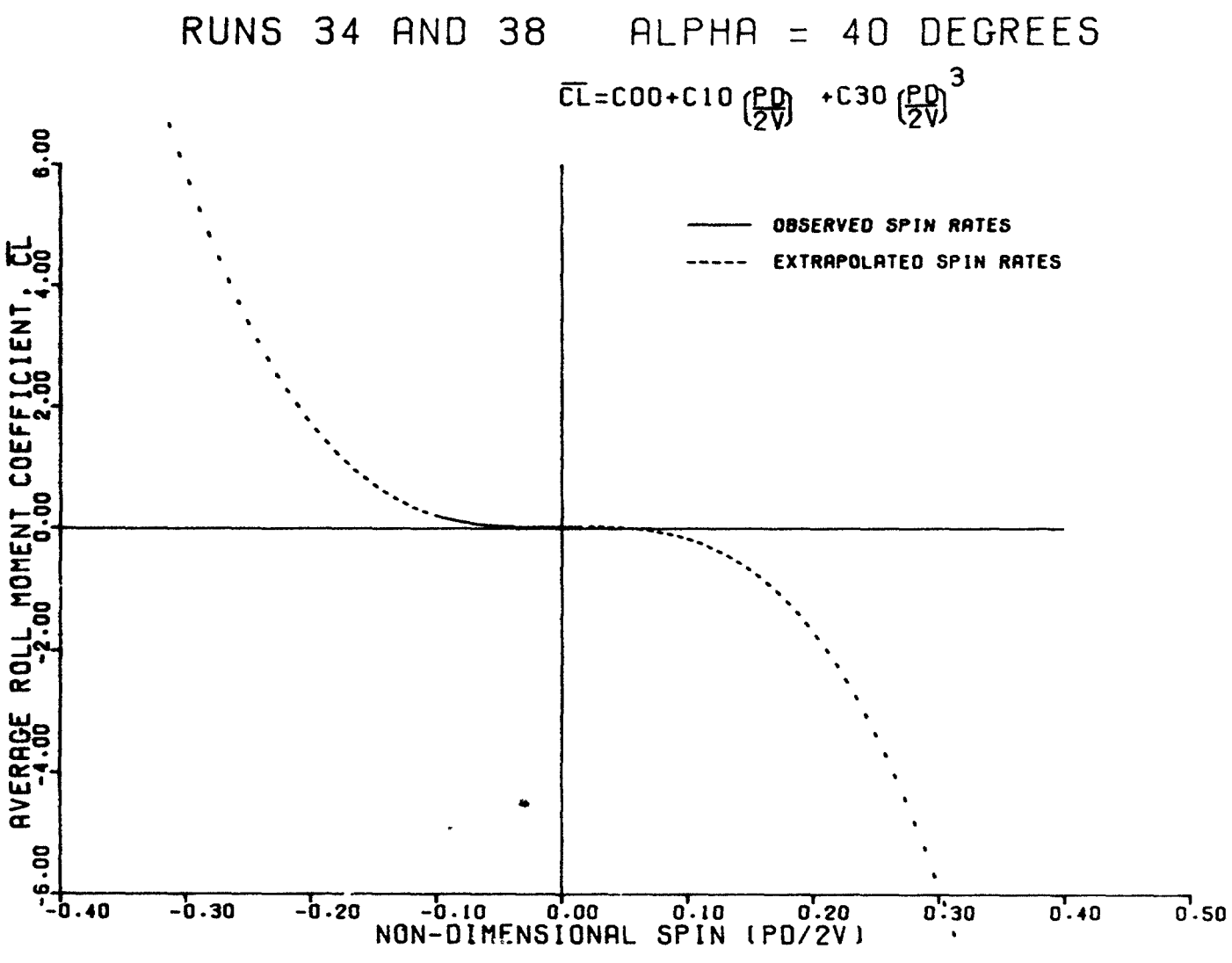

Figure C-8. Average Roll Moment Coefficient Versus Spin Rate at a 40° Angle of Attack for Runs 34 and 38

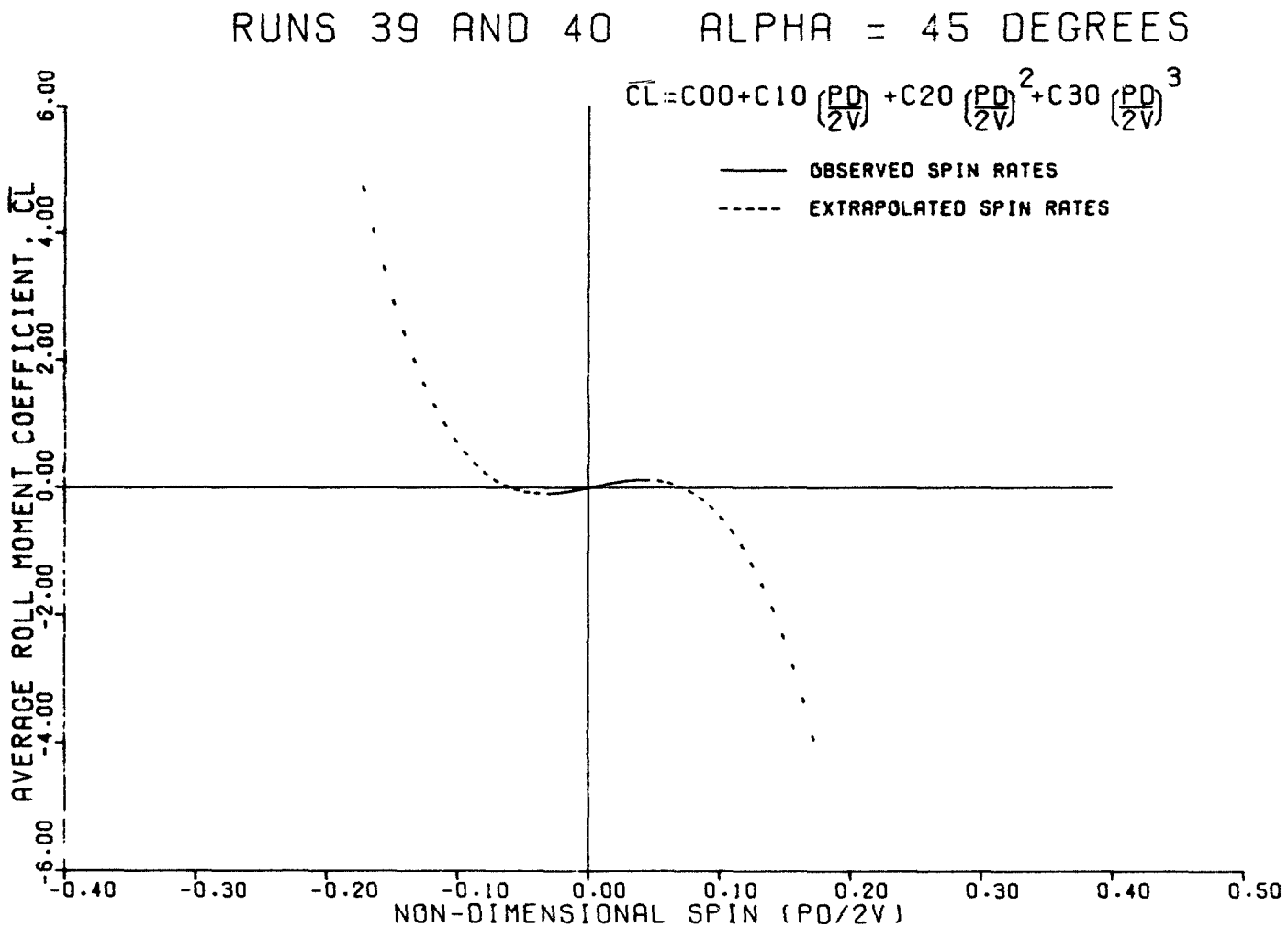

Figure C-9. Average Roll Moment Coefficient Versus Spin Rate at a 45° Angle of Attack for Runs 39 and 40

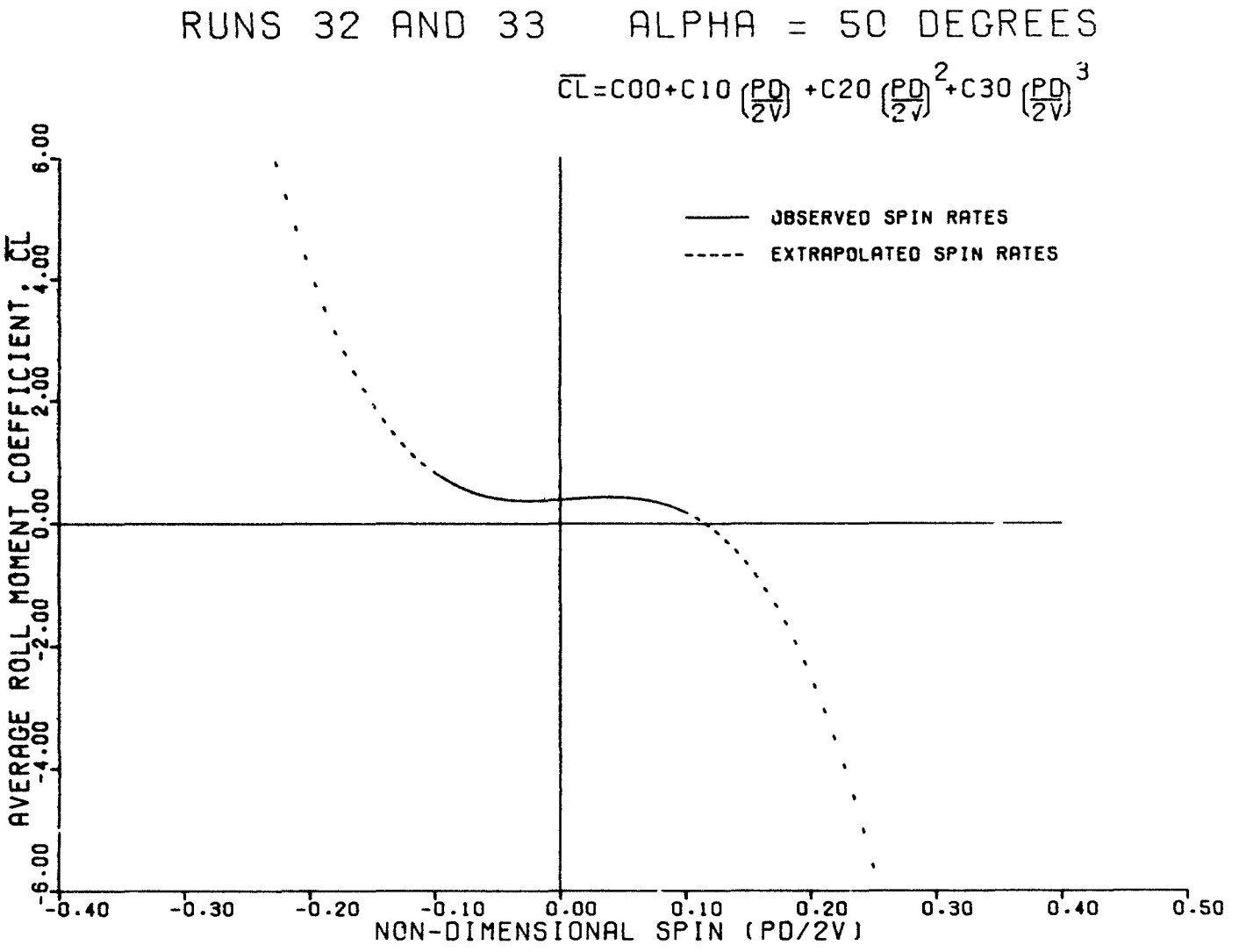

Figure C-10. Average Roll Moment Coefficient Versus Spin Rate at a 50° Angle of Attack for Runs 32 and 33

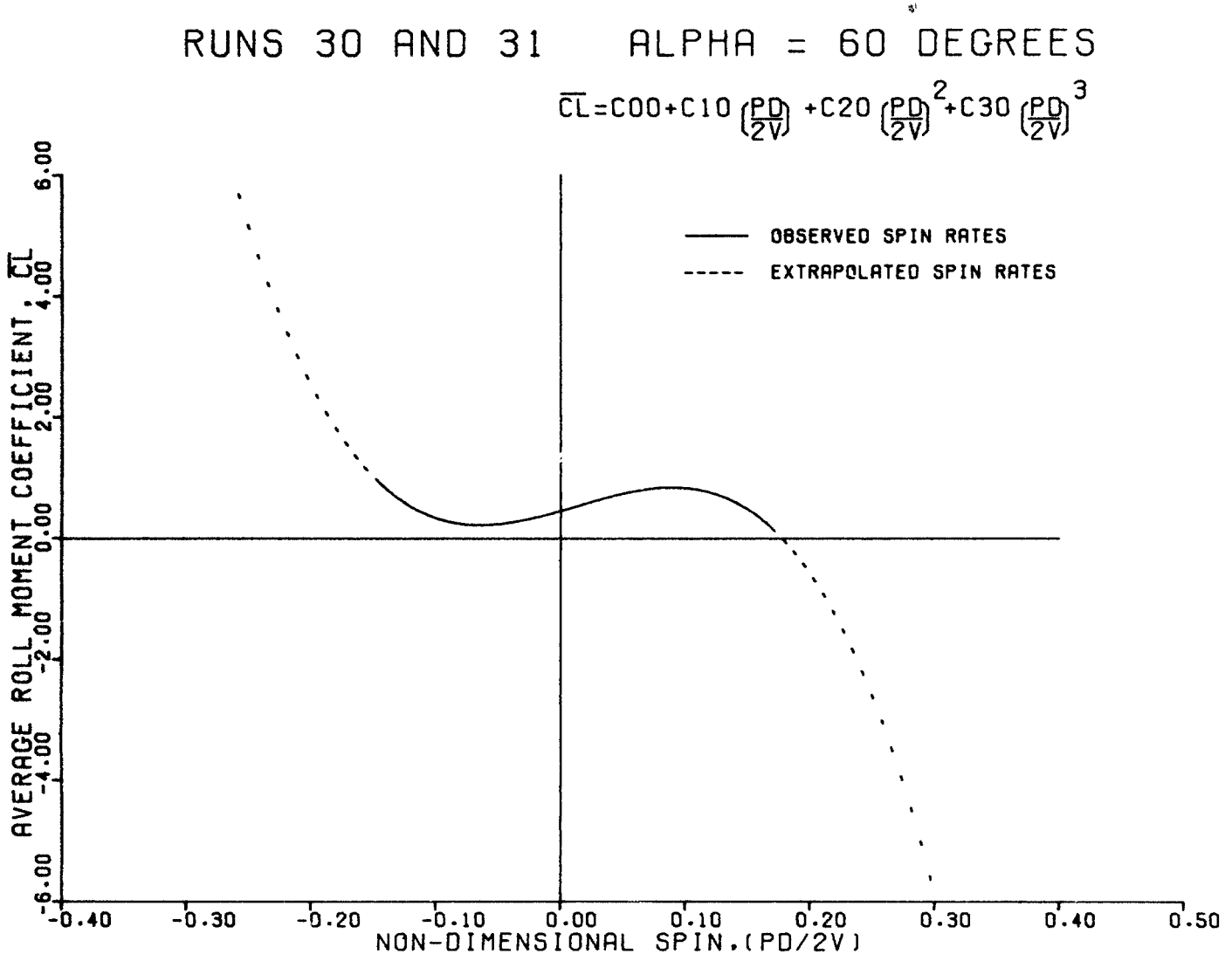

Figure C-11. Average Roll Moment Coefficient Versus Spin Rate at a 60° Angle of Attack for Runs 30 and 31

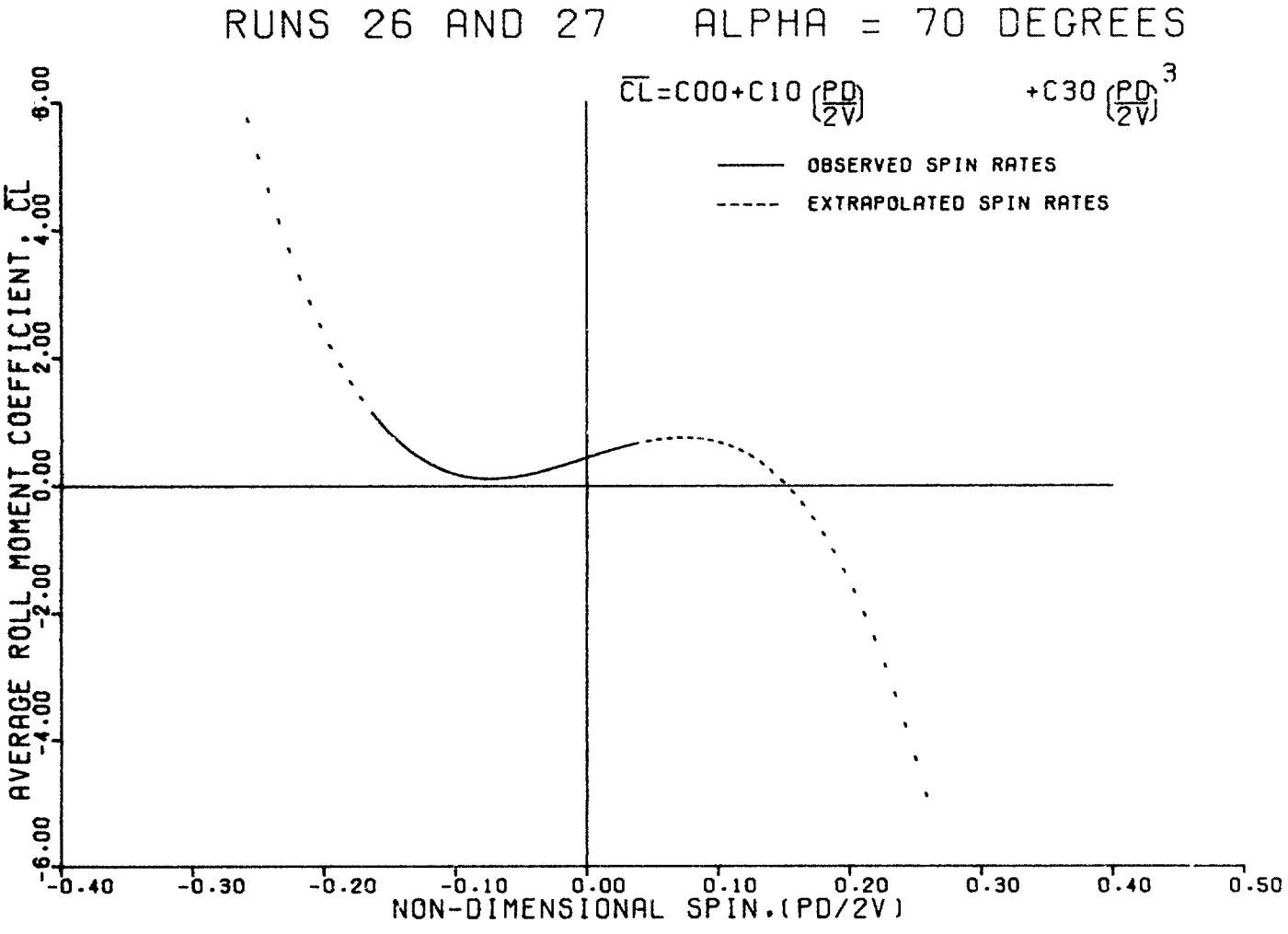

Figure C-12. Average Roll Moment Coefficient Versus Spin Rate at a 70° Angle of Attack for Runs 26 and 27

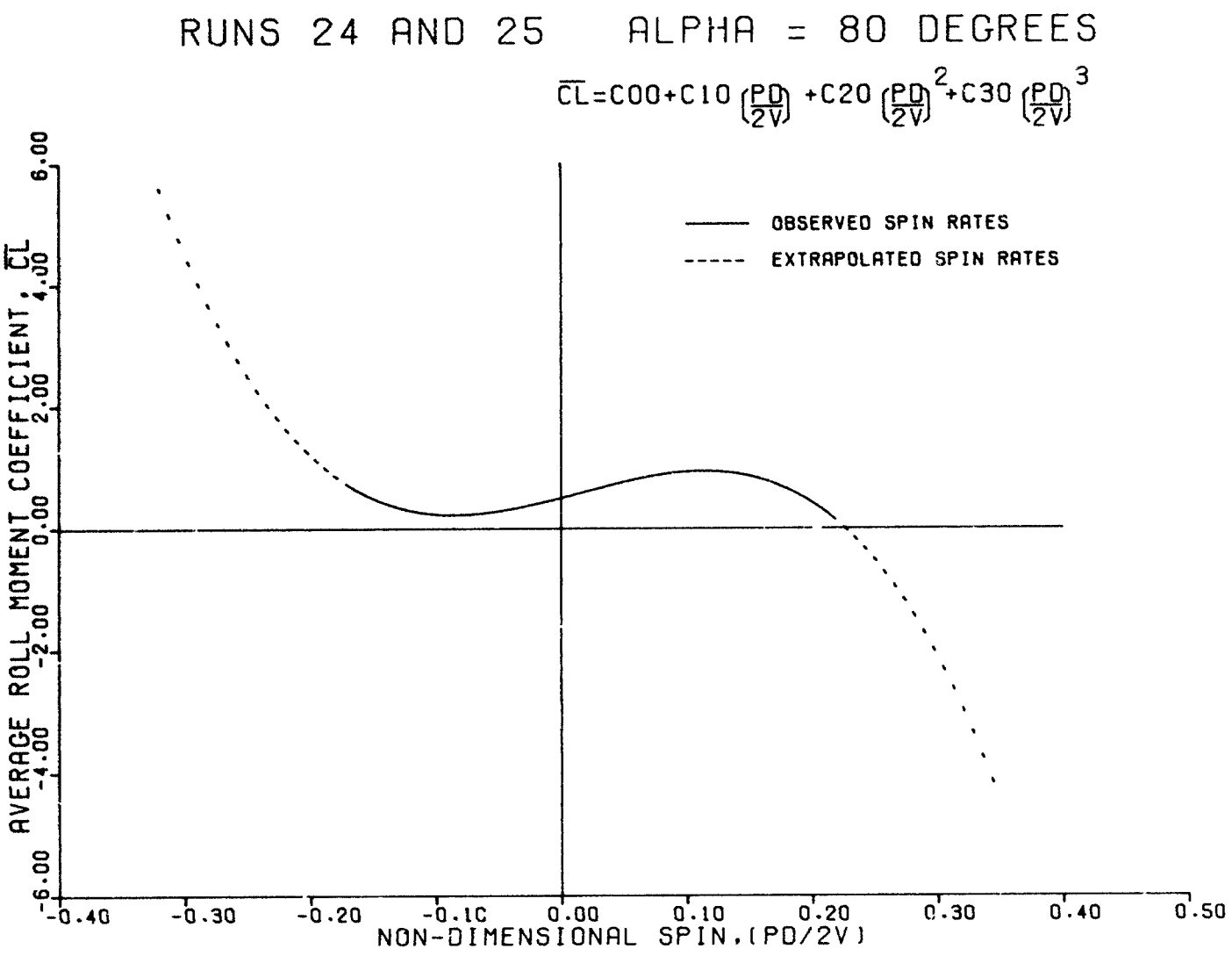

Figure C-13. Average Roll Moment Coefficient Versus Spin Rate at an 80° Angle of Attack for Runs 24 and 25

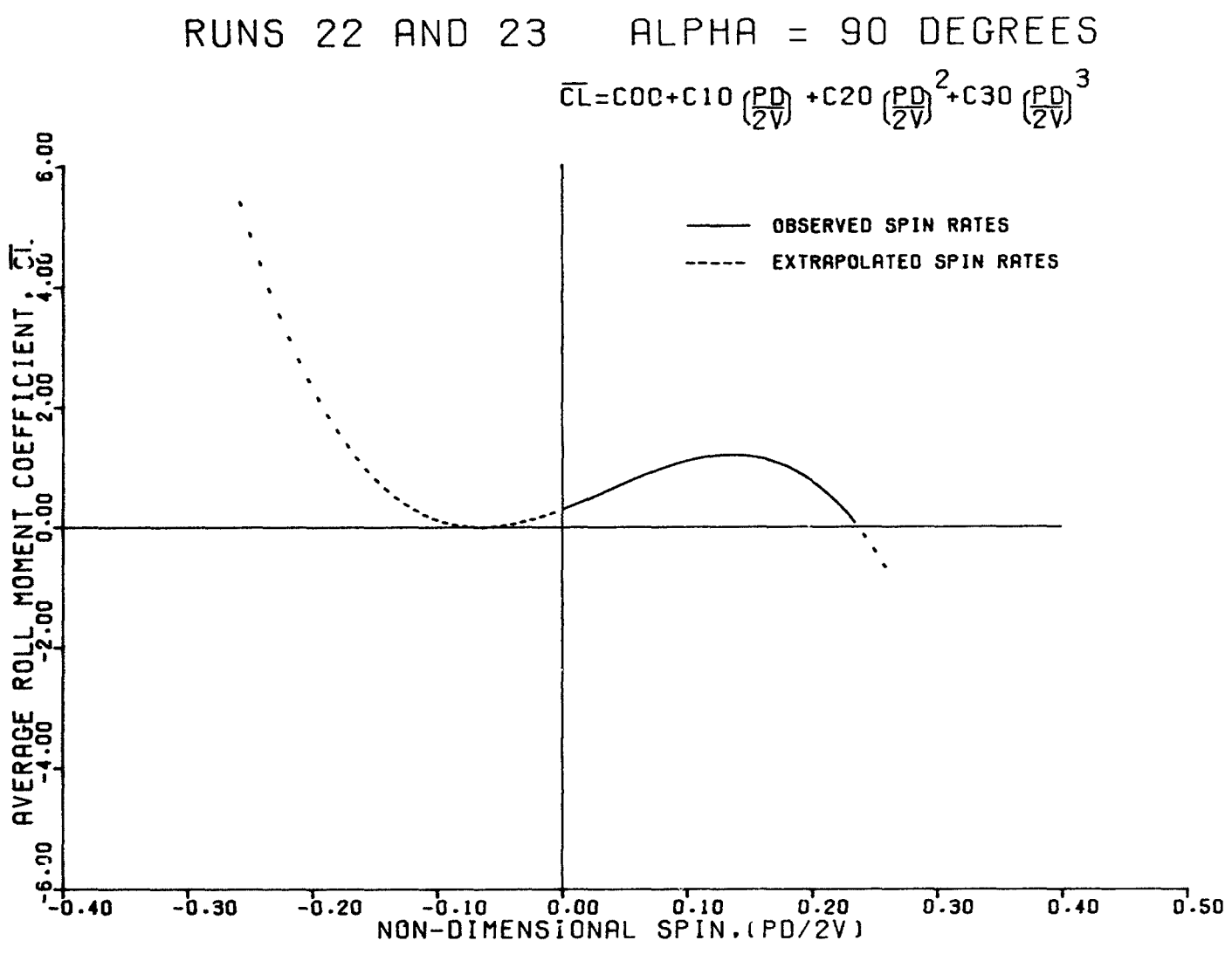

Figure C-14. Average Roll Moment Coefficient Versus Spin Rate at a 90° Angle of Attack for Runs 22 and 23

APPENDIX D

NOMENCLATURE

NOMENCLATURE

A	Body reference area (ft)
C_{ac}, S_{as}	Aerodynamic/mass asymmetry roll moment coefficients
C_{jk}	Roll moment coefficient, defined in Equation (1) (see Table 1)
$\overline{C_\ell}$	Average roll moment coefficient per revolution, defined in Equation (2)
C_{ℓ_p}	Linear roll damping moment coefficient
$C_{\ell_{p^2}}$	Quadratic roll damping moment coefficient
$C_{\ell_{p^3}}$	Cubic roll damping moment coefficient
$C_{\ell_{p(4\gamma)}}$, $C_{\ell_{p(8\gamma)}}$	Variation of the linear roll damping moment coefficient with roll angle
$C_{\ell_{(4\gamma)}}$, $C_{\ell_{(8\gamma)}}$, $C_{\ell_{(12\gamma)}}$, $C_{\ell_{(16\gamma)}}$, $C_{\ell_{(18\gamma)}}$	Induced static roll moment coefficients
C_{ℓ_δ}	Static roll moment coefficient
$C_{\ell_{\delta(4\gamma)}}$, $C_{\ell_{\delta(8\gamma)}}$	Variation of the static roll moment coefficient with roll angle
d	Body reference diameter (ft)
I_x	Axial moment of inertia, slug (ft^2)
p	Roll rate (rad/s)
Q	Dynamic pressure, $pV^2/2$ (lb/ft^2)
$\underset{\sim}{Q}$	QAd/I_x

NOMENCLATURE (Continued)

S_{jk}	Time (s)
V	Velocity (ft/s)
X_A, Y_A, Z_A	Coordinates of wind tunnel axis system, defined in Figure 3
X_B, Y_B, Z_B	Coordinates of model body axis system, defined in Figure 3
α	Angle of attack (rad or deg)
γ	Roll orientation angle (rad or deg)
$\dot{\gamma}$	Roll rate, $\gamma = p$ (rad/s)
$\ddot{\gamma}$	Roll angular acceleration, $\ddot{\gamma} = \dot{p}$ (rad/s)
δ	Fin cant deflection angle (rad or deg)

DISTRIBUTION

Commander
Naval Air Systems Command
Washington, DC 20360
ATTN: AIR-320, Mr. Bill Volz
AIR-320, Dr. H. Mueller
Technical Library (2)

Commander
Naval Sea Systems Command
Washington, DC 20360
ATTN: SEA-03, Mr. Lionel Pasiuk
Technical Library (2)

Commander
Naval Material Command
Washington, DC 20360
ATTN: Mr. Sid Jacobson (MAT-032)
Dr. John Huth
Technical Library (2)

Commander
Naval Weapons Center
China Lake, CA 93555
ATTN: Code 4063, Mr. Ray Van Aken
Code 4063, Mr. R. E. Meeker
Code 4063, Mr. R. M. Rogers
Technical Library

Army Air Mobility Research and Development
Laboratory
Ames Directorate
NASA, Ames Research Center
Moffett Field, CA 94035
ATTN: F. Lazzeroni (Mail Stop N216)
G. Laub (Mail Stop N216)

Commander
Pacific Missile Test Center
Point Mugu, CA 93041
ATTN: Mr. Joe Rom
Technical Library (2)

DISTRIBUTION (Continued)

Commander
David W. Taylor, Naval Ship Research and
Development Center
Washington, DC 20007
ATTN: S. Gottlieb
Martin Cook
Technical Library

Chief of Naval Research
Department of the Navy
Washington, DC 20360
ATTN: Technical Library (2)

Director
Naval Strategic Systems Project
Office (PM-1)
Department of the Navy
Washington, DC 20360
ATTN: Technical Library (2)

Superintendent
U.S. Naval Academy
Annapolis, MD 21402
ATTN: Head, Weapons Department
Head, Science Department
Technical Library (2)

Superintendent
U.S. Naval Postgraduate School
Monterey, CA 95076
ATTN: Head, Mechanical Engineering Department
Head, Department of Aeronautics
Technical Library (2)

Officer in Charge
U.S. Naval Scientific and Technical
Intelligence Center
U.S. Naval Observatory
Washington DC 20360
ATTN: Technical Library (2)

DISTRIBUTION (Continued)

Office of Naval Research
Pentagon
Washington, DC 20350
ATTN: Dr. R. J. Lundegard
Mr. Da. ' Seigel
Dr. Bob Whitehead
Mr. Mort Cooper
Mr. Ralph Cooper
Technical Library (2)

Deputy Chief of Naval Operations
(Development)
The Pentagon
Washington, DC 20350
ATTN: Technical Library (2)

Commanding Officer
Naval Air Development Center
Warminister, PA 18974
ATTN: Technical Librar, (2)

Commanding Officer
Naval Air Engineering Center
Aeronautical Structures Department
Lakehurst, NJ 19112
ATTN: Technical Library (2)

Commanding Officer
Naval Ordnance Station
Indian Head, MD 20640
ATTN: Technical Library (2)

Commandant of the Marine Corps
Headquarters, Marine Corps
Washington, DC 20380
ATTN: Technical Library (2)

Commanding General
Marine Corps Development and Education
Command
Quantico, VA 22134
ATTN: Director, Development Center
Chief, S and R Division
Chief, Air Operations Division
Chief, Ground Operations Division

DISTRIBUTION (Continued)

Commander
Ballistic Research Laboratory
Aberdeen Proving Ground, MD 21005
ATTN: Dr. C. H. Murphy
Mr. L. McAllister
Dr. A. Platou
Mr. B. McCoy
Technical Library (2)

Commander
Department of the Army
U.S. Army Armament Research and Development Command
Dover, NJ 07801
ATTN: Mr. A. Loeb
Mr. Mertz
M. Cline
Technical Library (2)

Commander
U.S. Army Missile Command
Redstone Arsenal, AL 35809
ATTN: Mr. Ray Deep (DRSMI)
Dr. D. J. Spring (DRSMI)
Technical Library (2)

Commander
U.S. Army Material Development and Readiness Command (AMCRD-TP)
5001 Eisenhower Avenue
Alexandria, VA 22304
ATTN: Technical Library (2)

Office of Chief of Research and Development
Washington, DC 20310
ATTN: Technical Library (2)

Commander
Army Chemical Center
Edgewood, MD 21040
ATTN: Technical Library (2)

DISTRIBUTION (Continued)

Commander
Frankford Arsenal
Philadelphia, PA 19104
ATTN: Mr. W. Gadomski
Technical Library (2)

Commander
Harry Diamond Laboratories
Washington, DC 20013
ATTN: Technical Library (2)

Commanding Officer
U.S. Army Combat Development Command
Field Artillery Agency
Fort Sill, OK 73503
ATTN: President, U.S. Army Field
Artillery Board
Marine Corps Liaison Officer
Technical Library (2)

Commanding Officer
Aeronautical Research Laboratory
Wright-Patterson Air Force Base
Dayton, OH 45433
ATTN: Head, Aeronautical System Division
Technical Library (2)

Commanding Officer
USAF Office of Scientific Research
Washington, DC 20330
ATTN: Technical Library (2)

Commanding Officer
Arnold Engineering Development Center
USAF
Tullahoma, TN 37389
ATTN: Mr. J. Uselton
Mr. L. M. Jenke
Mr. W. B. Baker, Jr.
Technical Library (2)

Headquarters, USAF
Systems Command
Andrews Air Force Base, MD 20331
ATTN: Technical Library (2)

DISTRIBUTION (Continued)

Headquarters, USAF
Washington, DC 20330
ATTN: Technical Library (2)

Commanding Officer
Flight Research Center
Edwards Air Force Base, CA 93523
ATTN: Technical Library (2)

Commanding Officer
Air Force Rocket Propulsion Laboratory
(AFSC)
Department of the Air Force
Edwards, CA 93523
ATTN: Major Washburn

Commanding Officer
U.S. Air Force Systems Command
Regional Offices
c/o Department of the Navy
Washington, DC 20360
ATTN: Technical Library (2)

Commanding Officer
U.S. Air Force Armament Laboratory
(AFATL)
Eglin Air Force Base, FL 32542
ATTN: Dr. Daniel
Mr. C. Butler
Mr. C. Matthews
Mr. K. Cobb
Mr. E. Sears
Technical Library (2)

Superintendent
U.S. Air Force Academy
Colorado Springs, CO 80912
ATTN: Technical Library (2)

Commanding Officer
Air Force Flight Dynamics Laboratory
Wright-Patterson Air Force Base, OH 45433
ATTN: Mr. E. Flinn (FCG)
Dr. G. Kurylowich (FGC)
Technical Library (2)

DISTRIBUTION (Continued)

Applied Physics Laboratory
The John Hopkins University
8621 Georgia Avenue
Silver Spring, MD 20910
ATTN: Dr. L. L. Cronvich
Mr. Edward T. Marley
Dr. Gordon Dugger
Technical Library (2)

Director
Advanced Research Projects Agency
Department of Defense
Washington, DC 20305
ATTN: Technical Library (2)

Director
Defense Research and Engineering
Department of Defense
Washington, DC 20305
ATTN: Technical Library (2)

Commander
George C. Marshal Flight Center
Huntsville, AL 35804
ATTN: Technical Library (2)

NASA Goddard Space Center
Greenbelt, MD 20771
ATTN: Technical Library (2)

NASA Lewis Research Center
Cleveland, OH 44101
ATTN: Technical Library (2)

NASA
Washington, DC 20546
ATTN: Technical Library (2)

NASA Ames Research Center
Moffett Field, CA 94035
ATTN: Mr. Vic Peterson
Mr. John Rakich
Technical Library (2)

DISTRIBUTION (Continued)

NASA Langley Research Center
Langley Station
Hampton, VA 23365
ATTN: Mr. Bud Bobbitt
Mr. Jerry South
Mr. C. M. Jackson, Jr.
Mr. W. C. Sawyer
Technical Library (2)

Virginia Polytechnic Institute and
State University
Department of Aerospace Engineering
Blacksburg, VA 24060
ATTN: Prof. J. A. Schetz
Technical Library (2)

Stanford Research Institute
Menlo Park, CA 94025
ATTN: Dr. Milton Van Dyke
Technical Library (2)

Raytheon Company
Spencer Laboratory
Burlington, MA 01803
ATTN: Steve Pealsing
Box SL 7162

North Carolina State University
Department of Mechanical and Aerospace
Engineering
Box 5246
Raleigh, NC 27607
ATTN: Prof. F. R. DeJarnette
Technical Library (2)

The University of Tennessee
Space Institute
Tullahoma, TN 37388
ATTN: Dr. J. M. Wu
Technical Library (2)

Director
Defense Research and Engineering
Department of Defense
Washington, DC 20301
ATTN: Bartley Osborne, R&AT Office